The Story of the Carrara Sub-Basin - Biomarker Distribution and Thermal Maturity of Source Rocks from NDI Carrara 1

By

Liam Johnson

This thesis is presented in partial fulfilment of the requirements for the Master of Earth Sciences (Advanced) at The Australian National University

Research School of Earth Sciences

May 2022

I. Thesis declaration

This thesis contains no material which has been accepted for the award of any other degree or diploma in any university. To the best of the author's knowledge, this thesis contains no material previously published or written by another person, except where due reference is made in the text.

Signed:

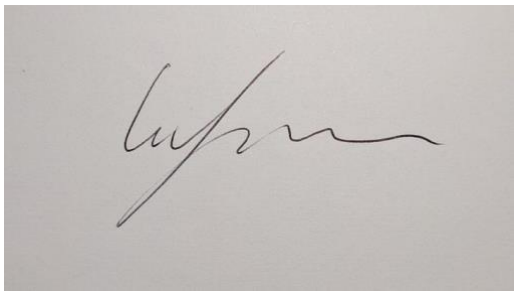

Liam Johnson
27th of May 2022

Word count of main text: 15790

II. Table of Context

TABLE OF CONTENTS

III. Abstract

The NDI Carrara 1 drill hole was drilled as part of the Mine Ex CRC National Drilling Initiative in September-December 2020 in collaboration with Geoscience Australia and the Norther Territory Geological Survey. In this project, 17 rock samples and 3 oil stains from the Carrara 1 drill core were analysed using Gas Chromatography and Mass Spectrometry (GC/MS) to provide a comprehensive assessment of biomarkers and the thermal maturity of the Carrara Sub-basin in Northern Australia. According to aromatic hydrocarbon maturity assessment of phenanthrenes and methylphenanthrenes, the interval from the top of the core to 630 m is in the peak oil window and the source rocks are likely highly generative in terms of liquid hydrocarbons. In addition, prokaryote and eukaryote biomarkers are detected in high abundance providing valuable insights into life during the Cambrian period. In contrast, biomarkers are below detection limits in the Proterozoic section of the core (630-1750.85 m) with the notable exception of acyclic saturated hydrocarbons which are detected in some of the shallower Proterozoic samples. Thermal maturity estimates computed using aromatic hydrocarbons illustrate that maturity increases downcore indicating that these compounds are syngenetic and that the source rocks are overmature in terms of liquid hydrocarbon generation and are likely in the late stages of wet gas generation or a producing dry gas. In addition, the distribution of biomarkers and thermal maturity is consistent with an unconformity at 630 m and a fault repeated sequence between 630-800 m from 925-1130 m. Finally, the distribution of acyclic saturated hydrocarbons and polyaromatic hydrocarbons provide evidence for secondary migration of liquid hydrocarbons in at least one sample of the Carrara 1 drill core.

IV. Acknowledgments

First and foremost, I would like to extend my sincere gratitude to my supervisors Professor Jochen Brocks and Dr Emmanuelle Grosjean for the opportunity to undertake this research as part of the Brocks lab group at the ANU in partnership with Geoscience Australia. Thank you for your continued guidance and support during the entirety of this master's project. I'd also like to give my sincere appreciation to Geoscience Australia for the research scholarship which was absolutely critical in giving me time to work on the project and complete it to a high standard. I would also like to thank Geoscience Australia for providing the Carrara 1 samples and preparing them for laboratory work. I wish to acknowledge the help and guidance of our lab supervisor Janet Hope for her expertise in the lab and for her guidance towards the necessary skills to perform the laboratory component to a high standard. My gratitude extends to the entire cohort of the Brocks lab group for their suggestions and guidance. Finally, I wish to thank my friends and family, and in particular my mum, dad, and best friend Danny, for their unwavering love and support throughout this entire project.

V. Main text

1: Introduction

1.1. - Overview

Planet Earth is a dynamic and extraordinarily complicated assemblage of interconnected systems that have evolved together for 4.6 billion years. The history of the Earth, including the evolution of life and the waxing and waning of environments and coastlines, are stored in the geological record, in rocks waiting to be uncovered. In addition, these geological basins that hold the secrets of deep time contain the resources and materials to build a strong industry and economy, and more importantly, a greater understanding of the resource potential of an area and how it can be best utilised prudently and sustainably for long term benefits. The exploration of early life and hydrocarbon resources such as oil and gas are complimentary to one another since both require a quantification of hydrocarbon molecules (Peters et al. 2005). In the case of Pre-Ediacaran life, macrofossils are of little use since life at this time was mostly microscopic and lacked hard skeletons (Porter 2020). Subsequently, one of the most effective techniques available to analyse the rock record in deep time is the study of molecular fossils, or biomarkers – the extremely stable diagenetic hydrocarbon products of biologically derived parent molecules (Peters et al. 2005). Biomarkers show varying degrees of biological and environmental specificity allowing some to serve as powerful tools for understanding past life and environmental conditions on Earth (Eigenbrode 2011; Welander 2019). By analysing the rock record for evidence of these molecules and many other important biomarkers, Brocks et al. (2017) were able to create a biomarker record which illustrates the relative abundance of different groups of life through time (See Brocks et al. 2017; Brocks 2018).

In addition to providing valuable evidence of early life and environments on Earth, one of the most common applications of biomarkers and other informative hydrocarbons is to provide insight into the resource potential of a geological basin (Brocks & Summons 2014; Mackenzie 1984; Radke et al. 1997). There are numerous saturated and aromatic biomarkers that can be used to estimate thermal maturity and thus source rock generative potential as a consequence of differing thermal stability among isomers (Brocks & Summons 2014; Peters & Moldowan 1993; Peters et al. 2005; Radke et al. 1983). For example, isomerisation at C_{20} of the C_{29} sterane molecule leads to a 20S and an 20R isomer (Peters et al. 2005). The S isomer has a higher thermal stability compared to the R isomer and thus a calculation of 20S/(20S+20R) can provide an estimate of thermal maturity (Brocks and Summons 2014; Peters & Moldowan 1993; Peters et al. 2005). Thermal maturity is most often used to estimate the extent of hydrocarbon generation source rock in parallel with Rock-Eval pyrolysis data (Peters et al. 2005). Through mathematical manipulation of maturity dependent biomarker quantifications, the thermal maturity of source rocks can be assessed by characterising the sample as either immature, mature or overmature in terms of liquid hydrocarbon

generation (Brocks & Summons 2014; Peters & Moldowan 1993; Peters et al. 2005). Thermal maturity is equally important to the study of early life since maturity it is a function of pressure and heat associated with long-term burial of hydrocarbons. Rocks with high maturity and have experienced high levels of thermal degradation are often devoid of biomarkers (Jarrett et al. 2019a; Peters et al. 2005). Consequently, it is equally beneficial to identify mature and highly generative source rocks with an abundance of hydrocarbons and biomarkers to deepen our understanding of early life on Earth and make prudent decisions for long-term resource exploration and management (Mackenzie 1984; Peters et al. 2005).

1.2. Geological context

During the course of this project 17 core samples and three oil stains collected from the NDI Carrara 1 drill core were analysed using Gas Chromatography/Mass Spectrometry (GC/MS) to determine the biomarker abundance and distribution in addition to the thermal maturity of the Carrara 1 Sub-basin (See Appendix A and Table 1). All of the samples selected for this study had Total Organic Carbon (TOC) > 0.5, with the exception of the deepest sample 7533872 (1593.78 m) which had a TOC ≈ 0.0% and was utilised as a blank. NDI Carrara 1 is the first stratigraphic drill hole taken from the Carrara Sub-basin, a large sedimentary depocentre recently discovered based on interpretation of the L210 South Nicholson Deep Crustal Reflection Seismic Survey (Carr et al. 2019, 2020). The survey was a major deliverable of the Australian government's Exploring for the Future (EFTF) initiative led by Geoscience Australia which aims to provide an improved understanding of the nation's minerals, energy, and groundwater resource potential (Carr et al. 2019, 2020). The first phase of the EFTF ran from 2016-2020 and was aimed at increasing resource exploration in frontier regions of Northern Australia by providing valuable geoscience data (Carr et al. 2019, 2020; Carson et al. 2022).

The Carrara Sub-basin is part of the larger South Nicholson Basin (SNB), which straddles the Northern Territory and Queensland, Australia (See Figure 1). The Carrara Sub-basin is up to 8 km deep, 120 km wide and 190 km from north to south (Carson et al. 2022). Preliminary analysis indicates that it contains thick sequences of Proterozoic carbonates, shales and siliciclastic rocks overlain by 630 m of Cambrian aged Georgina basin sediments (Grosjean et al. 2022; Lauire 2022). Sensitive High Resolution Ion Microprobe (SHRIMP) zircon U-Pb geochronology of lithic tuffs illustrate that the interval between 1653 m and 1012 m was deposited ≈ 1588–1612 million years ago (Ma) which makes this interval stratigraphically equivalent to the middle to upper Lawn Hill Formation and the upper McArthur and Nathan groups of the southern McArthur-basin, all of which are highly prospective in terms of sediment hosted base metal mineralisation and unconventional hydrocarbons (Carson et al. 2022; Grosjean et al. 2022). The Carrara 1 drill core itself was retrieved in late 2020 for extensive isotopic, geochronological, organic, and inorganic geochemistry and geobiological analysis as a collaboration between Geoscience Australia (GA), the Norther Territory Geological Survey (NTGS) and the Mineral Exploration

Cooperative Research Centre (MinEx CRC) (Carson et al. 2022; Grosjean et al. 2022). The core reached a depth of 1750.85 m intersecting Cambrian sediments of the Georgina basin and underlying Proterozoic sediments. The attribution of the Carrara Sub-basin as equivalent to highly prospective basins in northern Australia provides an exciting opportunity for geochemical investigation to identify rocks with good hydrocarbon generative potential paving the way for future hydrocarbon exploration. Additionally, geobiological study of biomarkers throughout the core will provide valuable data to increase the resolution and reliability of the biomarker record. The southern McArthur basin is host to the oldest indigenous biomarkers discovered thus far providing extremely valuable information about early life during the Paleoproterozoic (Vinnichenko et al. 2020). Since the Carrara sub-basin is stratigraphically equivalent, there is the exciting prospect that it too will host extremely old and particularly informative biomarker information.

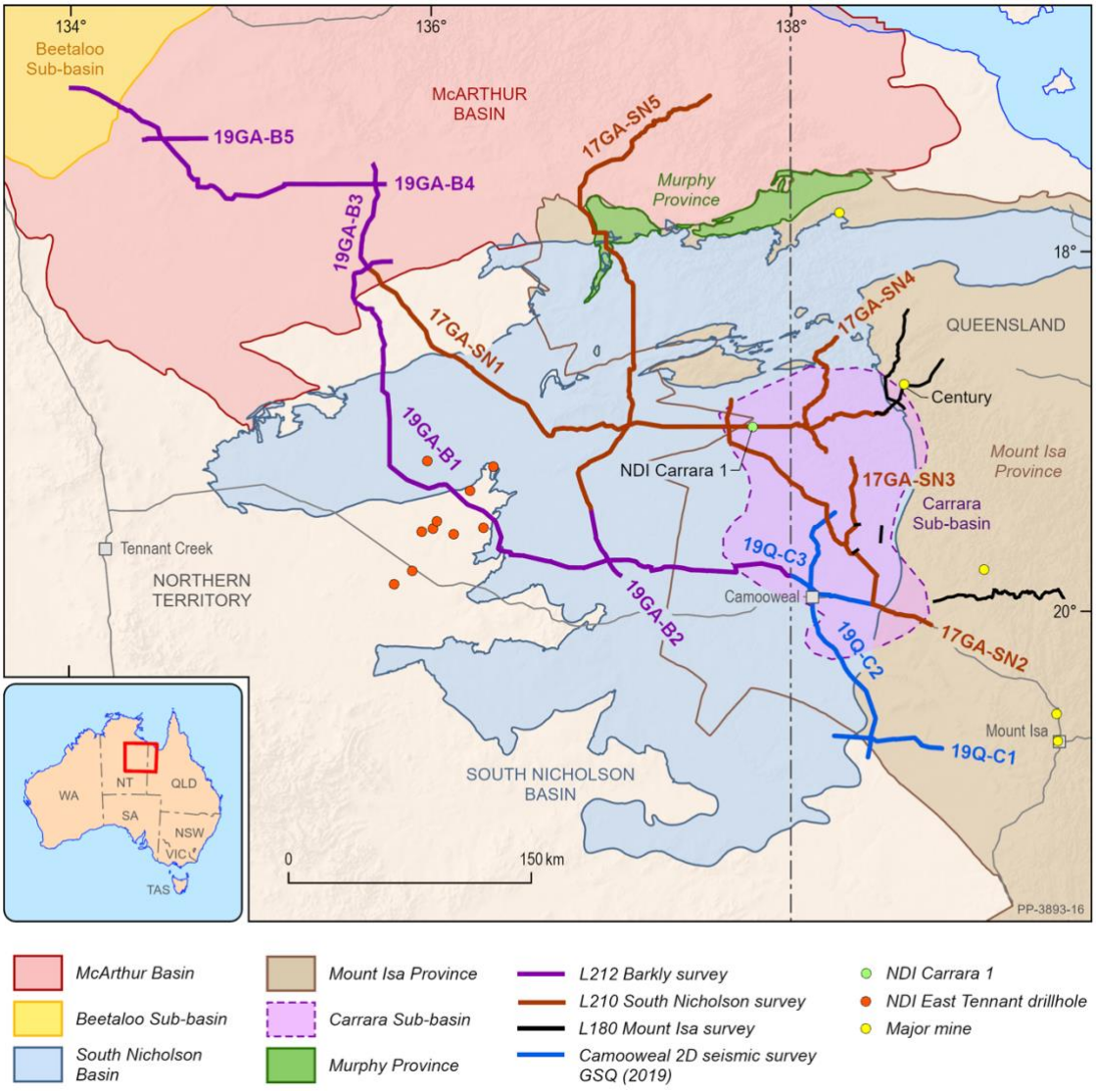

Figure 1 Location of the Carrara 1 drill core (NDI Carrara) embraced between the Mount Isa province and McArthur basin. Note the presence of the highly productive Pb-Zn Century mine which sits on the border of the Carrara sub basin. (Figure from Carson et al. 2022 Geoscience Australia)

Table 1 Selected Carrara 1 samples and rock eval parameters for source rocks

Sample ID	Sample type	Depth top	Depth bottom	TOC (%wt) [a]	S1[b]	S2 [c]	T_{max} [d] (°C)	HI [e]	PI[f]
7533132	Source rock	361.71	371.79	1.37	0.10	3.68	430	269	0.03
7533139	Source rock	394.97	395.12	4.65	1.46	28.22	435	607	0.05
7533159	Source rock	494.48	494.60	1.37	0.09	3.98	427	291	0.02
6725604	Oil stain	528.33	n.d	n.d	n.d	n.d	n.d	n.d	n.d
7533185	Source rock	610.47	610.62	1.36	0.05	4.09	427	300	0.01
7533204	Source rock	689.82	689.95	5.50	0.59	5.39	453	98	0.10
7533210	Source rock	719.21	719.38	1.16	0.22	1.17	441	100	0.16
7373044	Oil stain	763.10	n.d	n.d	n.d	n.d	n.d	n.d	n.d
7373046	Oil stain	763.10	n.d	n.d	n.d	n.d	n.d	n.d	n.d
7533225	Source rock	794.71	794.86	0.93	0.30	0.58	421	62	0.34
7533569	Source rock	925.37	925.53	0.81	0.08	0.17	465	21	0.33
7533584	Source rock	998.66	998.76	1.24	0.05	0.35	494	28	0.12
7533609	Source rock	1069.16	1069.32	1.93	0.04	0.06	500	3	0.40
7533625	Source rock	1150.08	1150.21	1.87	0.03	0.05	442	3	0.34
7533635	Source rock	1199.60	1199.72	0.90	0.01	0.02	443	2	0.35
7533644	Source rock	1244.79	1244.95	3.17	0.02	0.08	442	2	0.22
7533668	Source rock	1345.03	1345.17	1.46	0.02	0.02	446	2	0.45
7533682	Source rock	1405.10	1405.26	1.57	0.02	0.02	417	1	0.50
7533705	Source rock	1461.32	1461.45	0.68	0.00	0.00	434	0	0.99
7533872	Source rock	1593.64	1593.78	0.01	0.00	0.00	379	16	0.44

[a] Total Organic Carbon
[b] Thermally extracted free hydrocarbons in the sample (mg HC/g rock)
[c] Hydrocarbon generating potential (mg HC/g rock)
[d] The temperature at the apex of the S2 peak
[e] Hydrogen index = (S2/TOC) x 100, mg HC/g TOC
[f] Production index = S1/[S1 + S2]

1.3. Aims and objectives

1.3.1. Determine the presence, abundance, and distribution of biomarkers in the drill core to gain a deeper understanding of life in deep time and reinforce the reliability of the biomarker record

Based on the current biomarker record, it is likely that bitumens and oils derived from the Cambrian samples will contain a plethora of biomarkers including steranes and hopanes produced by crown group taxa of eukaryotes and bacteria respectively (Brocks et al. 2016, 2017, 2018; Vinnichenko et al. 2020). It is very unlikely that the Proterozoic samples will contain any eukaryote biomarkers since the

Proterozoic marine ecosystems were dominated by bacteria with very little evidence of eukaryote activity (Brocks et al. 2005, 2016, 2017, 2018; Butterfield 2017; Porter 2020). Subsequently, we expect Proterozoic samples to potentially yield bacterial biomarkers such as hopanes and trimethyl aryl isoprenoids and only trace amounts (if any) of eukaryotic steranes. (Brocks et al. 2016, 2017; Vinnichenko et al. 2020; Hoshino et al 2017). Currently, the oldest indigenous biomarkers are from the 1.73 Ga Wollogorang formation in the southern McArthur Basin (Vinnichenko et al. 2020). In the study conducted by Vinnichenko et al. (2020), "Acyclic isoprenoids, saturated carotenoid derivatives, bacterial hopanes and aromatic hopanoids and steroids" were all below detection limits (Vinnichenko et al. 2020, p. 544). However, the study identified trimethyl aryl isoprenoids which are attributed to green and purple sulfur bacteria (Brocks and Schaeffer 2008; Jarret et al. 2019a) and represent the oldest indigenous biomarkers to date. We will attempt to identify these molecules in the Carrara 1 drill core to provide further evidence for signatures of life during the Paleoproterozoic.

1.3.2. Estimate the thermal maturity of Carrara 1 source rocks and oil stains to determine the extent of hydrocarbon generation and oil migration

There are numerous, well-established molecular methods used to determine the thermal maturity of a source rock (Peters et al. 2005). The most successful methods analyse the ratios of different isomers of the same molecule which are stable under different thermal conditions, and mathematically correlate these ratios to vitrinite reflectance (R_0) (Hackley et al. 2013; Peters et al. 2005). Vitrinite reflectance is a method that measures the amount of light reflected of a polished surface of vitrinite and can provide an accurate assessment of thermal maturity (Mukhopadhyay 1994; Senftle & Landis 1991). Vitrinite is an organic maceral derived from lignin and cellulose of modern vascular plants and it becomes more reflective as a function of thermal exposure (Mukhopadhyay 1994). However, since it originates in vascular plants, vitrinite is not found in sediments older than 420 Ma, when vascular plants first appear, and other methods are required to determine thermal maturity of ancient sediment (George & Ahmed 2002). The saturated and aromatic biomarkers used to approximate thermal maturity can be distinguished based on their ability to withstand varying degrees of thermal degradation (Peters et al. 2005). For example, some sterane indicators provide useful information for samples that range from immature to mature but cannot provide any data for over-mature rocks since most sterane isomers reach equilibrium and stabilise or, in very over-mature rocks, are destroyed altogether (Peters et al. 2005). This study will examine the abundance and distribution of the phenanthrene molecule and its alkylated isomers, 2, 3, 9 and 1-methylphenanthrenes to estimate the thermal maturity of the Carrara 1 drill core. Thermal maturity approximations based on phenanthrenes and methylphenanthrenes can also provide important data to determine the consistency of a drill core, the presence of unconformities, volcanic intrusions, burial history, and oil migration events (Alalade 2013;

Petmecky 1999; Stewart et al. 2005). Since thermal maturity is an important parameter to consider when attempting to estimate the generative potential of a source rock, it is of great importance to organisations and industry concerned with oil and gas exploration.

2: Literature review

2.1. Biomarkers

The Cambrian period is characterised by the appearance of life with hard parts like armour, spines, and teeth (Briggs & Derek 2015). As the fossil record clearly illustrates, these lifeforms are more likely to fossilise and the diversity and abundance of life during the Cambrian and periods thereafter can be generally well understood via the fossil record (Briggs & Derek 2015; Butterfield 2003). It is still possible, as we move backward in time, to find fossil evidence of life, for example, the Ediacaran period is home to an obscure and intriguing collection of lifeforms (Bobrovskiy et al. 2018). Ediacaran biota were soft bodied organisms of which at least some represent the earliest known metazoan animals (Bobrovskiy et al. 2018). It is also characterised by Ediacaran style preservation whereby the fossil protrudes from the bedding surface in a positive epirelief type fossil (Kerber et al. 2021). This rare type of fossilisation is an exception in the fossil record and is likely related to clay mineral authigenesis allowing the soft bodies of Ediacaran biota to become fossilised (Kerber et al. 2021). As we step further back in time, before the emergence of animals and large body plans, fossils become scarce (Butterfield 2013). Organic walled microfossils representing the remains of bacteria and early eukaryotes can be identified in diagenic chert or flattened remains of shale (Woltz et al. 2021) providing valuable insights into first appearance of eukaryotes in the fossil record (Miao et al. 2020) and changes in the abundance and diversity of bacteria and eukaryotes throughout the Proterozoic (Budd and Mann 2018; Knoll et al. 2006; Porter 2020). However, microfossils alone are not sufficient to accurately report Proterozoic ecosystems and biology (Porter 2020; Summons et al. 2021). In addition, the fossil record is prone to taphonomic bias, severely limiting the apparent diversity of biology in a given sediment and even under perfect conditions, it is extremely unlikely that cells without hard coverings will be preserved (Butterfield 2014). It can also be extremely difficult to properly assign fossils to a group or domain (Butterfield 2014). For example, it is common practice to assign cells larger than 60μm to the eukarya domain, but there are several species of bacteria that can reach this size, e.g., chroococcacean cyanobacteria (Butterfield 2014).

Biomarkers have been used since the 1970's to assess the organic matter content of rocks and oils as an alternative and complimentary analysis to microfossils (Brocks et al. 2008). They can be of particular importance when analysing Proterozoic sediments where physical fossils become rare (Brocks et al. 2008; Vinnichenko et al. 2020). Biomarkers are complex organic molecules composed of carbon, hydrogen and other elements that are derived from once living organisms (Peters et al. 2005). Biomarkers are distinct and more informative than other products of diagenetic processes i.e., methane, because (i) they are composed of repeating sub-units indicating that they were derived form once living organisms, (ii) the parent molecule of which the biomarker is derived can be attributed to a specific organism or group of organisms, and (iii)

the carbon backbone of the biomarker is stable during sedimentation and burial (Peters et al. 2005). Biomarkers show varying degrees of biological and environmental specificity and analysis which identifies and quantifies their abundance and diversity can be extremely informative for understanding biological communities and environments on the early Earth (Eigenbrode 2011; Peters et al. 2005). For example, steranes are a group of biomarkers that have been analysed extensively. Steranes are derived from parent lipids called sterols, produced in the cell membrane of most modern eukaryotes and a small number of bacteria who attained the ability to produce sterols via horizontal gene transfer, gene loss and gene gain (Hei et al. 2016; Pierce et al. 2003; Wei et al. 2016; Welander 2019). Using methods such as GC/MS, steranes can be identified in sediments and quantified to provide estimates of the abundance of sterol synthesising organisms (Anbar & Knoll 2002; Peters et al. 2005).

However, biomarkers are not without their limitations. First, biomarkers are prone to taphonomic bias. This is particularly a challenge when analysing sediments from the Proterozoic due to a phenomenon called the "mat-seal effect" (Pawlowska et al. 2013). Without bioturbation from grazing and burrowing animals, (which appear in the Ediacaran period) (Bobrovskiy et al. 2019), benthic microbial mats are free to form thick cohesive structures that have semi-impermeable internal layers (Des marais 1995; Pawlowska et al. 2013). When phytoplankton die and fall through the water column towards the seafloor, benthic mats create a physical barrier which catch the dead plankton before they reach the sediment, inhibiting burial and subsequent digenic processes that are required for biomarker formation (Pawlowska et al. 2013). Additionally, the mats create a chemical barrier for phytoplankton as they sink towards the ocean floor. The combination of microbial activities in the mat result in fluctuating redox gradients which enables a plethora of lipid degrading pathways as plankton land on the mat (Pawlowska et al. 2013). Studies have shown that depending on the type of microbial mat, lipids can degrade some 57-97% in the top 2 cm of the mat (Jahnke et al. 2004; Wieland et al. 2008). This process severely biases the preservation of biomarkers to those originating from the microbial mat community while excluding plankton derived biomarkers (mostly steranes) (Pawlowska et al. 2013).

The taphonomic consequences of the mat-seal effect are nicely illustrated in results from GC/MS analysis of sediments covering the Proterozoic-Ediacaran transition (Pawlowska et al. 2013). Proterozoic sediments are characterised by a large unresolved complex mixture (UCM), a high concentration of monomethyl alkanes (MMA) and dimethyl alkanes (DMA) and either noticeably high or low concentrations of isoprenoids such as pristane and phytane compared to Phanerozoic oils and sediments (Pawlowska et al. 2013). These characteristic features of Proterozoic sediments are likely the consequence of the bias of input and burial of organic matter due to the mat-seal effect (e.g., Pawlowska et al. 2013). The mat-seal effect illustrates that unlike their Phanerozoic counterparts, Proterozoic sediments are dominated by input from benthic mats and might exclude planktonic organic matter. The potential for taphonomic bias, especially

when quantifying biomarkers from the Proterozoic, must be considered and used in parallel with other methods to track evolutionary history in deep time.

Unlike the fossil record, biomarker data can be distorted and in extreme cases, completely lost due to anthropogenic contamination (Brocks 2011). These contaminants can be introduced during sample collection in the form of drilling fluids and diesel which may contain Phanerozoic hydrocarbons (Brocks 2011; French 2015; Hallman et al. 2011). They can also be introduced in the lab environment or during storage where hydrocarbons in the air, from people's skin, and from polyethylene plastic bags can contaminate a sample with a huge range of modern hydrocarbons (Brocks 2011; Brocks et al. 2008). When a sample becomes contaminated, indigenous biomarkers can become overprinted by contaminants affecting their abundance making it difficult to discern between autochthonous and allochthonous biomarkers during analysis (Brocks et al. 2008; Hallman et al. 2011). As the source and severity of contamination has been realised over the last decade, several procedures have been developed to decrease the risk of contamination and to remove contaminated material before analysis (Brocks 2011; Brocks et al. 2008). In the Brocks laboratory at the Australian National University, it is now common practice to remove the exterior portion of a sample before crushing to remove any surficial contaminants (Brocks et al. 2008). By removing the exterior and analysing it separately to the interior, exterior/interior experiments can be run to determine the extent of contamination and indicate sections where overprinting might have occurred (e.g., see Brocks et al. 2008). Though removing the exterior can dramatically decrease the severity of contamination, the interior of the rock can still be affected (Brocks 2011). Petroleum contaminants can permeate centimetres deep into rock samples after just several hours leaving the interior sections of the sample contaminated (Brocks 2011). Interestingly, heavier hydrocarbons take longer to pervade through the rock compared to smaller and lighter molecules which adds an extra dimension to exterior/interior experiments. For example, if the ratio of *n*-alkanes in the exterior/interior increased as a function of mass, the sample is almost certainly contaminated since, lighter molecules will more easily permeate a sample compared to larger molecules (Brocks 2011). Many organic geochemical laboratories now run a sand blank in parallel with the samples to control for laboratory contamination (Brocks et al. 2008; Brocks 2011). The blank undergoes the same laboratory processes and procedures as the actual samples which means that any contamination from the laboratory can be easily identified in the blank and necessary actions can be taken to either re-run the samples after removing the contaminant from the laboratory, subtract the concentration of the blank from the affect sample or removing the affected data from the study (Brocks et al. 2008).

2.2. Early life

Eukaryotes comprise the domain of life characterised by the presence of a nucleus and complex morphological traits (Martin 1977; Woese et al. 1990). Their existence is one of the most profound features

of planet Earth and their emergence likely represents the greatest shift in the Earth's biosphere in its 4.6-billion-year (Ga) history (Brocks et al. 2015; Butterfield 2015). When we consider the diversity of life on Earth today, we note a huge range of eukaryotes from animals to fungi that have been extremely successful during the Phanerozoic (Butterfield 2015). However, crown group eukarya only diversified c.a. 800 Ma (Brocks et al. 2017, Brocks et al. 2015; Porter 2020). They were preceded by a plethora of microscopic eukaryotes including chlorophyte and rhodophyte algae, which represent the earliest known crown-group eukaryotes c.a. 1050 million years ago (Ma) (Brocks et al. 2017). While there were eukaryotes that existed before 1050 Ma, they are enigmatic, and it is unclear if they belong to crown or stem-group eukaryotes, which are the organisms that existed between the First Eukaryote Common Ancestor (FECA) and the Last Eukaryote Common Ancestor (LECA). Despite the difficulty of analysing life in deep time, various studies have utilised a variety of geochemical, biochemical, and paleontological techniques to constrain the emergence of LECA and begin to probe into history of the eukaryote domain (Porter 2020).

The microfossil record indicates that the earliest crown group eukaryote was a rhodophyte alga called *Bangiomorphia pubescens* and it is thought to have lived 1.05 Ga (Butterfield et al. 1990; Gibson et al. 2018). However, this designation has been challenged over the years due recent evidence that suggests the morphological features observed in *B. pubescens* used to assign it to crown group eukaryotes could have evolved several times independently in other crown and stem group eukaryotes (Yang et al. 2016). Subsequently, some argue that *B. pubescens* existed before the divergence of LECA and is thus a stem group eukaryote (Chernikova et al. 2011; Porter 2020). Molecular clocks indicate that LECA appeared between 800-1800 Ma. This huge range is due to uncertainties originating in the fossil record, including the characterisation of *B. pubescens* (Porter 2020). The molecular clocks that include *B. pubescens* generally suggest an earlier emergence of LECA while those that omit *B. pubescens* argue that it was later (Porter 2021). This represents a huge gap in our understanding of eukaryote evolution but also the broader evolution of life on Earth (Butterfield 2015; Hallmann et al. 2011).

Eukaryotes are just one of the three domains of life, and this report will also investigate the presence of bacteria in the sediments of Carrara 1. Bacteria are likely the earliest representatives of life on Earth and were dominant in the oceans of the early Earth before the appearance of eukaryotes (Blumenber et al 2012; Brocks et al. 2005; Brocks et al. 2017; Vinnichenko et al 2020). There is strong evidence of bacteria during the Archean period as early as 3.5 billion years ago from the North Pole Dome in Western Australia in the form of fossilised stromatolite structures which are the result of bacterial mats being deposited, one on top of the next to create large domes of captured sediment (Fournier et al. 2021; Walter et al. 1980). However, not all bacteria produce structures like stromatolites that can be preserved in the fossil record, making their evolutionary history more obscure. Biomarkers provide an avenue to examine life in deep time since biomarkers are not biased towards soft and hard bodied organisms and are more easily assigned to a

particular group of organisms compared to ancient microfossils (Vinnichenko et al. 2020). However, there are very few geological basins in the world that still contain Paleoproterozoic rocks (1600-2500 Ma) and only one that contains indigenous biomarkers (For a summary, see Vinnichenko et al. 2020). Furthermore, as biomarkers are buried and exposed to heat and pressure, they begin to break down. Even a relatively small amount of burial metamorphism can completely destroy biomarkers (French et al. 2015) making the preservation of Mid-Proterozoic (1800-800 Ma) biomarkers even more difficult. Since the Carrara 1 drill core contains Paleoproterozoic rocks, there is a chance that it will contain indigenous biomarkers from this period adding valuable data to the extremely scarce Paleoproterozoic biomarker record helping us to uncover the history of life in deep time.

2.3. Thermal maturity and generative potential

The thermal maturity of a source rock is a crucial parameter to be considered in geobiological analysis since the extent of burial metamorphosis can severely impact the abundance of biomarkers (French et al. 2015). In addition, the thermal maturity measurement can provide information regarding the extent to which a source rock has generated hydrocarbons and help constrain the age of sediments (Farrimond et al. 1998; Peters et al. 2012; Tissot & Welte 1984). Thermal maturity indicates the extent of heat driven reactions experienced by the source rock as a function of pressure and time (Peters et al. 2012). Heat driven reactions change the organic content of the rock and thus the potential for hydrocarbon formation including oil, gas, and biomarkers (Peters et al. 2012). Thermal maturity estimations are especially useful to determine hydrocarbon potential when considered in parallel with Rock-Eval pyrolysis data. This is because it is often a combination of maturity and generative potential (indicated by Rock-Eval) that will ultimately lead to hydrocarbon generation. Rock-Eval for NDI Carrara 1 was performed by Grosjean et al. (2022) and is summarised in Table 1 of the present study. Parameters of particular interest for hydrocarbon generation are the hydrogen index (HI) and total organic carbon (TOC) (Table 1).

The earliest stages of thermal maturation generally termed ‘immature’, represent organic material such as bacterial and algal debris which has undergone diagenesis (reorganisation and polymerisation) but has not been affected by high temperatures. These processes lead to the formation of bitumen and a macromolecular network called kerogen (Peters et al. 2005). Kerogen is the most important source of organic carbon in sedimentary rocks and is divided into four groups (Type I, II, III and IV) based on chemical composition (Dow 1997; Wood & Hazra 2017). Kerogen is a necessary precursor from which oil and eventually gas will form but an immature source rock that only contains kerogen is practically worthless for those in oil and gas exploration (Peters et al. 2005). Further, kerogen is insoluble in organic solvents and therefore, biomarkers that might be present in the kerogen matrix cannot be analysed using

solvent extraction techniques. In immature samples, the more soluble bitumen provides the only source of free molecules that can be analysed. The second stage of thermal maturity represents mature organic matter where temperatures are high enough for catagenesis to begin (Selley 1998). During catagenesis, material becomes thermally altered and kerogen begins to 'crack' releasing molecules and forming oil (Peters et al. 2012; Selley 1998). Catagenesis begins to occur around 60°C and oil formation peaks at 120°C, therefore, source rocks and crude oil of this thermally maturity are ideal for molecular analysis and oil exploration (Peters et al. 2005). Finally, 'over-maturation' of source rocks begins to occur at yet higher temperatures (~ 200°C) where catagenesis melds into another process called metagenesis. At this temperature, the kerogen has yielded all possible petroleum and gas begins to form via three main routes summarised by Peters (2005).

1. 'Cracking' of highly mature organic material,
2. Decomposition of oil in petroleum source rocks, and
3. Secondary cracking of oil in reservoir rocks

Therefore, mature material is an essential component for natural gas exploration, however, overmature rocks are of limited use in understanding early life on Earth. Once samples reach the late oil window, most biomarkers are diminished or completely destroyed due to their instability under these high temperatures (Peters et al. 2005). Due to the importance of thermal maturity of source rocks for molecular analysis, geobiology and oil and gas exploration, it is imperative to have some indicator of thermal maturity (Boreham et al. 1988). There are several techniques that can be utilised to accurately determine the thermal maturity of source rock. The most commonly applied method is called vitrinite reflectance ($R_{V\,max}$% or R_0%) (Hackley et al. 2013; Tissot and Welte 1984). R_0 is determined by measuring the percentage of light reflected off a polished vitrinite surface of an organic rock (Hackley et al. 2013; Peters et al. 2005). The percentage of light reflected increases with thermal exposure (temperature plus time) at a known rate for each kerogen type and can therefore provide accurate estimations of the thermal maturity of a source rock (Kim 2011; Mukhopadhyay 1994). However, R_0 analysis has several limitations. It has been experimentally illustrated that there is natural variance and analytical uncertainties associated with the R_0 at any given locality (Katz and Lin 2021; Mukhopadhyay 1994; Bostick and Foster 1975). In addition, it is standard practice to report R_0 as an absolute value without the associated error and without considering the geological context and it would be more accurate to report R_0 as a trend rather than as discrete values (Katz and Lin 2021). Moreover, there is a significant difference between R_0 of whole rock samples and isolated kerogen analysis. This difference is not trivial and shifts the final interpretation of hydrocarbon phase boundaries (Katz and Lin 2021). Finally, vitrinite is derived from lignin and cellulose of modern plants and is therefore only applicable to rocks younger than 420 Ma (George & Ahmed; Mukhopadhyay 1994; Senftle & Landis 1991). Different phases of organic matter in older sedimentary

rocks will show different reflectance behaviour with maturation, thus deviating from the traditional R_0 scale.

As introduced in section 1.3.2, biomarkers are heavily relied upon to estimate thermal maturity and are generally considered to be a more reliable proxy for thermal maturity then vitrinite reflectance, especially for moderately mature samples where the bitumen content is high (Hackley et al 2013; Wood and Hazra 2017). The isomerisation of biomarker molecules is the main way that they can be used to estimate maturity. Certain biomarker isomers will be more thermally stable than others due to steric hindrance. This means that more sterically hindered isomers will decrease as a function of time relative to more stable isomers (He et al. 2019). Though saturated biomarkers can provide good estimates of thermal maturity, especially in less mature rocks, this study will use aromatic biomarkers exclusively due to their stability at high maturity (He et al. 2019; Welte & Tissot 1984). Thermal maturity is most commonly estimated using aromatic biomarkers by comparing the concentration of isomers that have different thermal stabilities based on methylation patterns and the number of aromatic rings (Brocks et al. 2003a; George 1992; He et al. 2019). For example, the abundance of phenanthrene (P) and its methylated isomers 3, 2, 9 and 1 methylphenanthrene (MP) can be quantified to estimate thermal maturity. Due to the stereochemistry of the MP molecule, 3-MP and 2-MP are thermally less stable than the 9-MP and 1-MP and their abundance will decrease as a function of heating as they are demethylated into P. With high thermal maturity, demethylation of the 9 MP and 1 MP isomers will also occur. Subsequently, the ratio of P/MP will generally increase with thermal maturity (Boreham et al. 1988; Brocks et al. 2003a). By using these thermal properties of P and MP, several maturity parameters have been developed. These include the methylphenanthrene index (MPI) (equation 1), the methylphenanthrene distribution factor (MPDF) (Radke & Welte 1983) (equation 2) and the methylphenanthrene ration (MPR) (Radke et al. 1984) (equation 3).

$$MPI = 1.5 \times \frac{2MP + 3MP}{P + 1MP + 9MP} \quad (1)$$

$$MPDF = \frac{2MP + 3MP}{2MP + 3MP + 1MP + 9MP} \quad (2)$$

$$MPR = \frac{2MP}{1MP} \quad (3)$$

Despite the accuracy of biomarkers as indicators of thermal maturity, they have their limitations. Firstly, studies suggest that organic matter input and biodegradation can affect the ratios and subsequently the measure of thermal maturity (Peters et al. 2005). More recently, there is evidence that high

concentrations of sulphur can enhance the isomerisation of steranes and homohopanes affecting the apparent thermal maturity (Wood & Hazra 2017). For example, Sun et al. (2016) analysed the geochemical properties of two stratigraphic units from the Late Cretaceous from South Texas, USA. Analysis of homohopanes and steranes indicate that the lower unit has a higher thermal maturity than the upper unit, while an overwhelming number of other hopanes and aromatic biomarkers suggest the opposite. The lower unit has very high concentrations of sulphur (up to 2.6%) and the researchers suggest that this decreases the time required for isomerisation to occur in the homohopanes and steranes, which subsequently provides an apparent higher thermal maturity.

3: Materials and Methods

3.2. Methodology

This section outlines the methods used to analyse the source rocks of Carrara 1 at the Brocks laboratory at the Australian National University. The oil stains were sampled and prepared at Geoscience Australia and the methodology for these is provided in Grosjean et al. (2022).

3.2.1. Contamination control experiments

There are several protocols described in detail by Brocks et al. (2017) which decrease the risk of contamination in biomarker analysis that were priorities throughout this study. Initially, 12 sand blanks were run which captured all steps and procedures from rock crushing to fractionation to assess the level of potential contaminants in the laboratory environment. Generally, the abundance of biomarkers in these blanks were below detection limits. It is now well understood that contaminants are also introduced during sample collection and storage (Brocks et al. 2008) and that the contaminants can diffuse into the surface of the rock via diffusion as discussed in detail by Brocks (2011). To remove any contaminants on and in the surface layers of the samples, approximately 3 mm of the outer surface of each rock specimen were removed using a wet solvent-cleaned Table saw (Nortel Machinery Inc.). The exterior (E) portion that was removed was set aside and analysed to determine the extent of contamination via E/I experiments (See section 4.1 in Chapter 4). The interior and exterior slices were then transferred to separate glass jars that had been baked at 300°C for 9 hours to remove contaminants and stored in the drying oven overnight to ensure any residual water was evaporated.

3.2.2 Rock powder preparation and bitumen extraction

The interior (I) and exterior (E) components were crushed into a fine grit using a solvent cleaned puck mill (Rocklabs) for 45 seconds each. The dry powder was transferred to metal bomb cells and loaded into the Dionex Accelerated Solvent Extractor (ASE 200) and run using method 3 (at 1000 PSI at 100°C) using 90% DCM and 10% methanol. The solvent was transferred to the TurboVap and reduced under a constant stream of N_2 gas at 45°C until they were dry. Using a glass pipette, ~ 2 ml of DCM was added to the cells and mixed by continually moving the solvent in and out of the pipette. Once the solvent was mixed well with the organics, the solution was transferred to 4 mL vials and reduced to ≈ 100 µl under a constant

stream of N_2 gas. Using the same mixing method described above, the organic solution was transferred to open columns (pasteur pipettes) filled with baked silica gel and left overnight.

3.2.3 Fractionation

2 ml vials with neck inserts were prepared and the following standards were added to the corresponding vials: for saturated hydrocarbons, 25 ng of D4 (10 μL) and 150 ng D10 pyrene (6 μL) were added, and for aromatic hydrocarbons, 150 ng D10 pyrene (6 μL) were added. These were put aside to air dry. By eluting the columns, the organic molecules in solution could be separated into individual 4 ml vials. Saturated hydrocarbons were eluted using 2 ml of n-hexane, aromatic hydrocarbons were eluted with 4 ml of n-hexane:DCM in a 1:1 ratio and polar compounds with 2 ml of DCM:methanol in a 1:1 ratio. (The DCM was added first since it is less dense to ensure proper mixing). The polar fractions weren't useful for the purposes of this study and were stored from this point forward. The 4 ml vials with the saturated and aromatic hydrocarbons were reduced using a light stream of N_2. This step was performed under constant supervision so the flow of N_2 could be cut off in time to prevent any organic material evaporating. The point that N_2 flow was stopped was dependent on the class of molecules. The saturated hydrocarbons were blown down until only a thin disc of liquid was present and the aromatic hydrocarbons were blown dry. A small amount of n-hexane was then added to the vials and mixed. The solution was transferred to the 2 ml vials prepared earlier with the standards.

3.2.4. GC/MS analysis

Gas Chromatography/Mass Spectrometry (GC/MS) analysis was undertaken using an Agilent 6890 GC coupled to a Micromass Autospec Premier double sector MS. The GC, as outlined in Brocks et al. (2017) "was equipped with a 60 m DB-5 capillary column (0.25 mm i.d., 0.25 μm film thickness; Agilent JW Scientific, Agilent Technologies), and helium was used as the carrier gas at a constant flow of 1 ml min^{-1}. Samples were injected in splitless mode into a Gerstel PTV injector at 60 °C (held for 0.1 min) and heated at 260 °C min^{-1} to 300 °C. The MS source was operated at 260 °C in electron ionization mode at 70 eV ionization energy and 8,000 V acceleration voltage. The GC oven was programmed from 60 °C (held for 4 min) to 315 °C at 4 °C min^{-1}, with a total run time of 100 min" (Brocks et al. 2017, p 582). Acyclic saturated hydrocarbons, and aromatic hydrocarbons were quantified using full scan Total Ion Current (TIC) analysis and saturated steranes, hopanes, tricyclic terpanes and trimethyl aryl isoprenoids were quantified using Metastable Reaction Monitoring (MRM).

4: Results

4.1 Syngeneity of biomarkers

A major challenge when interpreting the presence of biomarkers is determining if they are indigenous molecules or contaminants introduced during collection, storage, or analysis (Brocks 2011; Brocks et al. 2008). Most biomarkers were below detection limits in the four cumulative system blanks run in unison with the four sets of samples (Cambrian saturate and aromatic fraction and Proterozoic saturate and aromatic fraction) indicating that there was no major contamination introduced in the laboratory environment (Brocks et al. 2008). To confirm that the few contaminants detected in the blanks weren't responsible for the peaks measured in the samples, extract/blank (E/B) values were calculated based on the absolute concentrations of biomarkers in nanograms per gram of rock (ng/g) using equation 4 (Brocks et al. 2008; Jarret et al. 2013).

$$\frac{E}{B} = \frac{((A_{BM}/A_{std})\times M_{std})}{((A_B/A_{std})\times M_{std})} \quad (4)$$

Where A is peak area, M is mass, std is the D4 or D10 standard, BM is the biomarker of interest and B is the equivalent signal in the blank.

E/B experiments quantify the concentration of individual biomarkers in the interior portion of the sample compared to the corresponding sand blank to determine the extent of laboratory contamination (Brocks et al. 2008). According to Brocks et al. (2008) biomarker ratios from samples with E/B ratio < 20 are potentially significantly affected by laboratory contamination. All quantified biomarkers from NDI Carrara 1 have an E/B value > 20 except for C_{27}-C_{34} hopanes and C_{19}-C_{26} tricyclic terpanes in the source rocks below the unconformity (Table 2). Consequently, these biomarkers are not interpreted as indigenous and are omitted from the biomarker data reported as part of present study.

Table 2 Extract/Blank (E/B) ratios for hopanes in Proterozoic source rocks of Carrara 1

Sample ID	Depth (m)	E/B C_{27}[a]	E/B C_{29}[b]	E/B C_{30}[c]	E/B C_{31}[d]	E/B C_{32}[e]
7533204	689.82	10.80	7.49	5.36	14.38	0.00
7533210	719.21	5.87	3.34	5.06	4.49	0.00
7533225	794.71	0.00	9.62	0.00	0.00	0.00
7533569	925.37	0.00	5.29	0.00	0.00	0.00
7533584	998.66	1.10	0.44	0.90	0.75	0.00
7533609	1069.16	0.00	1.01	2.54	2.20	0.00
7533625	1150.08	0.72	0.64	1.03	0.00	0.00
7533635	1199.60	1.26	1.41	2.60	3.93	0.68
7533644	1244.79	1.26	1.06	2.29	2.35	0.55
7533668	1345.03	0.90	1.16	1.06	1.86	0.00
7533682	1405.10	0.88	1.04	1.46	1.94	0.75
7533705	1461.32	0.89	0.49	1.20	1.18	0.00

[a] E/B ratio for C_{27} hopanes. Isomers include C_{27} farri, C_{27} dia, Ts, Tm and C_{27} β
[b] E/B ratio for C_{29} hopanes. Isomers include C_{28} farri, C_{28} dia, C_{28} αβ and C_{28} βα
[c] E/B ratio for C_{30} hopanes. Isomers include C_{30} farri, C_{30} dia, C_{30} αβ and C_{30} βα
[d] E/B ratio for C_{31} hopanes. Isomers include C_{31} farri, C_{31} dia, C_{31} αβ and C_{31} βα
[e] E/B ratio for C_{32} hopanes. Isomers include C_{32} farri, C_{32} dia, C_{32} αβ and C_{32} βα

To identify contaminants introduced to the rock specimens before analysis, exterior/interior (E/I) experiments were utilised. In this type of experiment, biomarkers are quantified and compared for both the exterior and interior portions of the rock specimens (Brocks 2011). Indigenous hydrocarbons will commonly have an E/I ~ 1, while contaminants have an E/I >> 1. An E/I < 1 may be the result of evaporation from surfaces (or loss from solvent cleaning of rock specimens, a practice that should be avoided) (Brocks 2011; Vinnichenko 2020). E/I ratios of indigenous biomarkers commonly deviate from unity, e.g., falling into the range ~0.3 to 5, an effect attributed to natural spatial heterogeneities of hydrocarbons within the rock (Brocks et al. 2011). Diffusion of contaminants into the interior of the rock is characterised by increasing E/I ratio as a function of molecular mass since lighter molecules with lower adsorption and evaporation energies will permeate into the rock fissures faster than larger molecules (Brocks 2011). For more information see Brocks (2011) and for an interpretation of different E/I trends, see Brocks et al. (2008). *n*-alkanes are below detection limits in most of the Proterozoic bitumens in this study (see Figure 8) and thus sample 7533204 (689.82 m) and 7533609 (925.37 m) (two of the four sample which contain *n*-alkanes), were selected for E/I experiments. As illustrated by the E/I plots (Figure 2a and 2b), both samples have E/I values at or just below 1 for all homologues. In addition, there is no clear upwards trend with carbon number indicating that there was no diffusion of *n*-alkanes from the surface into the interior. These results indicate that the samples have not been affected by contamination introduced during storage or handling and the *n*-alkanes in these samples are interpreted to be indigenous biomarkers.

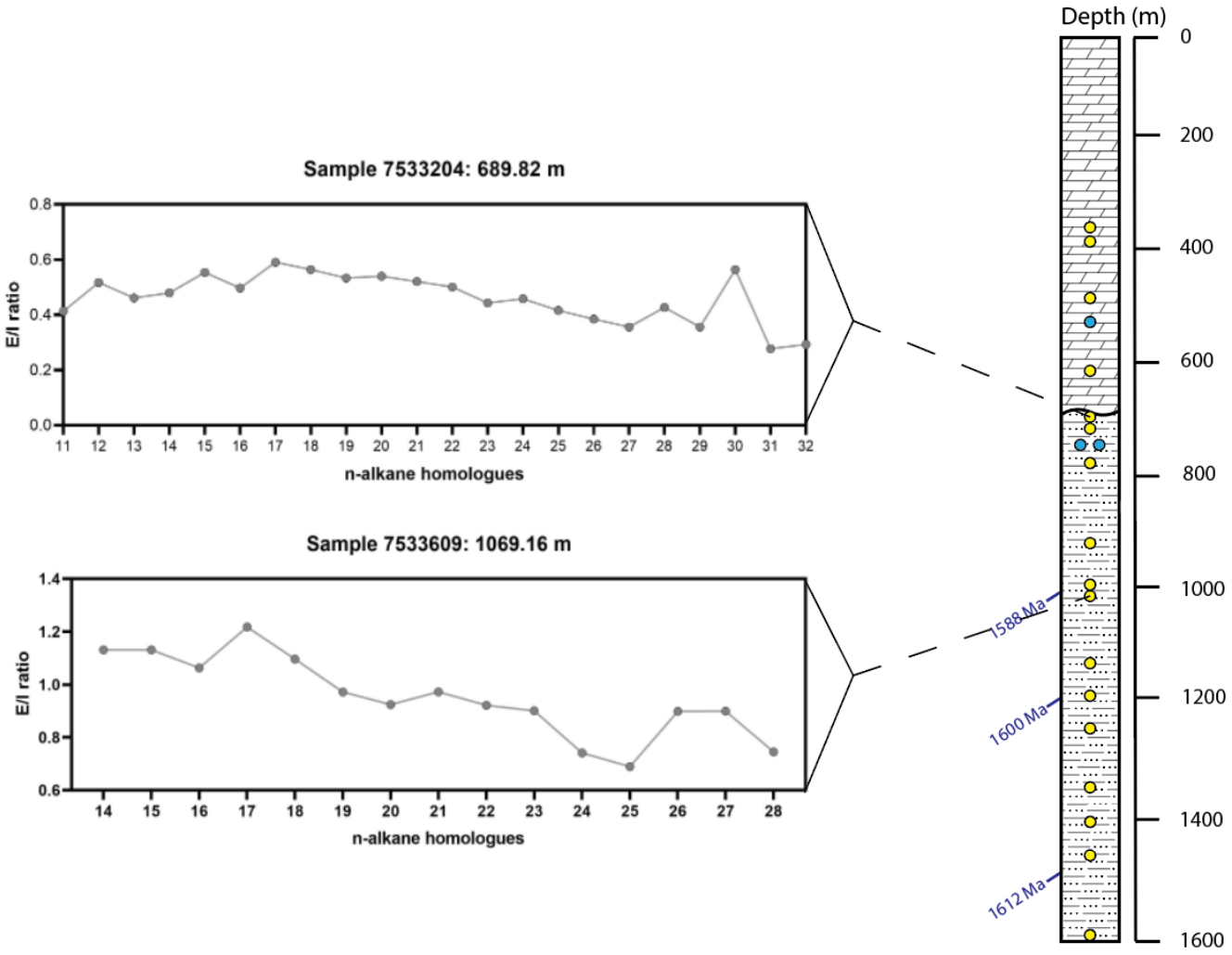

Figure 2 E/I plots for *n*-alkanes in sample 7533204 (a) and 7533609 (b) and their relative position in the Carrara 1 drill core.

Figure 3 illustrates the E/I values for the phenanthrene (P) and four methylphenanthrene (MP) molecules for samples below 790 m. E/I experiments were not conducted on source rocks and oil stains shallower than 790 m since P and MP exhibit large peak area in these bitumens and even if contamination is present, it would have little effect on these peaks. Most samples report E/I values ≤ 1 which indicates that the peaks are indigenous and not strongly affected by contamination. Sample 7533584 (998.66 m) is the only specimen with E/I values > 1 for P and MP but they still lie in a range to be considered indigenous (Brocks et al. 2011). However, this sample was closely monitored during evaluation as contamination cannot be completely ruled out. Therefore, all the P and MP in the bitumens of Carrara 1 are interpreted as indigenous and can be used to evaluate thermal maturity. It is important to note, however, that some of the deeper samples, especially 7533609 (1069.16 m), exhibit strongly fluctuating values across the isomers. This is most likely due to integration error effects since the abundance of these molecules are close to detection limits and there is a greater chance that co-eluting peaks might affect the peak areas.

(a)

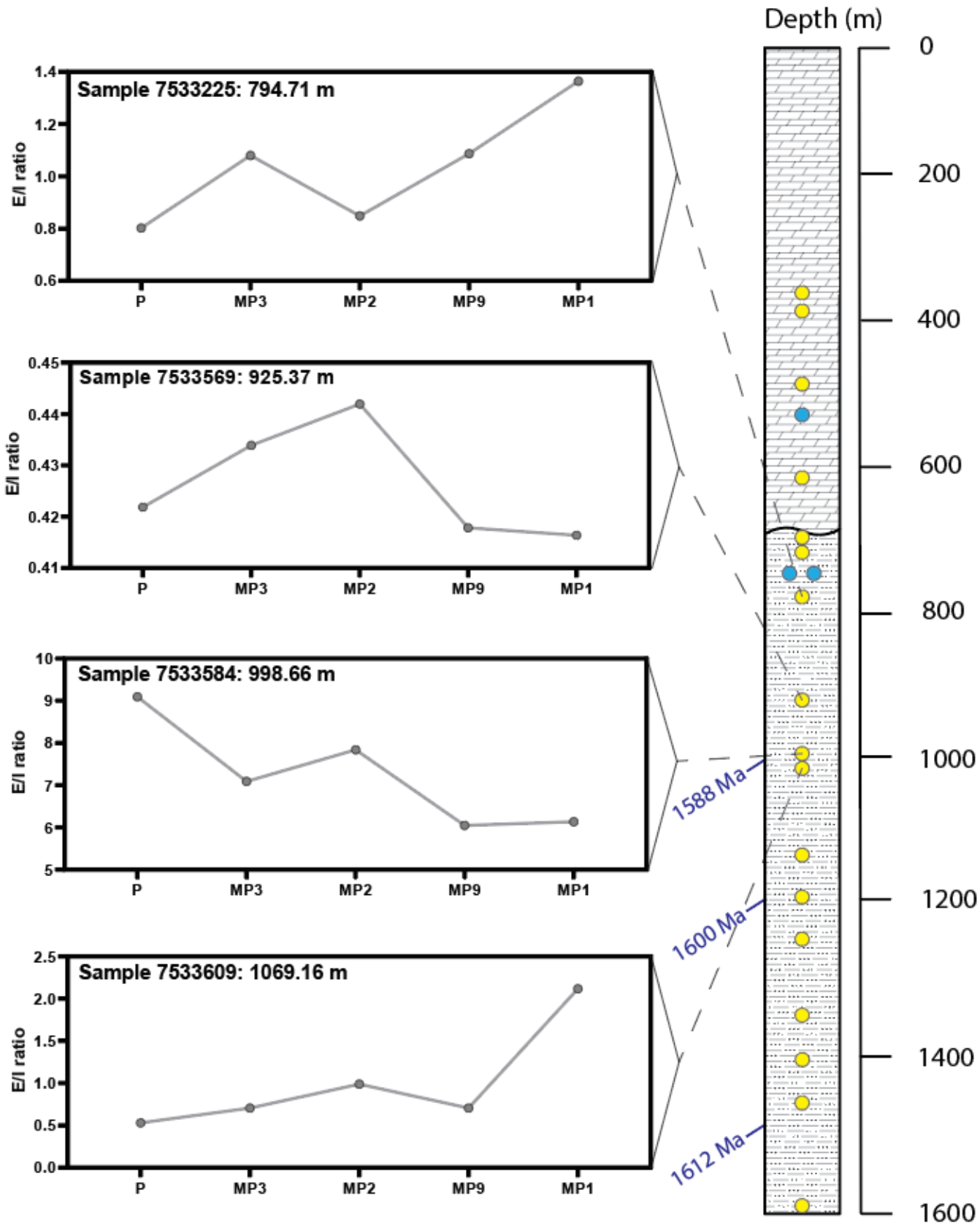
Depth (m)
0
200
400
600
800
1000
1200
1400
1600
Sample 7533225: 794.71 m
E/I ratio
1.4
1.2
1.0
0.8
0.6
P
MP3
MP2
MP9
MP1
Sample 7533569: 925.37 m
E/I ratio
0.45
0.44
0.43
0.42
0.41
P
MP3
MP2
MP9
MP1
Sample 7533584: 998.66 m
E/I ratio
10
9
8
7
6
5
P
MP3
MP2
MP9
MP1
1588 Ma
Sample 7533609: 1069.16 m
E/I ratio
2.5
2.0
1.5
1.0
0.5
0.0
P
MP3
MP2
MP9
MP1
1600 Ma
1612 Ma

(b)

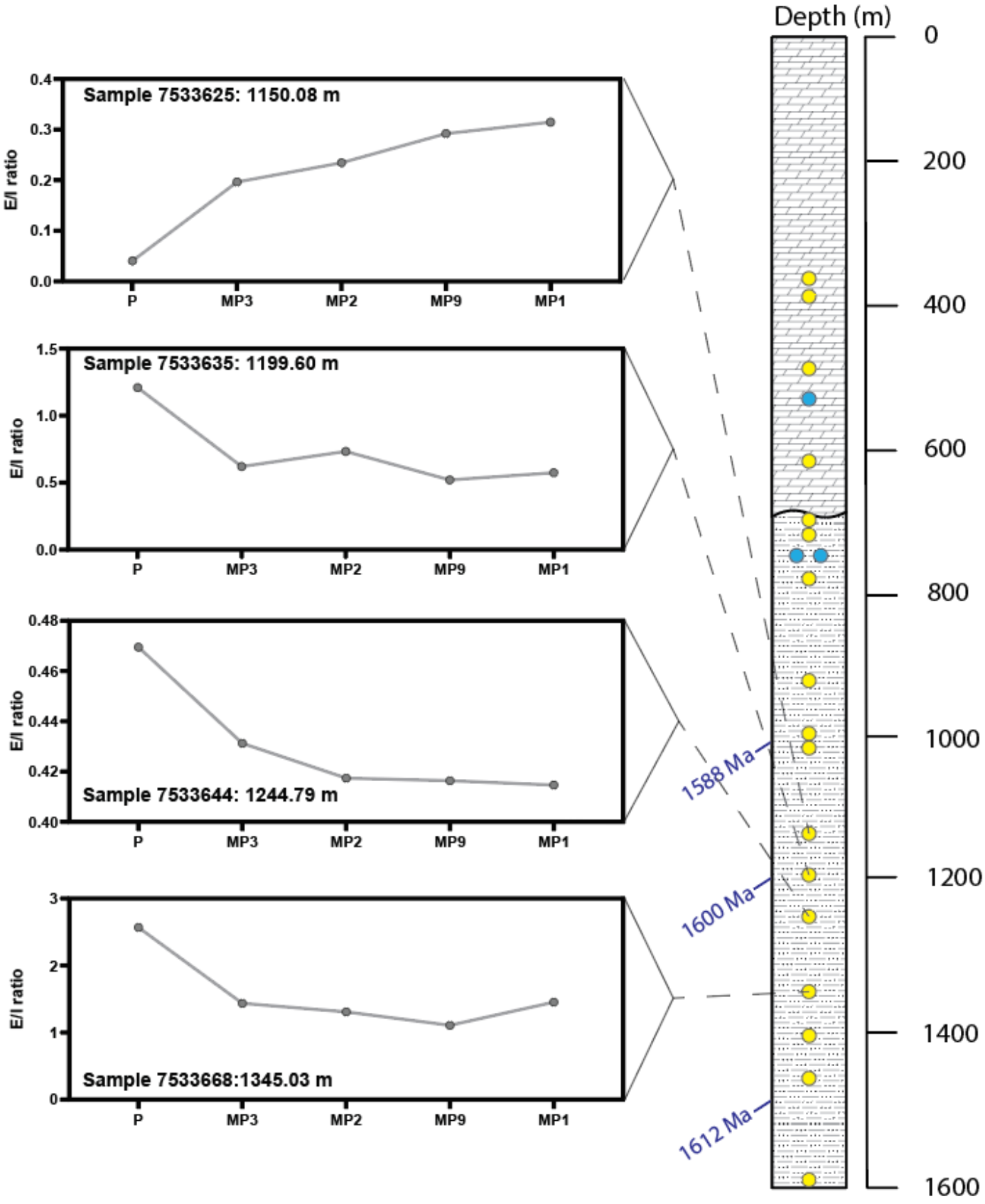
Depth (m)
0
200
400
600
800
1000
1200
1400
1600
Sample 7533625: 1150.08 m
E/I ratio
0.4
0.3
0.2
0.1
0.0
P
MP3
MP2
MP9
MP1
Sample 7533635: 1199.60 m
E/I ratio
1.5
1.0
0.5
0.0
P
MP3
MP2
MP9
MP1
Sample 7533644: 1244.79 m
E/I ratio
0.48
0.46
0.44
0.42
0.40
P
MP3
MP2
MP9
MP1
Sample 7533668:1345.03 m
E/I ratio
3
2
1
0
P
MP3
MP2
MP9
MP1
1588 Ma
1600 Ma
1612 Ma

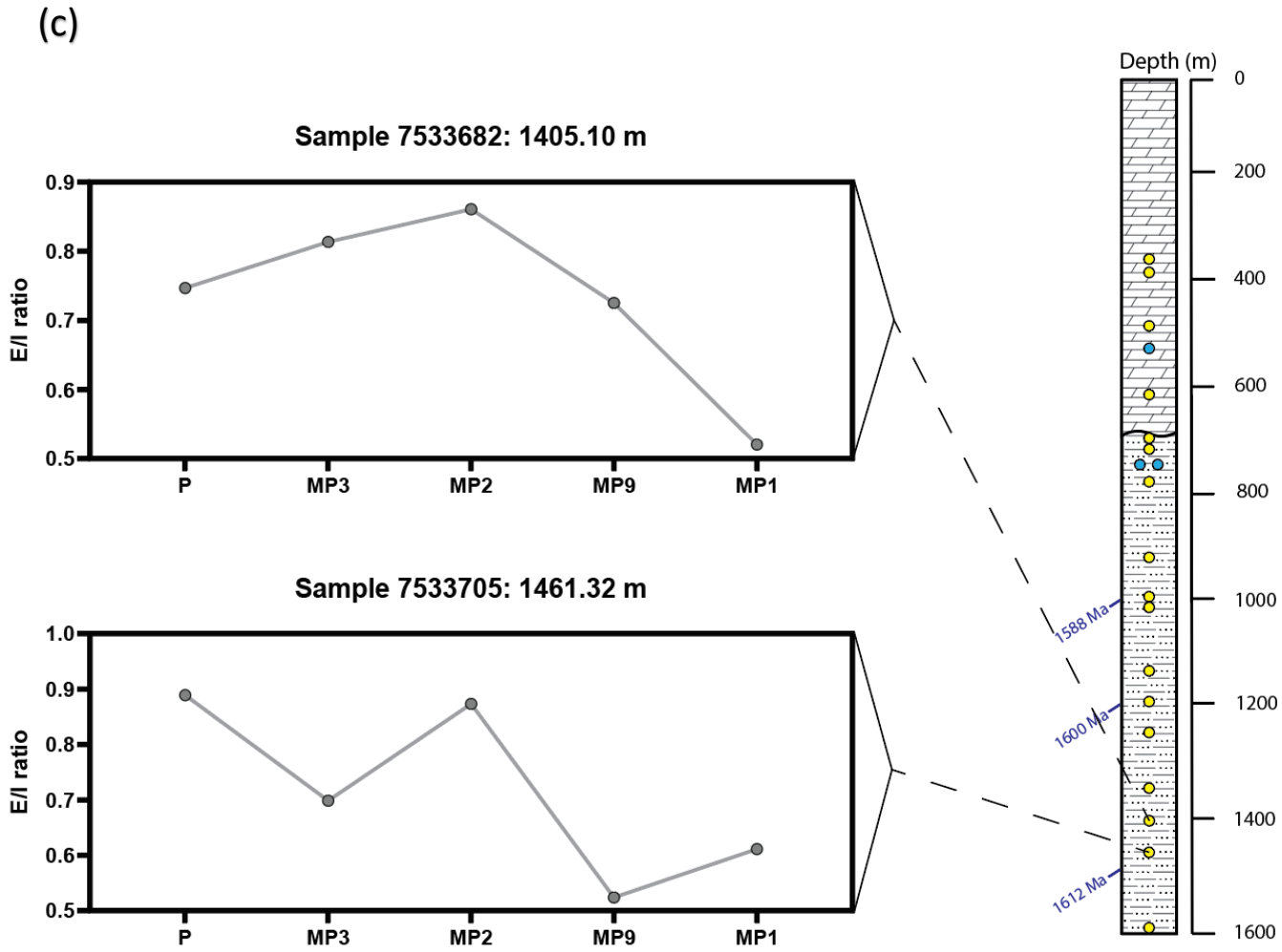

Figure 3 E/I plots for phenanthrenes and methylphenanthrenes for all samples below 790 m and their relative position in the Carrara 1 drill core.

4.2 Distribution of biomarkers

4.2.1. Acyclic saturated hydrocarbons

Full scan total ion currents (TIC) of acyclic saturated hydrocarbons are illustrated in Figure 8. *N*-alkanes are detected in all the Cambrian samples and five of the Proterozoic samples between 689 – 925 m below which they fall beneath detection limits with the notable exception of sample 7533609 (1069.16 m) which shows high concentrations of acyclic saturated hydrocarbons starkly contrasting their absence in overlying and underlying samples (Figure 8). The Cambrian source rocks, and oil stains have a maximum at either C_{17} or C_{19} and Proterozoic samples at C_{14} or C_{13} (Table 3). To determine the predominance of either odd or even *n*-alkanes, three Carbon Preference Index (CPI) parameters were calculated for each sample (Table 3). For the carbon number range C_{23}-C_{28}, the samples had a CPI from 0.99-1.16 indicating that while there might be a very slight odd over/even predominance, there is generally no preference (Marzi et al. 1993) (Table 3).

CPI1 provides the carbon preference for short chain *n*-alkanes from C_{14} – C_{22}. All of the Cambrian samples have CPI1 value > 1 (1.13-1.46) reflecting a slight odd/even predominance, especially in the oil stain 6725604 (528.33 m) CPI1 = 1.46, which indicates a strong odd/even predominance which is also reflected in the chromatogram (Figure 8d). The CPI1 values of the Proterozoic samples indicate that there is no strong preference, except for sample 7533609, 1069.16 m, (CPI1 = 0.50) which indicates a strong even/odd predominance. However, this is not reflected in the chromatogram (Figure 8m) and the reason for this could be due to integration errors associated with the high Unresolved Complex Mixture (UCM) which makes it difficult to determine where the peak starts or as a consequence of the edge effect, which is the evaporation of low molecular weight compounds such as C_{14} and C_{15}.

CPI2 estimates the carbon predominance of long chain *n*-alkanes from C_{25} – C_{36}. The Cambrian samples all have a CPI2 > 1.2 (1.48-1.25) except for 7533159 (CPI2 = 1.17) and 6725604 (CPI2 = 1.15) indicating that there is generally no strong preference which is illustrated in the chromatograms. CPI2 values for Proterozoic samples might indicate a very slight even/odd predominance with all values < 1.20 (1.02-1.12) (Table 3). However, this pattern is not observed in the chromatograms and there is generally no strong preference (Figure 8). MMAs and DMAs are also detected in all Cambrian samples but in much lower concentrations compared to *n*-alkanes (Figure 8.a). Regularly branched isoprenoids, namely pristane and phytane are also identified in all samples. Pristane/Phytane (Pr/Ph) ratios are reported in Table 3 and range between 2.08-0.23 with an average of 1.05.

Table 3 Geochemical parameters of *n*-alkanes in Carrara 1

Sample	Depth (m)	Max	Pr/Ph	Pr/nC17	Ph/nC18	CPI[a]	CPI1[b]	CPI2[c]
7533132	361.71	C_{17}	1.51	1.81	1.87	1.14	1.16	1.48
7533139	394.97	C_{17}	0.87	0.74	1.42	1.07	1.15	1.30
7533159	494.48	C_{19}	1.60	1.40	1.00	1.02	1.15	1.17
6725604	528.33	C_{17}	1.19	0.36	0.52	1.07	1.46	1.15
7533185	610.47	C_{19}	1.01	0.51	0.54	1.00	1.13	1.25
7533204	689.82	C_{14}	0.30	0.15	0.60	1.14	0.93	1.12
7533210	719.21	C_{14}	0.71	0.17	0.27	1.16	0.96	1.07
7373044	763.10	C_{14}	0.85	0.24	0.30	1.07	0.98	1.06
7373046	763.10	C_{17}	1.20	0.24	0.23	0.94	1.09	1.01
7533225	794.71	C_{14}	0.23	0.04	0.19	1.06	1.03	1.03
7533569	925.37	C_{14}	2.08	0.88	0.48	1.16	0.91	1.10
7533609	1069.16	C_{13}	1.10	3.09	0.77	0.99	0.50	1.02

[a] CPI = $((C_{23}+C_{25}+C_{27})+(C_{25}+C_{27}+C_{29}))/(2x(C_{24}+C_{26}+C_{28}))$ (Marzi et al. 1993)

[b] CPI 1 = $0.5x((C_{15}+C_{17}+C_{19}+C_{21})/(C_{14}+C_{16}+C_{18}+C_{20}))+((C_{15}+C_{17}+C_{19}+C_{21})/(C_{16}+C_{18}+C_{20}+C_{22}))$ (See Yu et al. (2016)

[c] CPI 2 = $0.5x((C_{25}+C_{27}+C_{29}+C_{31}+C_{33}+C_{35})/(C_{24}+C_{26}+C_{28}+C_{30}+C_{32}+C_{34}))+((C_{25}+C_{27}+C_{29}+C_{31}+C_{33}+C_{35})/(C_{26}+C_{28}+C_{30}+C_{32}+C_{34}+C_{36}))$ (See Yu et al. (2016)

4.2.2. Steranes

Steranes are a group of saturated hydrocarbon molecules derived from sterols produced by eukaryotic organisms and several bacteria (Brocks 2017; Peters et al. 2005). Figure 4 illustrates the relative abundance of the trifecta steranes (C_{27} cholestane, C_{28} ergostane and C_{29} stigmastane) that are identified using Metastable Reaction Monitoring (MRM) transitions $M^+ \rightarrow 217$ in all Cambrian rock samples and the oil stain from the Carrara 1 core (Figure 4 and Table 4). GC-MS analysis of the Cambrian samples reflect a typical early Phanerozoic biomarker distribution (Brocks et al. 2017) (Figure 5). Within the Cambrian bitumens and oil, on average cholestane represents 36.6% +/- 3.1% (standard deviation (SD) = 7.0%) of the total trifecta sterane distribution, on average ergostane is 21.0% (SD = 7.8%) and on average stigmastane makes up the majority of sterane diversity with 42.4% (SD = 9.8%) of the total. Steranes were below detection limits and not identified below the unconformity at 630 m.

4.2.3. Hopanes

Hopanes were measured using MRM transitions $M^+ \rightarrow 191$ as a homologue series from C_{27}-C_{35}. Carrara 1 samples above the unconformity at 630 m exhibit an abundance of hopane biomarkers from

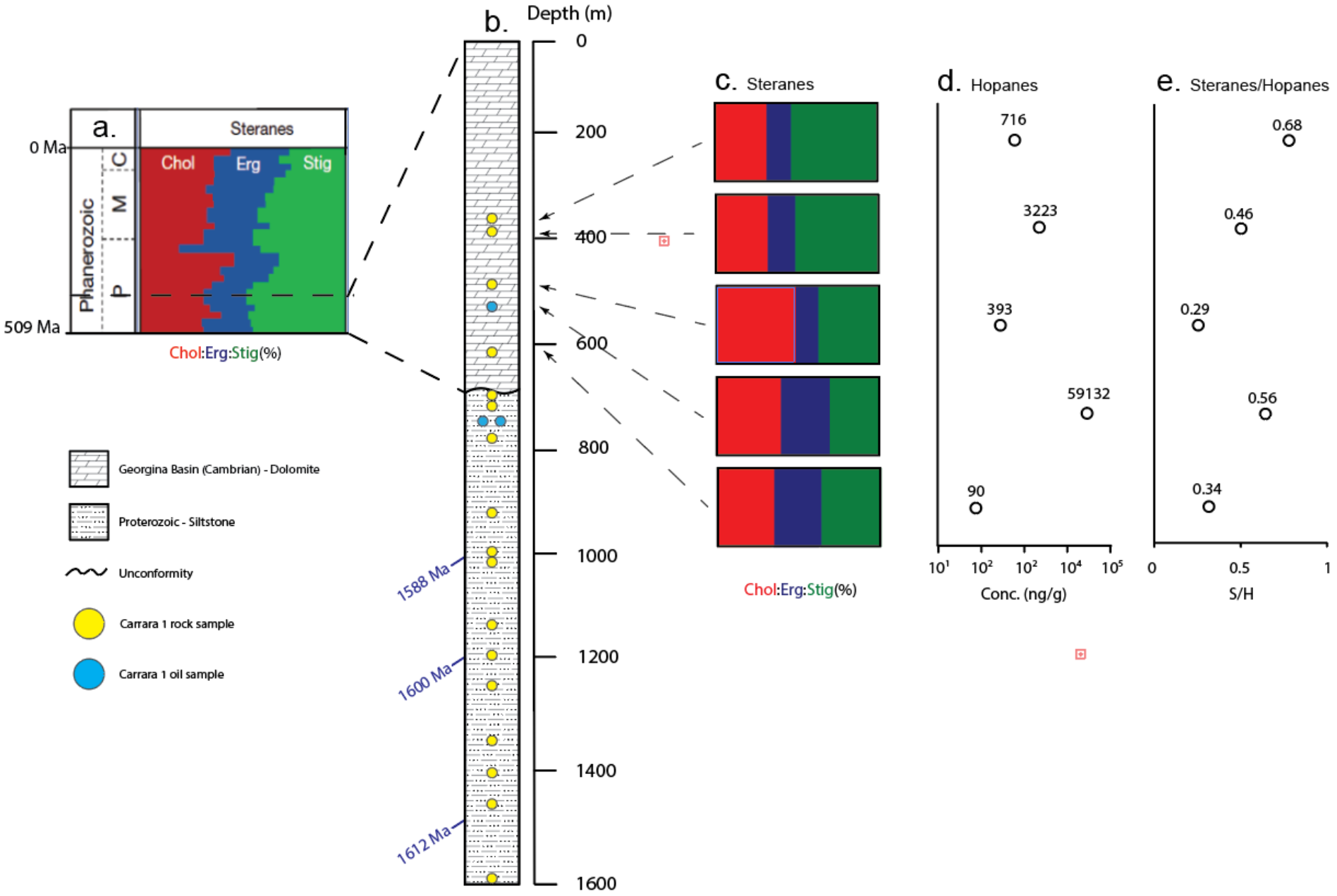

Figure 4 (a) illustrates a general Phanerozoic distribution of trifecta steranes (cholestane, ergostane and stigmastane (Modified from Brocks et al. 2017). This is correlated with the downcore plot of the Carrara 1 drill core where rock samples are represented by yellow dots and oil samples are represented as blue dots **(b).** Ages determined by U-Pb SHRIMP analysis is included on the left of core (Carson et al. 2022). **(c)** The sterane distribution for the five Phanerozoic samples illustrating the relative abundance of cholestane (red), ergostane (blue) and stigmastane (green). **(d)** The total concentrations of hopanes in the Cambrian samples, note the x axis is logarithmic **(e)** The sterane/hopane ratio (S/H).

C_{27} through to C_{35} (See Figure 4d and Table 4 for summed concentrations. Hopanes are only detected in trace concentrations in the Proterozoic section of the core and as discussed in section 4.1, E/B experiments indicate that these signals are most likely contamination from the laboratory environment and are not interpreted as indigenous (Table 2).

Table 4 Total concentrations (ng/g) of saturated hydrocarbons in the Cambrian samples of the Carrara drill core

Sample	Depth (m)	Sum of steranes[a]	Sum of hopanes[b]	Sterane/Hopane	Sum of tricyclic terpanes[c]	Sum of TMIA[d]
7533132	361.71	477.8	715.91	0.68	132.7	2909.8
7533139	394.97	1479.1	3223.1	0.46	518.3	11334.1
7533159	494.48	112.4	392.5	0.29	60.7	1637.3
6725604	528.33	33191.4	59132.2	0.56	0.04	0.0
7533185	610.47	31.0	90.4	0.34	9.2	2.1

[a] Sum of C_{27}, C_{28} and C_{29} steranes reported in ng/g of rock isomers include dia, αβ, βα, ββα, ααα*S* and αββ*S*
[b] Sum of $C_{27} - C_{35}$ hopanes reported in ng/g of rock isomers include farri, dia, αβ and βα
[c] Sum of $C_{19} - C_{16}$ tricyclic terpanes reported in ng/g of rock isomers include ββ, αβ, βα and αα
[d] Sum of $C_{13} - C_{26}$ trimethyl aryl isoprenoids reported in ng/g of rock isomers include 3,4,5 2,3,6 and 2,3,4

4.2.4. Tricyclic terpanes

Tricyclic terpanes or cheilanthanes are found in most oils and petroleum source rocks and were identified using MRM transition $M^+ \rightarrow 191$ as a pseudohomologue series from C_{19} to C_{26} in all Cambrian source rocks and the oil stain. Figure 5a illustrates the concentration of cheilanthanes across the pseudohomologue series for the Cambrian bitumens. The highest concentrations of cheilanthanes is at pseudohomologue C_{23} for all Cambrian bitumens except 7533132 (361.71 m) which has a maximum at $C_{21.}$ All samples have a minimum at C_{22} due to branching at this point on the isoprenoid side chain (Figure 5a). Cheilanthanes were also detected in trace concentrations from $C_{19} - C_{24}$ in the Proterozoic section of the core (Figure 5b). The maximum concentration is at either pseudohomologue C_{21} or C_{23} with a minimum at $C_{22.}$ All of the Proterozoic samples have at least one isomer that is absent or detected in only trace concentrations and to determine if these values are reliable, E/B ratios were computed for the entire pseudohomologue series (Table 5). Table 5 illustrates that cheilanthanes detected below 1000 m have E/B ratios < 20 and are thus potentially affected by laboratory contamination. In the remaining samples shallower than 1000 m, some of the isomers have E/B ratios < 20 and >20 which would indicate that some of these samples might contain indigenous cheilanthanes. However, it is important that cheilanthanes are detected as complete series to be considered indigenous, and since this is not the case in any of the samples, the detected peaks are more likely caused by some contaminant from the laboratory or misinterpretation of another peak eluting in the same position as the cheilanthane isomer. Therefore, we do not interpret these signals as indigenous cheilanthanes.

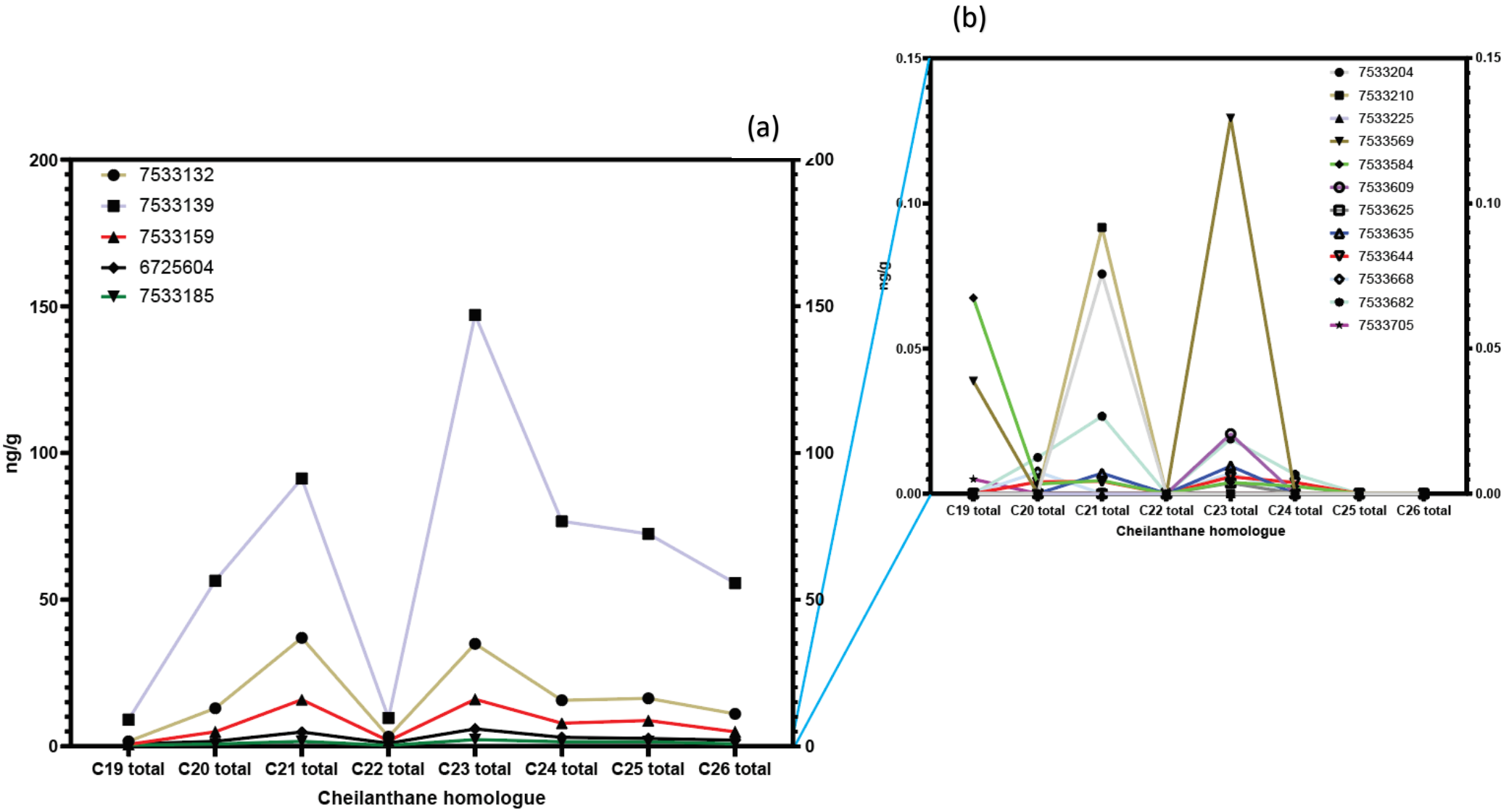

Figure 5 Concentrations of cheilanthanes in the homologue series from $C_{19} - C_{26}$ in (a) Cambrian samples and (b) Proterozoic samples. Isomers include ββ, αβ, βα and αα

Table 5 Extract/Blank (E/B) ratios for cheilanthanes in Proterozoic samples of Carrara 1

E/B	Depth (m)	C19 total	C20 total	C21 total	C22 total	C23 total	C24 total
7533204	689.82	0.00	0.00	207.76	0.00	0.00	0.00
7533210	719.21	0.00	0.00	251.76	0.00	0.00	0.00
7373044	763.10	0.00	0.00	0.00	0.00	0.00	0.00
7373046	763.10	0.00	0.00	0.00	0.00	0.00	0.00
7533225	794.71	0.00	0.00	0.00	0.00	0.00	0.00
7533569	925.37	24.99	0.00	0.00	0.00	31.59	0.00
7533584	998.66	43.49	0.00	1.31	0.00	0.95	6.00
7533609	1069.16	0.00	0.00	0.00	0.00	5.03	0.00
7533625	1150.08	0.00	0.00	0.00	0.00	0.90	0.00
7533635	1199.60	0.00	0.00	2.04	0.00	2.32	0.00
7533644	1244.79	0.00	0.00	1.24	0.00	1.43	9.17
7533668	1345.03	0.00	0.00	0.00	0.00	1.71	0.00
7533682	1405.10	0.00	0.00	7.71	0.00	4.60	15.67
7533705	1461.32	3.23	0.00	0.00	0.00	0.00	0.00

[a] E/B ratio for C_{19} cheilanthanes. Isomers include C_{19} 14α

[b] E/B ratio for C_{20} cheilanthanes. Isomers include $\beta\beta$ C_{20}, $\alpha\beta$ C_{20} and $\alpha\alpha$ C_{20}

[c] E/B ratio for C_{21} cheilanthanes. Isomers include $\beta\beta$ C_{21}, $\alpha\beta$ C_{21}, $\beta\alpha$ C_{21} and $\alpha\alpha$ C_{21}

[d] E/B ratio for C_{22} cheilanthanes. Isomers include $\alpha\beta$ C_{22} and $\beta\alpha$ C_{22}

[e] E/B ratio for C_{23} cheilanthanes. Isomers include $\beta\beta$ C_{23}, $\alpha\beta$ C_{23}, $\beta\alpha$ C_{23} and $\alpha\alpha$ C_{23}

[f] E/B ratio for C_{24} cheilanthanes. Isomers include $\beta\beta$ C_{24}, $\alpha\beta$ C_{24}, $\beta\alpha$ C_{24} and $\alpha\alpha$ C_{24}

4.2.5. Polyaromatic hydrocarbons

Polyaromatic hydrocarbons (PAHs) can provide crude estimates of the extent of biodegradation and thermal degradation, specifically by comparing the abundance of the parent PAH (pPAH), which are more thermally stable, to the abundance of corresponding alkylated PAHs (aPAHs), comparatively less stable. Therefore, the pPAH/aPAH ratio will generally increase as a function of thermal degradation.(Brocks et al. 2003a; George 1992). The PAHs quantified in the present study are reported in Table 6 as pPAH/aPAH ratios and illustrates the change in these ratios as a function of depth. Fluorene/methylfluorene (F/MF) exhibits relatively high values in the Cambrian samples compared to the Proterozoic samples which is opposite to the expected trend (George 1992). Phenanthrene/methylphenanthrene (P/MP) decreases as a function of depth until ~ 1000 m where the trend reverses and the P/MP increases. Such reversal patterns have been reported previously and is most commonly associated with the conversion of MP to P at very high maturities (Boreham et al. 1998). Pyrene/methylpyrene (Py/Mpy) increases with depth reflecting the thermal stability

of parent pyrene as is expected for pyrolytically altered bitumen (Brocks et al. 2003a; George 1992). Benzo[a]pyrene/methylphenanthrene and benzo[ghi]perylene/methylphenanthrene are reported in sample 7533185 and then drop below detection limits until they are reported again at ≈ 1150 m presumably indicating generation of these two higher parent PAH at the highest temperatures (Figure 4).

Table 6 Polyaromatic Hydrocarbon (PAH) concentrations in Carrara 1

Sample	Depth (m)	F/MF [a]	P/MP [b]	Py/Mpy [c]	Benzo[a]Py/MP [d]	Benzo[ghi]Pe/MP [e]
7533132	361.71	1.09	0.58	0.40	-	-
7533139	394.97	2.04	0.48	0.35	-	-
7533159	494.48	0.41	0.34	0.31	-	-
6725604	528.33	-	-	-	-	-
7533185	610.47	0.28	0.33	0.33	0.01	0.02
7533204	689.82	0.18	0.28	0.33	-	-
7533210	719.21	0.27	0.16	0.23	-	-
7373044	763.10	-	-	0.15	-	-
7373046	763.10	-	-	-	-	-
7533225	794.71	1.50	0.15	0.31	-	-
7533569	925.37	0.67	0.19	0.23	-	-
7533584	998.66	-	0.15	0.30	-	-
7533609	1069.16	0.43	0.25	-	-	-
7533625	1150.08	0.12	0.46	0.66	-	-
7533635	1199.60	-	0.26	0.64	0.02	0.02
7533644	1244.79	0.14	0.54	0.74	0.01	-
7533668	1345.03	-	0.28	0.62	0.05	0.03
7533682	1405.10	0.28	0.72	0.89	0.01	0.01
7533705	1461.32	-	0.35	1.00	0.03	0.01

[a] Fluorene/Methyl fluorenes (MF 3, MF 2, MF 1 and MF 4): measured using summed trace at *m/z* 166 and 180.
[b] Phenanthrene/Methylphenanthrenes (MP 2, MP 3, MP 9 and MP 1): measured using summed trace at *m/z* 178 and 192.
[c] Pyrene/Methylpyrene (Mpy 2, Mpy 4 and Mpy1) measured using summed trace at *m/z* 202 and 216.
[d] Benzo[a]pyrene/Methylphenanthrenes (MP 2, MP 3, MP 9 and MP 1): measured at *m/z* = 252 and 192 respectively.
[e] Benzo[ghi]perylene/Methylphenanthrenes (MP 2, MP 3, MP 9 and MP 1): measured at *m/z* = 276 and 192 respectively.

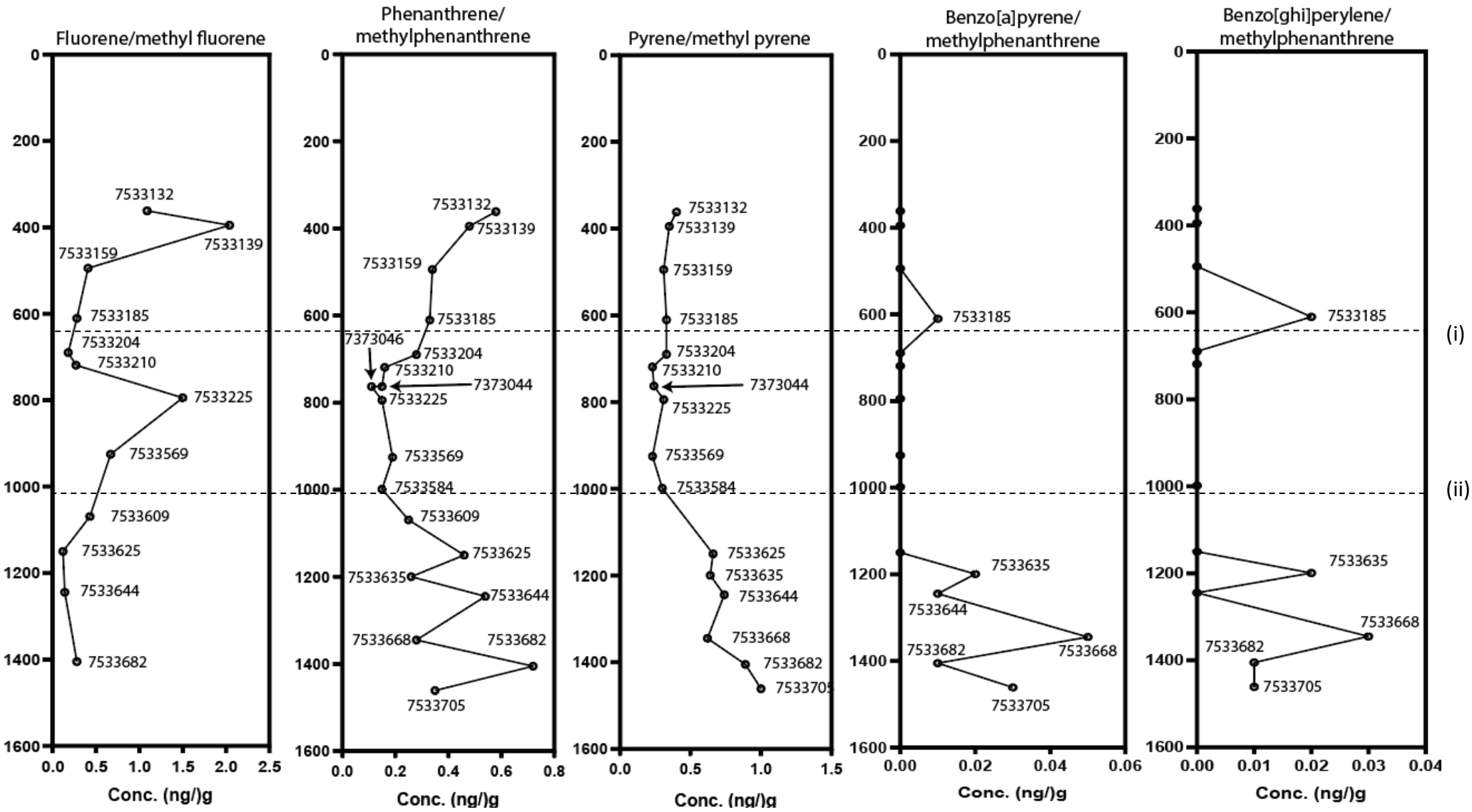

Figure 6 The various ratios of parent and alkylated poly aromatic hydrocarbons (PAHs) in Carrara 1. Missing data points indicate PAH were below detection limits. The dashed lines indicate (i) the unconformity between the Precambrian and Cambrian 630 m and (ii) 1012 m below which, samples are absolutely dated to be Paleoproterozoic.

4.2.6. Trimethyl aryl isoprenoids

Intact C_{40} carotenoids were not detected in any of the Carrara 1 samples, however the diagenic breakdown products of carotenoids, 2,3,4, 2,3,6 and 3,4,5 trimethyl aryl isoprenoids (TMAI) were detected in a pseudohomologue series from C_{10} – C_{23} in the three shallowest Cambrian samples and the two shallowest Proterozoic samples at *m/z* 133+134. Identification of TMAIs can be difficult since many isomers and homologues share elution positions with trimethyl alkyl benzenes (TMAB) and other interfering molecules (Jarrett et al. 2019a). TMAI with a short to medium chain length (generally C_{11} – C_{18}) are especially susceptible to this and it is crucial to clearly distinguish TMAIs against TMABs before a confident interpretation is made. Figure 7a and 7b illustrate the chromatograms corresponding to *m/z* 133+134 for the Cambrian and Proterozoic samples respectively. Peaks in the correct eluting positions of the three isomers of TMAIs and to TMAB were identified in Carrara 1 samples by juxtaposing them with a Cambrian sample from the BMR Mount Isa 1 drill core from the Georgina basin that is known to have a high concentrations of TMAIs (Pagès et al. 2016). In addition, Jarrett et al. (2019) provides a comprehensive identification of TMAB and other interfering signals by juxtaposing their data with a sample from the Barney Creek Formation (Brocks et al. 2005). Though there are several isomers that are obviously coeluting with TMAB for example, 2,4,5 TMAI at C_{13}, 3,4,5, TMAI at $C_{15,}$ 2,3,4 TMAI at $C_{16,}$ 2,3,4 TMAI at C_{18} and 3,4,5 TMAI at $C_{22,}$ (See Figure 7a and 7b), in most cases, the three TMAI isomers could be distinguished from the TMAB and other interfering signals in the Cambrian samples from C_{10} – C_{23}. However, identification is much more difficult in the Proterozoic samples due to the high concentration of TMABs and other interfering signals (Figure 7). For example, there is a relatively large peak in the correct elution position for C_{17} 2,3,4 TMAI however, since C_{17} is a branching point along the isoprenoid side chain, this signal should be very low compared to the C_{18} and C_{19} isomers which are below detection limits. Therefore, it is not possible to determine whether any of the Proterozoic peaks are TMAI and detailed MRM experiments on two different columns are needed to distinguish them. For example, see Vinnichenko et al. (2020). This sort of experiment is out of the scope of this project and thus, to err on the side of caution, no TMAIs are identified in the Proterozoic samples of the Carrara 1 drill core.

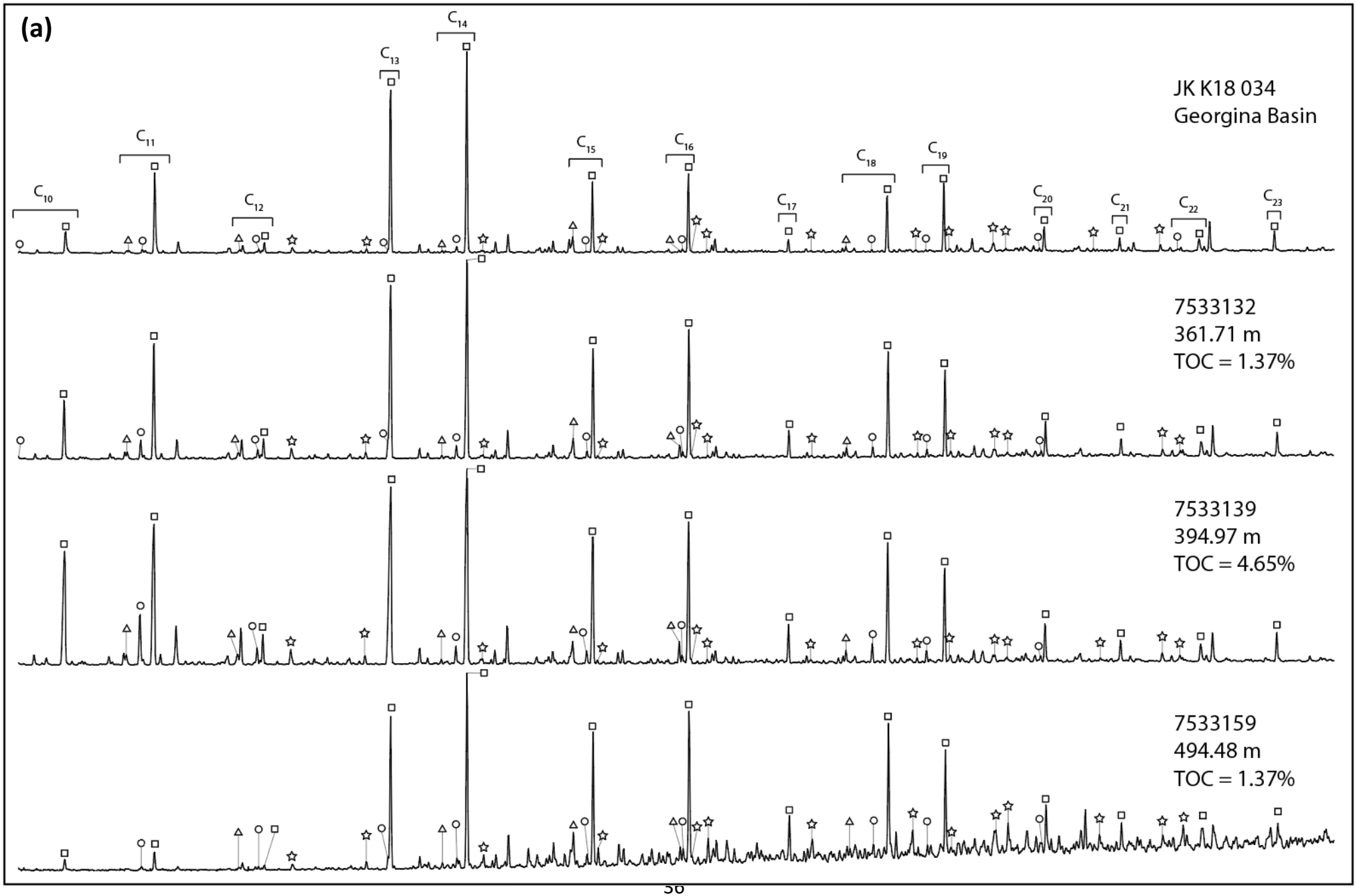
(a)
C10
C11
C12
C13
C14
C15
C16
C17
C18
C19
C20
C21
C22
C23
JK K18 034
Georgina Basin
7533132
361.71 m
TOC = 1.37%
7533139
394.97 m
TOC = 4.65%
7533159
494.48 m
TOC = 1.37%

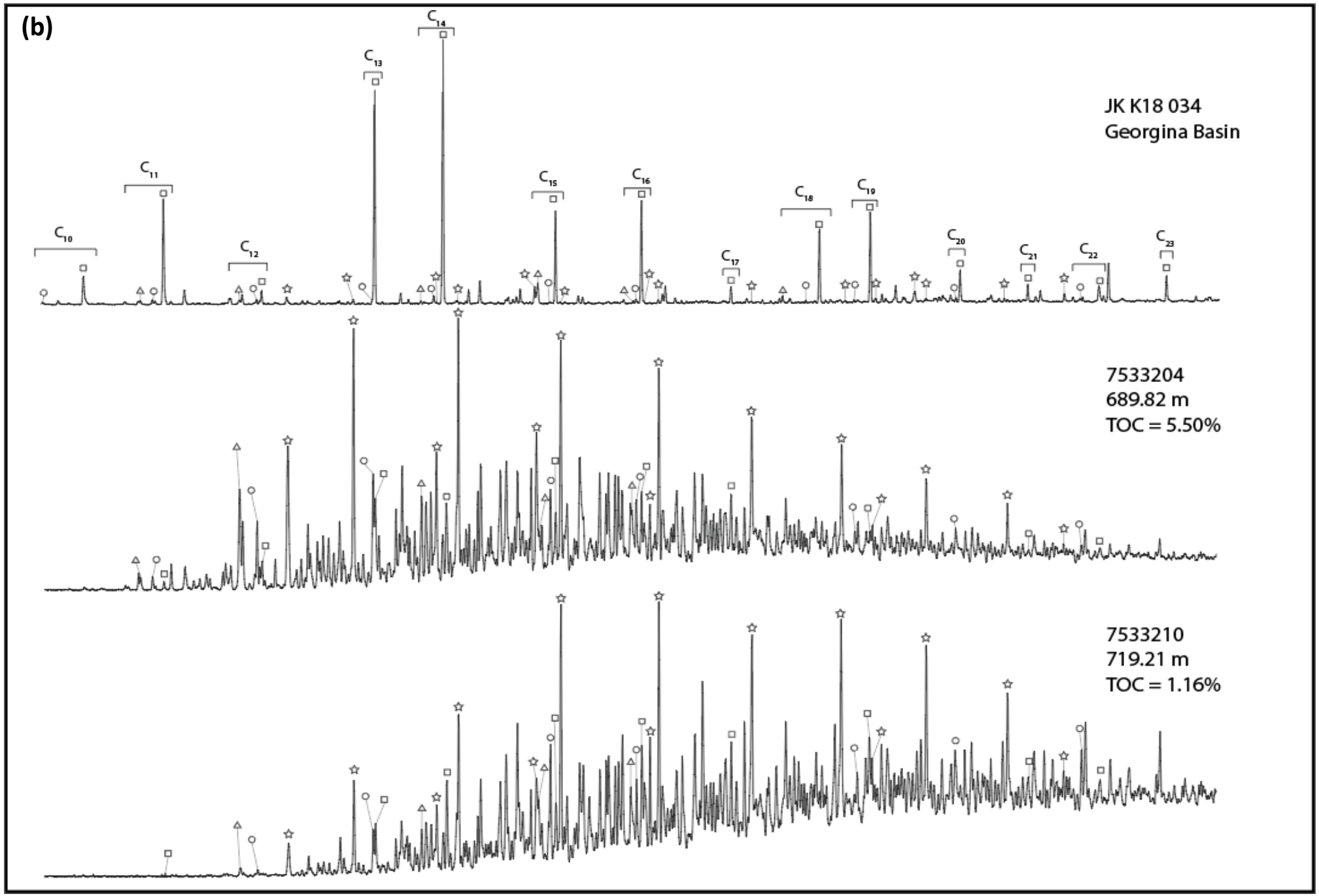

Figure 7 Chromatograms of Cambrian and Proterozoic samples that contain trimethyl arylisoprenoids (TMAI). Squares illustrate the 2,3,6 TMAI isomer, circles are the 2,3,4 TMAI isomer, triangles are the 3,4,5 isomer and stars are interfering trimethyl benzenes (TMAB)

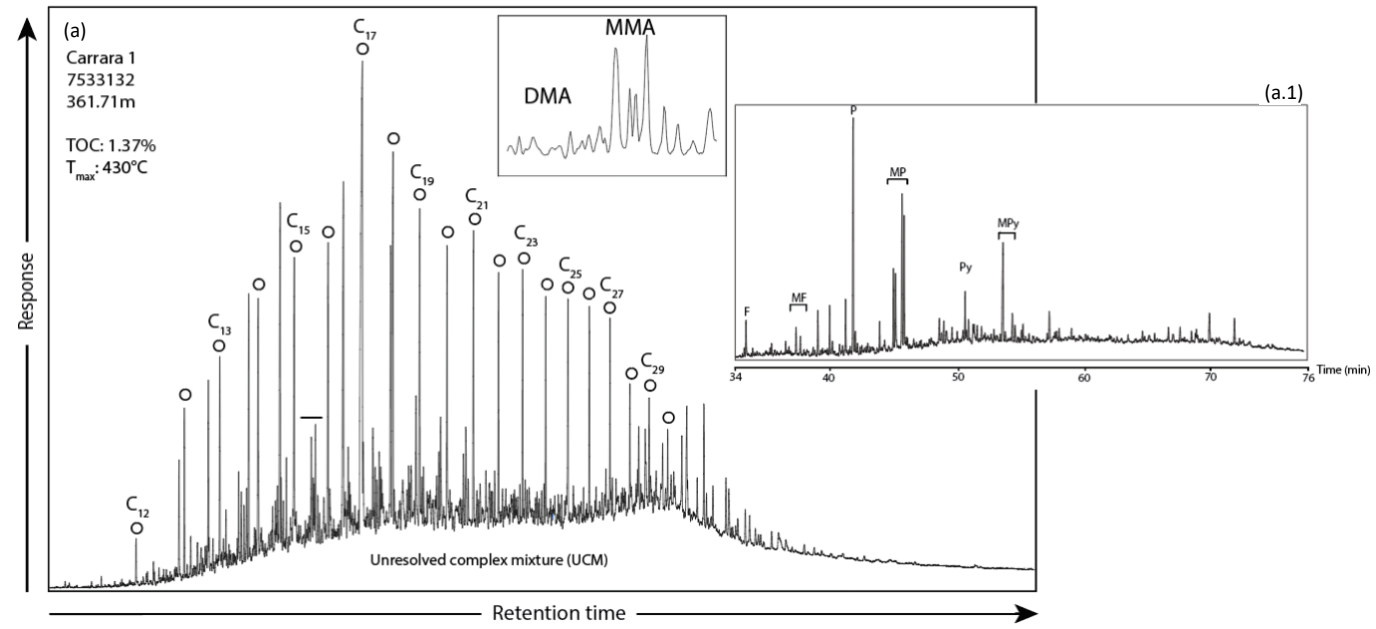
(a)
Carrara 1
7533132
361.71m
TOC: 1.37%
T_{max}: 430°C
MMA
DMA
(a.1)
P
MP
MPy
Py
MF
F
Time (min)
Response
Unresolved complex mixture (UCM)
Retention time

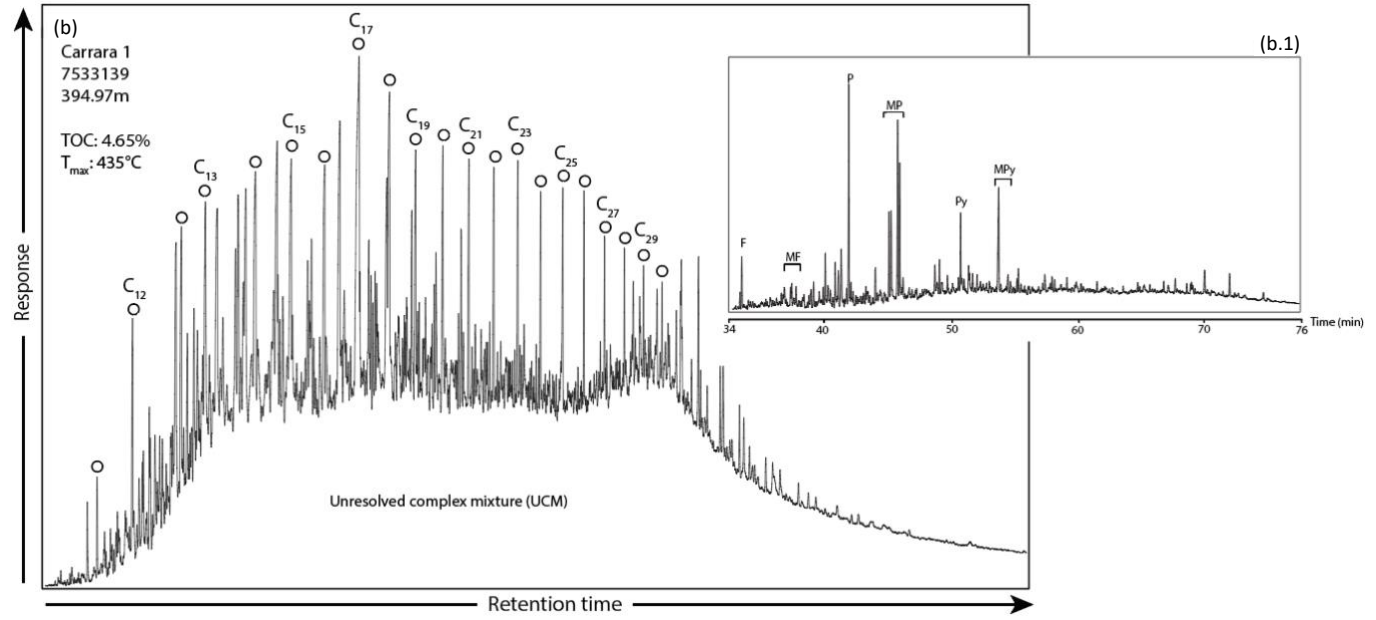
(b)
Carrara 1
7533139
394.97m
TOC: 4.65%
T_{max}: 435°C
(b.1)
P
MP
MPy
Py
MF
F
Time (min)
Response
Unresolved complex mixture (UCM)
Retention time

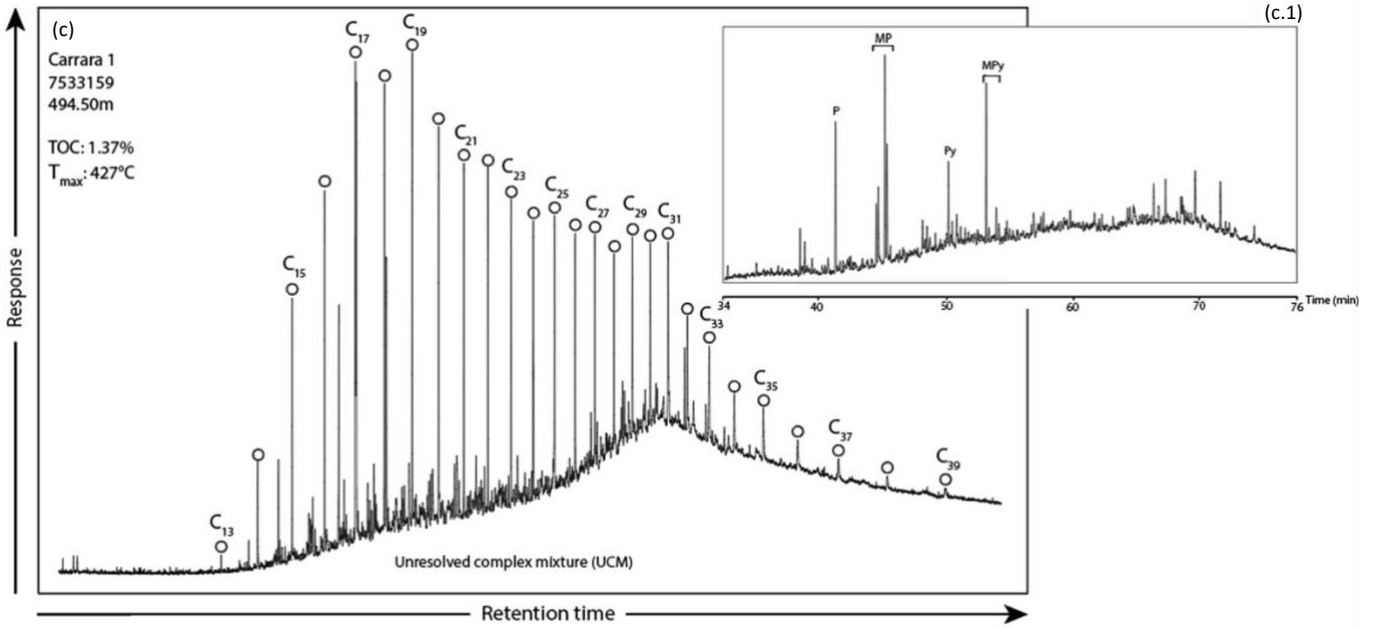
(c)
Carrara 1
7533159
494.50m
TOC: 1.37%
T_{max}: 427°C
(c.1)
MP
MPy
P
Py
Time (min)
Response
Unresolved complex mixture (UCM)
Retention time

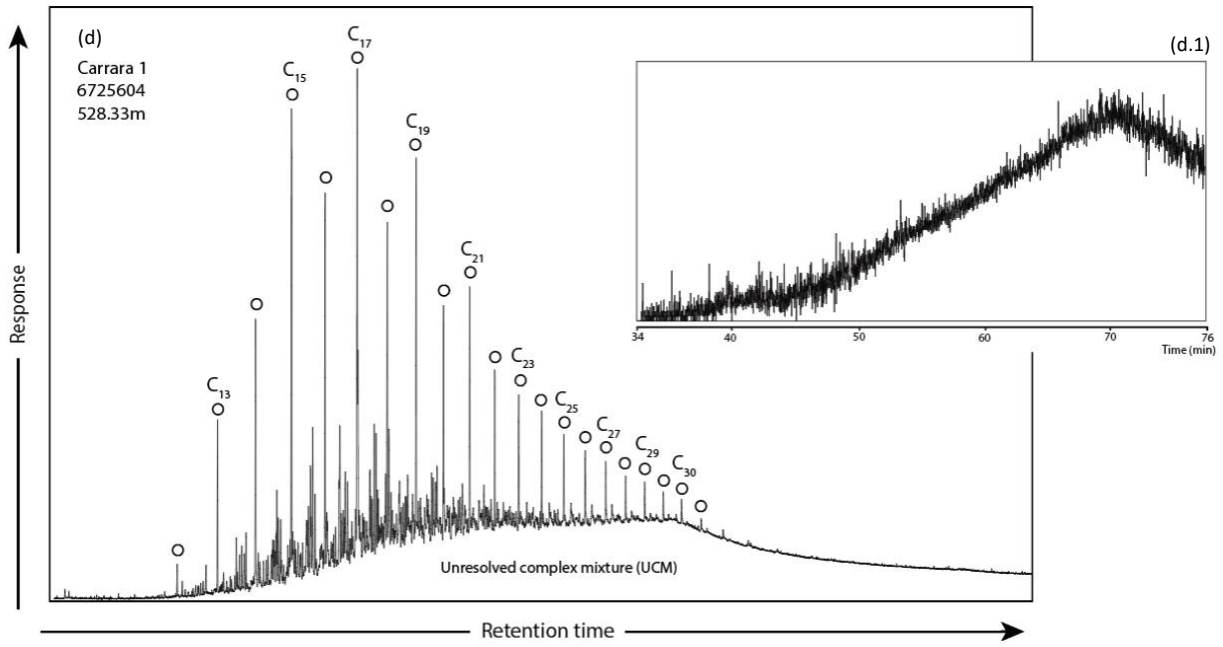
(d)
Carrara 1
6725604
528.33m
(d.1)
Response
Retention time
Unresolved complex mixture (UCM)
Time (min)

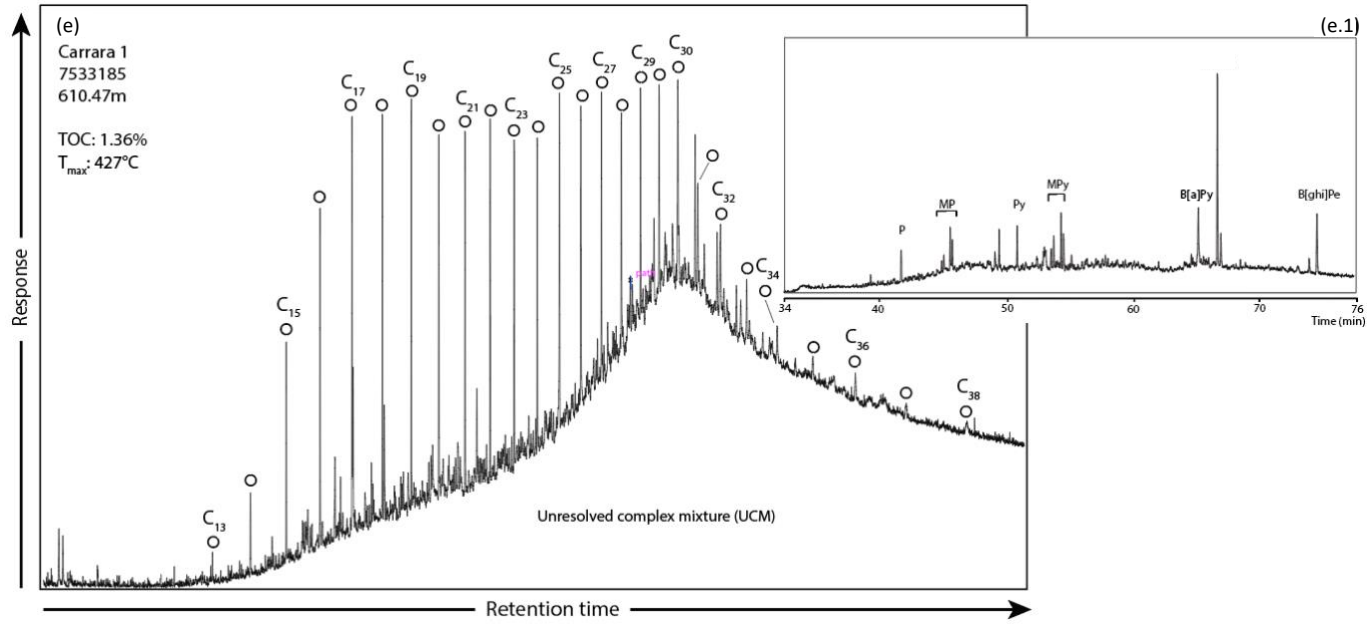
(e)
Carrara 1
7533185
610.47m
TOC: 1.36%
Tmax: 427°C
(e.1)
Response
Retention time
Unresolved complex mixture (UCM)
P
MP
Py
MPy
B[a]Py
B[ghi]Pe
Time (min)

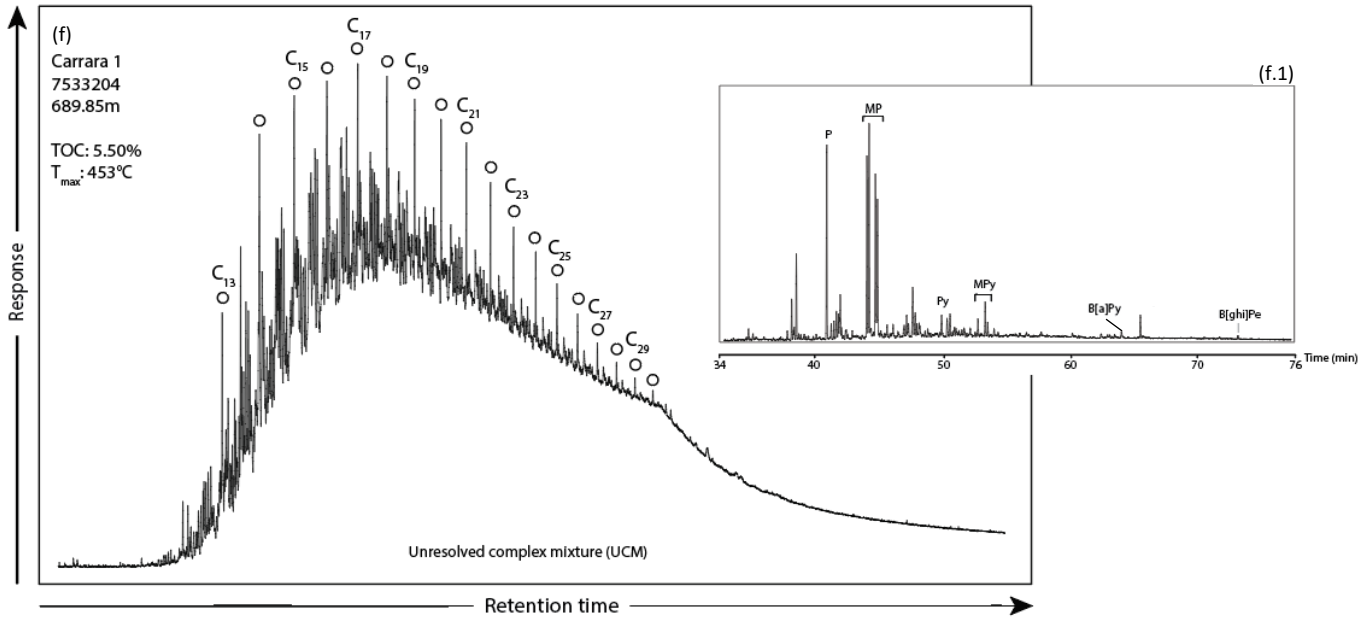
(f)
Carrara 1
7533204
689.85m
TOC: 5.50%
Tmax: 453°C
(f.1)
Response
Retention time
Unresolved complex mixture (UCM)
P
MP
Py
MPy
B[a]Py
B[ghi]Pe
Time (min)

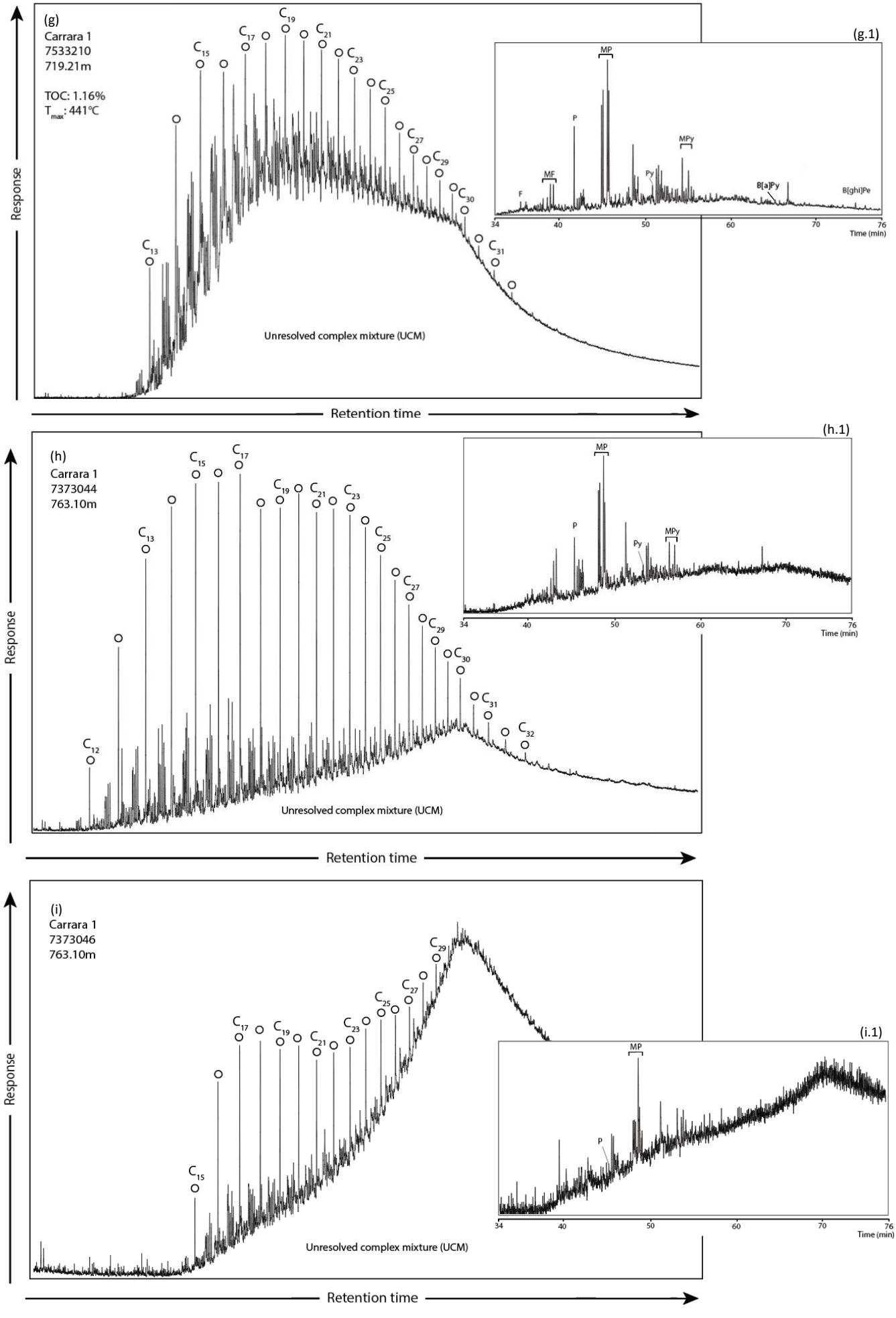
(g)
Carrara 1
7533210
719.21m
TOC: 1.16%
T$_{max}$: 441°C
Response
Retention time
Unresolved complex mixture (UCM)
(g.1)
MP
P
MPy
MF
Py
F
B[a]Py
B[ghi]Pe
Time (min)
(h)
Carrara 1
7373044
763.10m
(h.1)
(i)
Carrara 1
7373046
763.10m
(i.1)

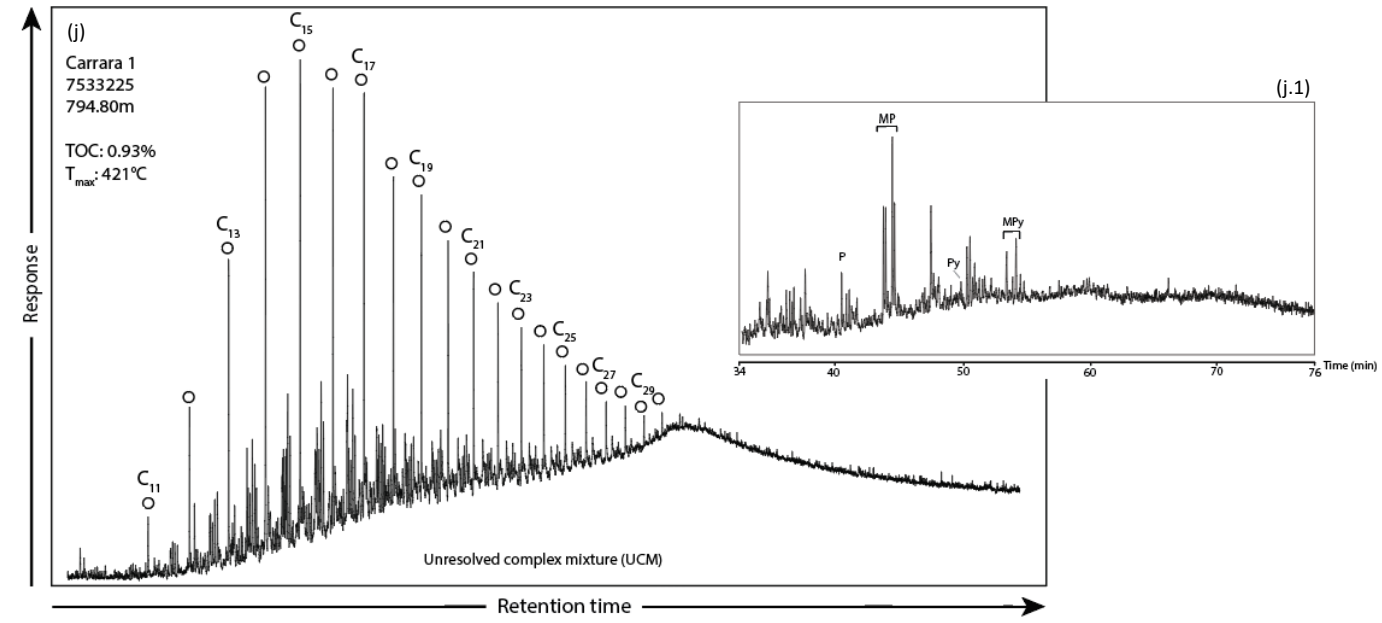
(j)
Carrara 1
7533225
794.80m
TOC: 0.93%
T_{max}: 421°C
Response
C_{11}
C_{13}
C_{15}
C_{17}
C_{19}
C_{21}
C_{23}
C_{25}
C_{27}
C_{29}
Unresolved complex mixture (UCM)
Retention time
(j.1)
MP
P
Py
MPy
34
40
50
60
70
76
Time (min)

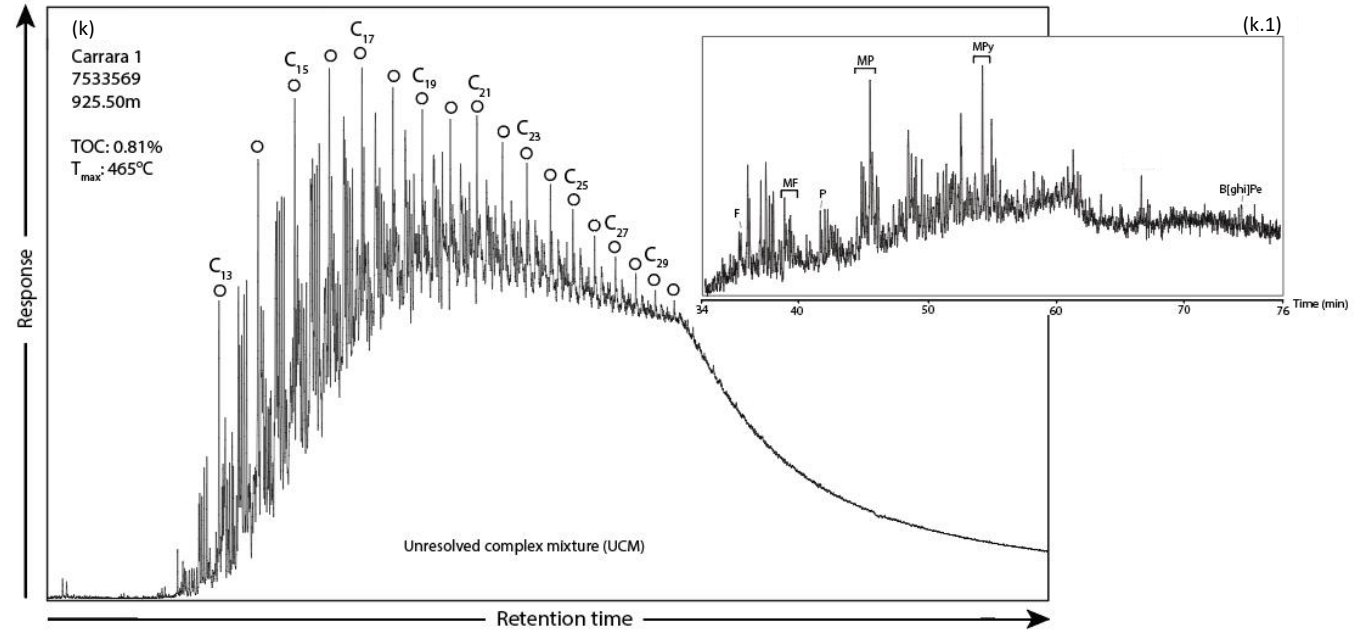
(k)
Carrara 1
7533569
925.50m
TOC: 0.81%
T_{max}: 465°C
Response
C_{13}
C_{15}
C_{17}
C_{19}
C_{21}
C_{23}
C_{25}
C_{27}
C_{29}
Unresolved complex mixture (UCM)
Retention time
(k.1)
MP
MPy
MF
P
F
B[ghi]Pe
34
40
50
60
70
76
Time (min)

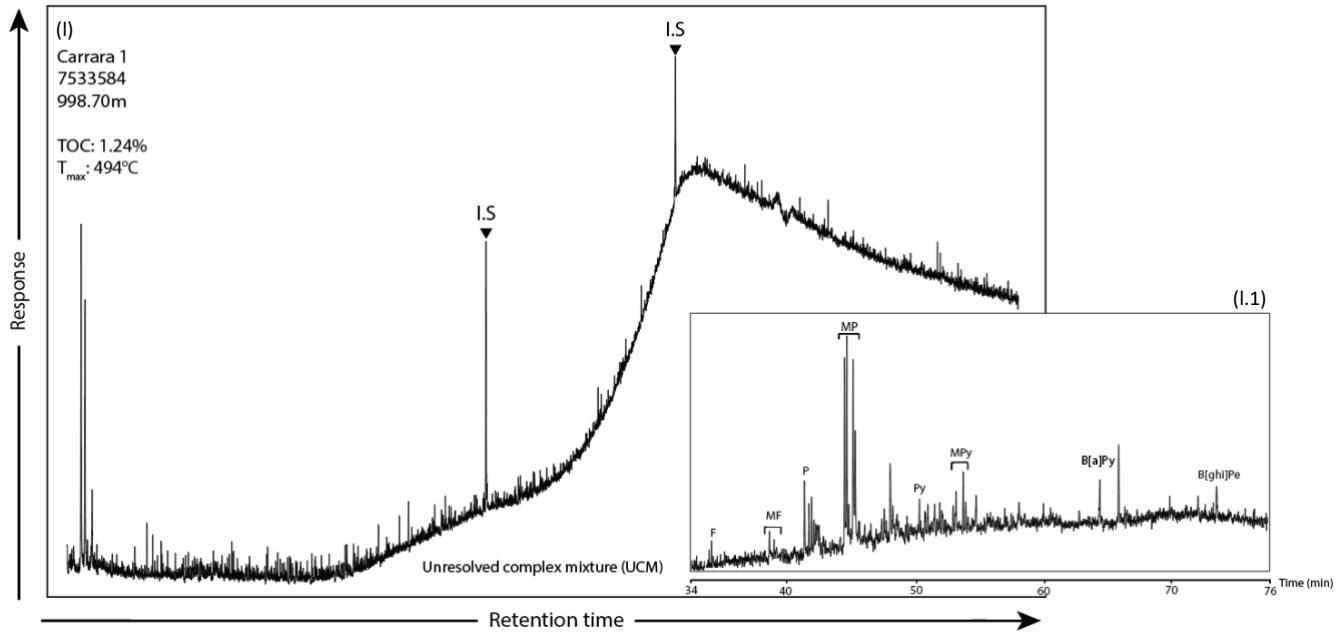
(l)
Carrara 1
7533584
998.70m
TOC: 1.24%
T_{max}: 494°C
Response
I.S
I.S
Unresolved complex mixture (UCM)
Retention time
(l.1)
MP
MPy
P
Py
MF
F
B[a]Py
B[ghi]Pe
34
40
50
60
70
76
Time (min)

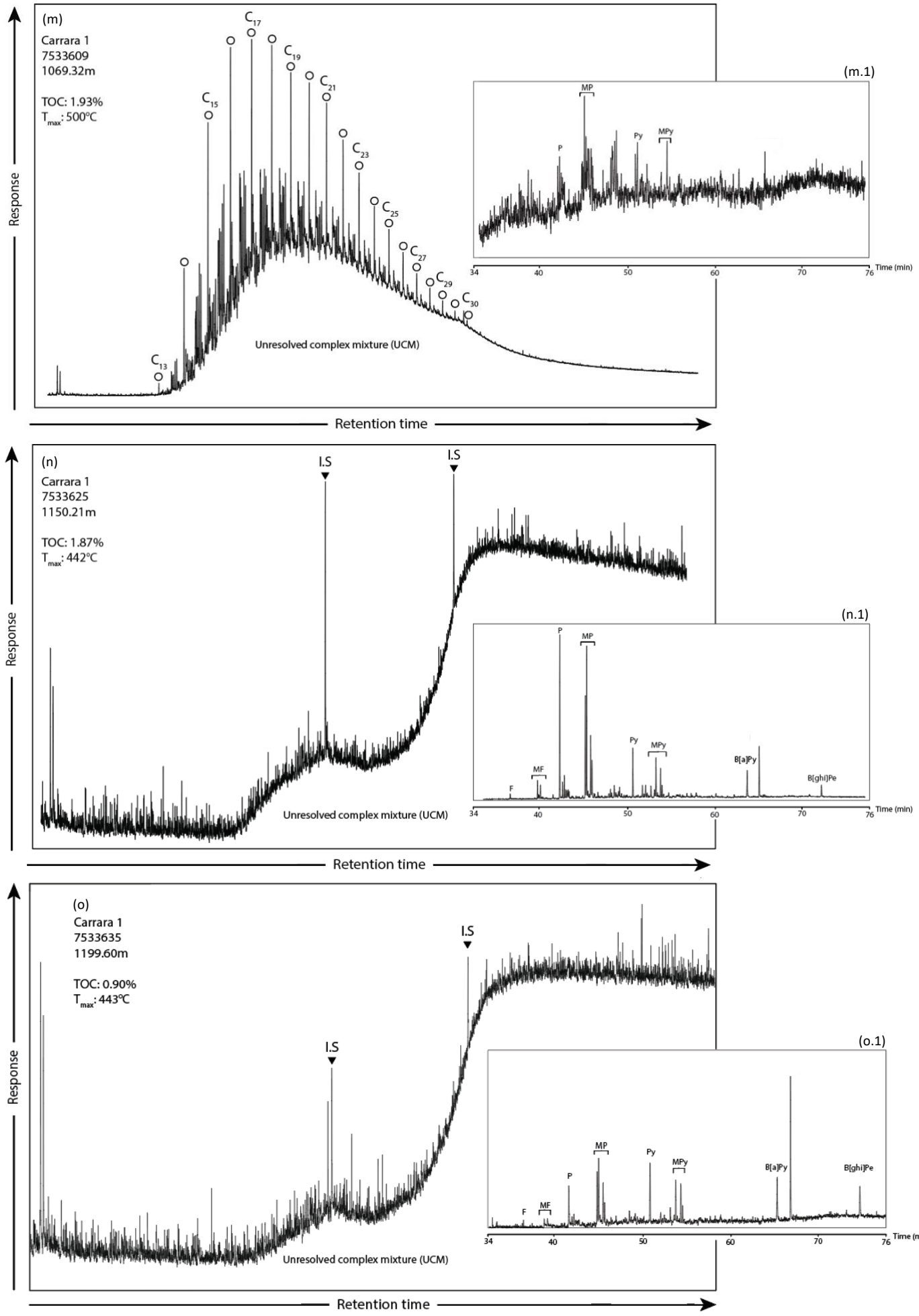
(m)
Carrara 1
7533609
1069.32m
TOC: 1.93%
T_{max}: 500°C
C_{13}
C_{15}
C_{17}
C_{19}
C_{21}
C_{23}
C_{25}
C_{27}
C_{29}
C_{30}
Unresolved complex mixture (UCM)
Response
Retention time
(m.1)
MP
P
Py
MPy
34
40
50
60
70
76
Time (min)
(n)
Carrara 1
7533625
1150.21m
TOC: 1.87%
T_{max}: 442°C
I.S
I.S
Unresolved complex mixture (UCM)
Response
Retention time
(n.1)
P
MP
Py
MPy
MF
F
B[a]Py
B[ghi]Pe
34
40
50
60
70
76
Time (min)
(o)
Carrara 1
7533635
1199.60m
TOC: 0.90%
T_{max}: 443°C
I.S
I.S
Unresolved complex mixture (UCM)
Response
Retention time
(o.1)
MP
Py
P
MPy
B[a]Py
B[ghi]Pe
F
MF
34
40
50
60
70
76
Time (min)

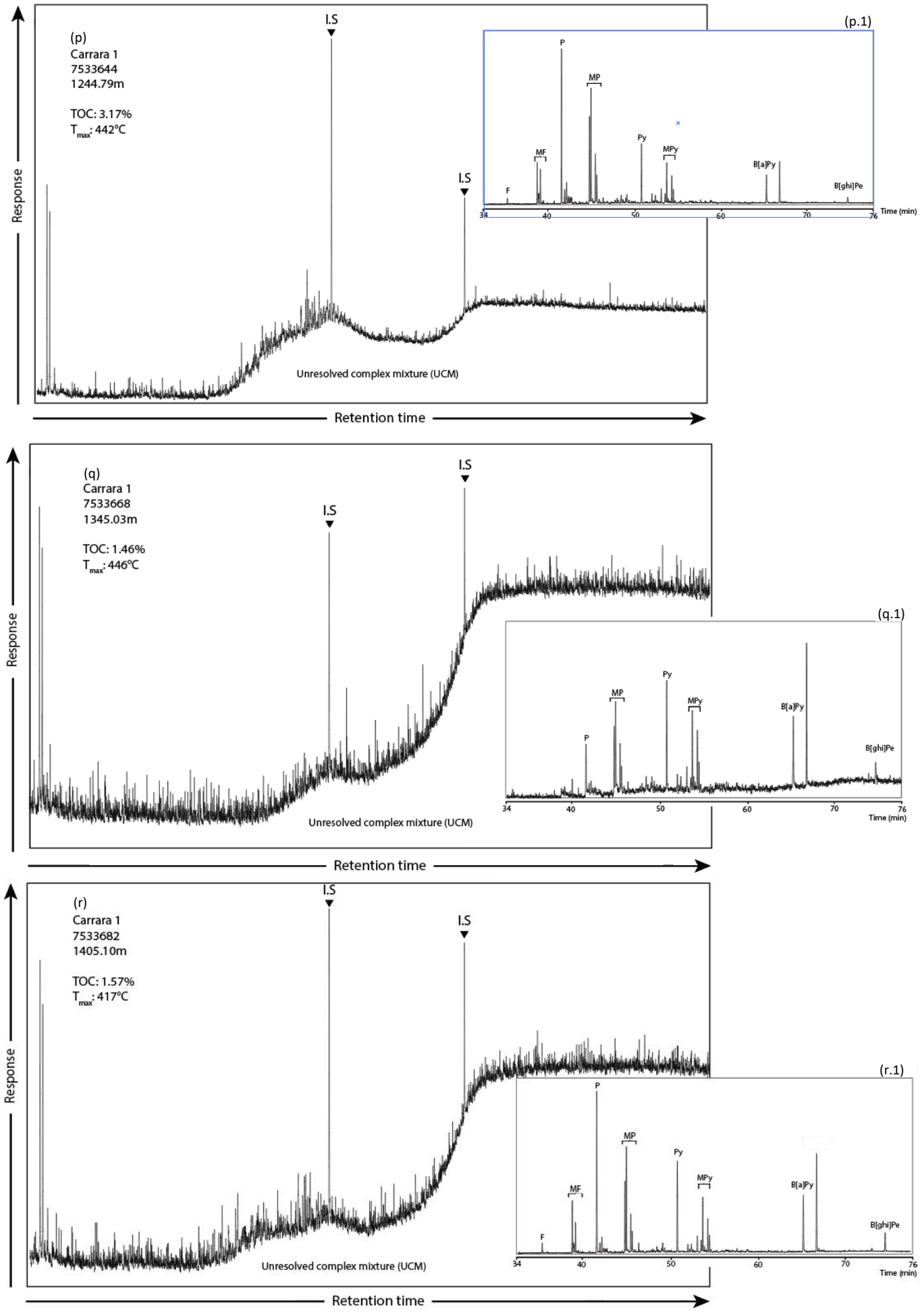
(p)
Carrara 1
7533644
1244.79m
TOC: 3.17%
T max: 442°C
I.S
I.S
Response
Unresolved complex mixture (UCM)
Retention time
(p.1)
P
MP
Py
MF
MPy
F
B[a]Py
B[ghi]Pe
34
40
50
60
70
76
Time (min)
(q)
Carrara 1
7533668
1345.03m
TOC: 1.46%
T max: 446°C
I.S
I.S
Response
Unresolved complex mixture (UCM)
Retention time
(q.1)
Py
MP
MPy
B[a]Py
P
B[ghi]Pe
34
40
50
60
70
76
Time (min)
(r)
Carrara 1
7533682
1405.10m
TOC: 1.57%
T max: 417°C
I.S
I.S
Response
Unresolved complex mixture (UCM)
Retention time
(r.1)
P
MP
Py
MF
MPy
B[a]Py
F
B[ghi]Pe
34
40
50
60
70
76
Time (min)

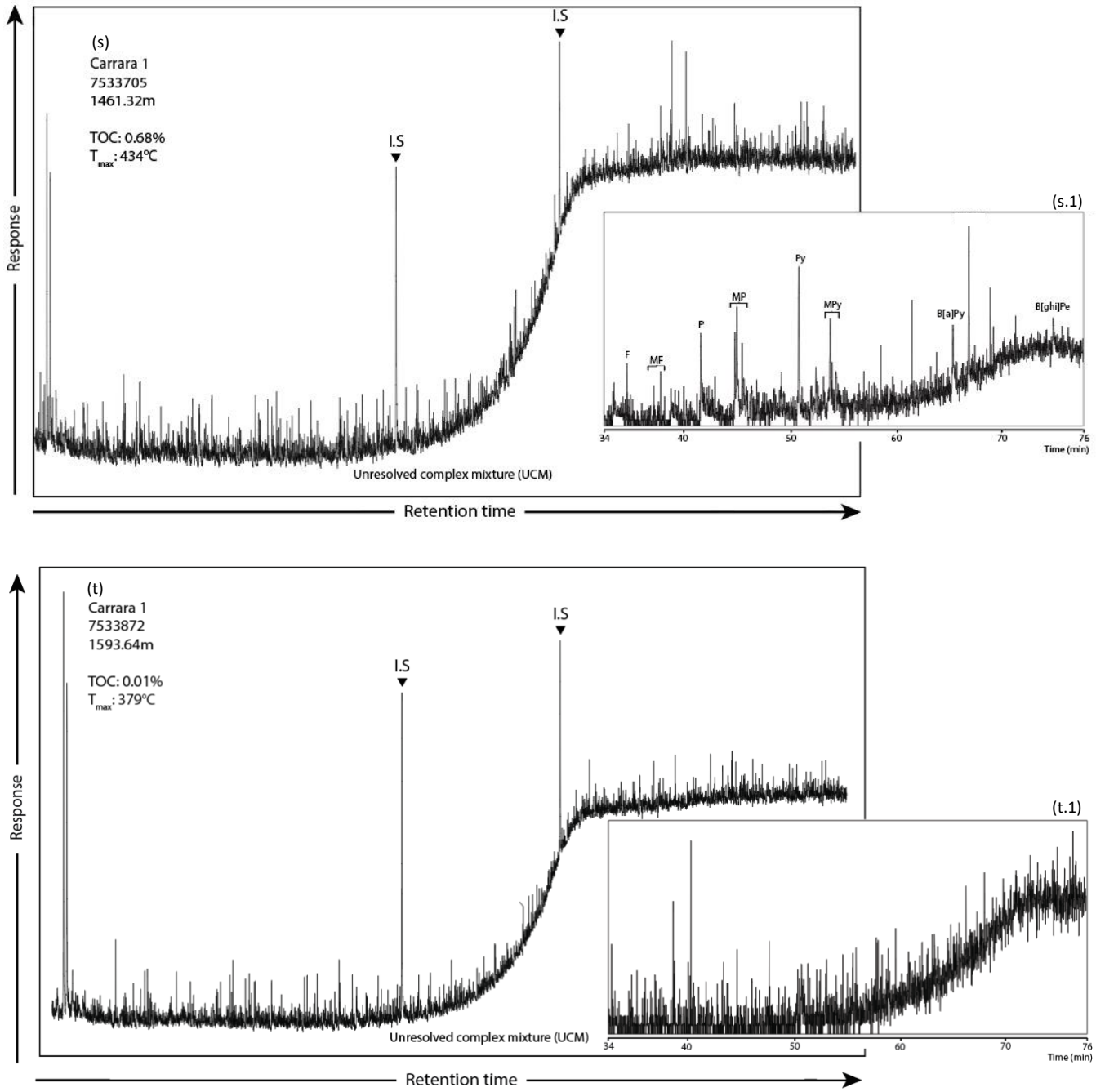

Figure 8 Full scan TIC chromatograms of saturated hydrocarbon fractions of all samples illustrating the distribution of acyclic saturated hydrocarbons (large chromatograms). Open circles identify n-alkanes and I.S is the added internal standards. The inserts illustrate the summed chromatogram of m/z 166, 180 ,178, 192, 202, 216, 252 and 276 representing selected polyaromatic hydrocarbons (PAHs). F = Fluorene, MF = Methylfluorene, P = Phenanthrene, MP = Methylphenanthrene, Py = Pyrene, Mpy = Methylpyrene, B[a]Py = Benzo[a]pyrene and B[ghi]Pe = Benzo[ghi]perylene.

4.3 Thermal maturity

Figure 9 illustrates three maturity parameters based on P and MP calculated for Carrara 1 source rocks and oils. They are the methylphenanthrene distribution factor (MPDF), the methylphenanthrene ratio (MPR) and the methylphenanthrene index (MPI). There is a strong trend in which maturity increases downcore reaching a maximum maturity at ≈1200-1400 m (Figure 9). Notably, the Cambrian oil stain, 6725604 (528.33 m), didn't contain any detectable P and MP and thus, thermal maturity estimates haven't been made for this sample. All three parameters indicate that sample 7533204, (which, at 689.85 m is the first sample below the unconformity at 630 m) has an unusually high maturity for its depth correlating more closely with samples below 1000 m. The Proterozoic oil stains illustrate maturity that is consistent with surrounding samples. In terms of generative potential of source rocks, P and MP data on its own is relatively uninformative. The P and MP maturity parameters can be mathematically manipulated to correlate with vitrinite reflectance (R_0) as calculated vitrinite reflectance equivalents (R_c) using equation 5, 6 and 7 from Kvalheim et al. (1987) and Radke and Welte (1983) and (1984) respectively.

$$Rc(MPDF) = 0.166 + 2.2424 \times MPDF \quad (5)$$

$$Rc(MPI) = 0.6 \times MPI1 + 0.4 \quad (6)$$

$$Rc(MPR) = 0.99 * log_{10}(MPR) + 0.94 \quad (7)$$

It is important to note that when working with extremely high thermal maturities, P and MP maturity estimates can become unpredictable and unreliable and should be interpreted with caution (Boreham et al. 1988; Brocks et al. 2003a; Raymond and Murchison 1992). It has been illustrated that samples with Rc(MPI) > 1.7%, can be affected by a reversal in the conventional trend in maturity as a consequence of demethylation of MP to P (Boreham et al. 1988; Radke et al. 1982b). If a reversal has occurred, Boreham et al. (1988) define a separate equation that should be used to determine a more accurate estimate of Rc(MPI):

$$Rc(MPI) = -0.55 * MPI + 3.0 \quad (8)$$

Table 7 and Figure 10 report R_c(MPDF), R_c(MPR) and R_c(MPI), based on equation 5, 6 and 7. The R_c values for Carrara 1 calculated using bitumen reflectance values (VREq) from Ranasinghe and Crosdale (2022) are also reported in Figure 10. In addition, the threshold values for hydrocarbon generative

windows defined by Tissot and Welte (1984) have been added to Figure to provide a rough estimate of the generative windows of the samples. R_c(MPDF) reports a maturity trend that ranges from Rc = 0.49% just above the unconformity to 1.09% directly below it and reaching a maximum of 1.46% at 1244 m (Table 7 and Figure10). The steep increase in maturity across the unconformity of 0.6% is likely the result of the loss of sediment at the erosional unconformity (Grosjean et al. 2022). Using equation 6 which assumes P and MP have not experienced a reversal, R_c(MPI) illustrates a similar trend with increasing maturity from R_c = 0.65% above the unconformity to 1.10% below it, reaching a maximum of 1.50% at 1345 m (Table 7 and Figure 10). Again, there is a steep jump of 0.45% in maturity likely due to the unconformity. Applying equation 8, for R_c(MPI) assuming the Paleoproterozoic samples have experienced a reversal in P and MP, returns much higher maturities reaching a maximum of 2.40% at 1405 m (Table 7 and Figure 10). VREq values also increase as a function of depth. The VREq above and below the unconformity is 0.69% and 1.44% respectively again illustrating the increase in maturity as a consequence of the unconformity (Table 7 and Figure 10). The VREq values for the Paleoproterozoic samples are much higher and more closely resemble R_c(MPI) using equation 8, reaching a maximum of 2.44% at 1405 m. Though R_c(MPDF), R_c(MPR) and VREq report different absolute values, they illustrate a very similar trend in maturity as a function of depth. Since they are based on different properties (molecular isomerisation and the reflectance of bitumen), this trend in maturity indicates that the aromatic hydrocarbons are indigenous and not migrated or notably affected by contaminants

Table 7 Maturity estimates of Carrara 1 source rocks and oils

Sample	Depth (m)	MPI	MPDF	MPR	Rc(MPI)[a]	Rc(MPI)[b]	Rc(MPDF)[c]	Rc(MPR)[d]	VREq[e]	P/MP
7533132	361.71	0.44	0.31	0.78	0.53	-	0.64	0.76	0.71	0.58
7533139	394.97	0.46	0.29	0.55	0.55	-	0.62	0.79	0.63	0.48
7533159	494.48	0.46	0.56	1.53	0.54	-	0.54	0.83	0.69	0.34
6725604	528.33	-	-	-	-	-	-	-	-	-
7533185	610.47	0.42	0.42	0.89	0.52	-	0.49	0.68	-	0.33
7533204	689.82	1.16	0.47	1.44	1.03	-	1.09	1.12	1.44	0.28
7533210	719.21	0.86	0.38	1.15	0.82	-	0.78	0.89	1.30	0.16
7373044	763.10	0.94	0.44	1.00	0.88	-	0.83	0.94	-	0.15
7373046	763.10	0.83	0.39	0.83	0.80	-	0.71	0.86	-	0.11
7533225	794.71	1.05	0.53	1.52	0.96	-	0.89	1.10	-	0.15
7533569	925.37	0.71	0.56	1.67	0.72	-	0.69	1.00	1.65	0.19
7533584	998.66	1.29	0.71	4.10	1.12	-	1.03	1.12	1.66	0.15
7533609	1069.16	1.23	0.63	2.67	1.08	2.33	1.10	1.16	-	0.25
7533625	1150.08	1.41	0.72	4.07	1.21	2.22	1.42	1.55	2.26	0.46
7533635	1199.60	1.48	0.71	4.89	1.26	2.19	1.24	1.36	-	0.26
7533644	1244.79	1.33	0.72	4.10	1.15	2.27	1.46	1.54	2.30	0.54

7533668	1345.03	1.83	0.68	3.00	1.50	1.99	1.42	1.62	2.35	0.28
7533682	1405.10	1.09	0.31	0.78	0.98	2.40	1.45	1.55	2.44	0.72
7533705	1461.32	1.50	0.29	0.55	1.27	2.18	1.35	1.41	2.42	0.35

[a] R_c(MPI) calculated using equation 3 in Boreham et al. (1988) and equation 2 in this report
[b] R_c(MPI) calculated using equation 5 in Boreham et al. (1988) and equation 7 in this report
[c] R_c(MPDF) calculated using equation 4 in Kvaldheim et al. (1987) and equation 2 in this report
[d] R_c(MPR) calculated using equation 3 in this report (See Radke et al. (1984)
[e] VREq calculated using bitumen reflectance by Ranasinghe & Crosdale (2022)

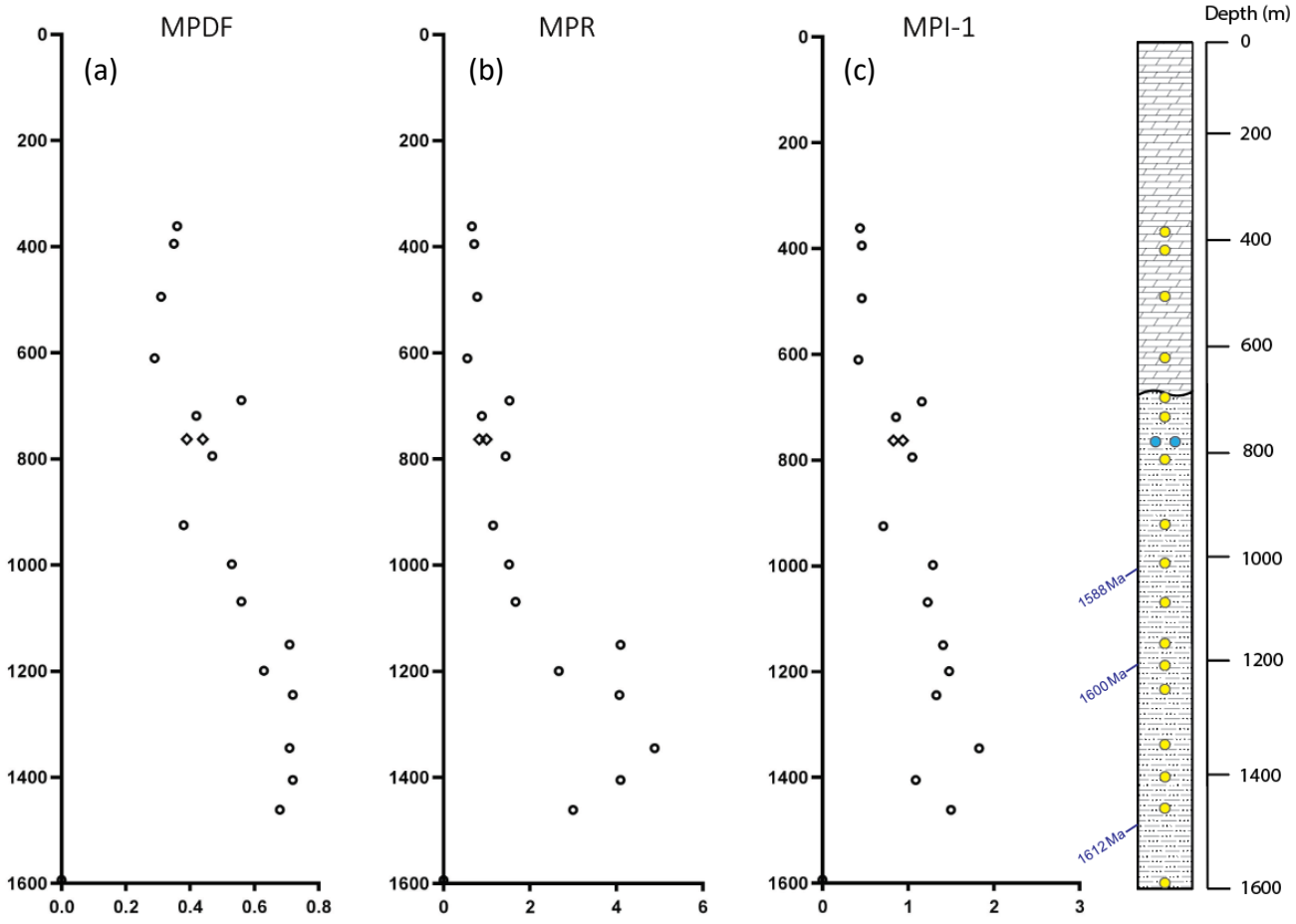

Figure 9 Maturity parameters based on phenanthrene (P) and methylphenanthrene (MP) concentrations correlated with the downcore plot of the Carrara 1 drill core. Open circles are rocks samples and diamonds are oil stains.

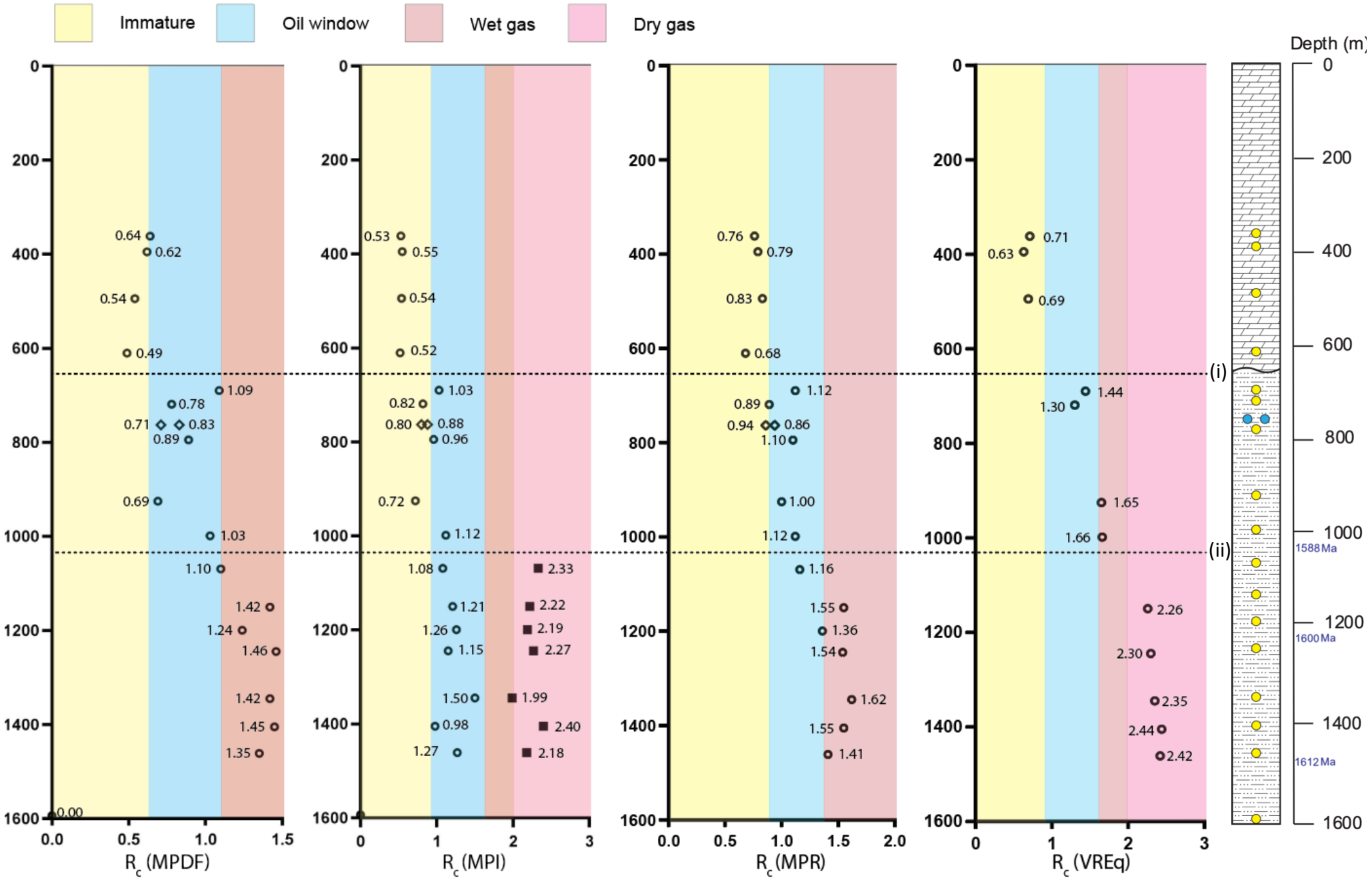

Figure 10 (a) Vitrinite reflectance (R_c) based on MPDF. **(b)** R_c based on MPI-1, circles using equation 6, squares using equation 8 to account for a potential reversal in P and MP with maturity. **(c)** R_c based on MPR. **(d)** R_c using bitumen reflectance (VRE_q) from Ranasinghe & Crosdale (2022). The approximate hydrocarbon generative windows defined by Tissot and Welte (1984) have been added to the Figure to provide a rough estimate of the generative window each sample. The dashed lines correlate with (i) the unconformity at 630 m and (ii) 1012 m below which, samples are absolutely dated to be Paleoproterozoic.

5: Discussion

5.1 Thermal maturity and generative potential of Carrara 1 source rocks

5.1.1. Thermal maturity of Cambrian samples (top – 630 m)

The R_c values based on P and MP suggest that the Cambrian samples are in the peak oil window indicating that they have excellent source rock generative potential (Table 10) (Tissot & Welte 1984). R_c(MPDF) ranges from 0.49-0.64%, R_c(MPI) is 0.52-0.55% and R_c(MPR) is 0.68-0.83% (Table 7 and Figure 10). Rock-eval data including TOC and the hydrogen index (HI) for Carrara 1 samples (Table 1 and summarised by Grosjean at et. (2022)), confirm that the samples are characteristic of highly generative source rocks. Furthermore, the presence of fluorescing lamalginite and liptinite reported by Ranasinghe and Crosdale (2022) provide further evidence that this stratigraphic section is in the peak oil window (Ranasinghe and Crosdale 2022). The presence of an oil stain (6725604, 528.33 m) indicates that this section has at least at some point, produced oil. As previously mentioned, none of the Carrara 1 samples have any detectable vitrinite which is required to calculate R_0 (Ranasinghe and Crosdale 2022). However, it is possible to use bitumen, one of the most common organoclasts found in Palaeozoic rocks Ranasinghe and Crosdale (2022), to determine vitrinite reflectance equivalent (VREq) by mathematically manipulating the measured reflectance of bitumen using the equations summarised by Luo et al. (2021). Ranasinghe and Crosdale (2022) calculated the VREq of 25 samples from the Carrara 1 drill core and determined a VREq range from 0.63-2.96 for the entire core and 0.63-0.71 for the Cambrian samples (Ranasinghe and Crosdale 2022) VREq reported by Ranasinghe and Crosdale (2022) correlates well with R_c computed using the P and MP parameters adding credibility to the maturity of this stratigraphic sequence (see Table 7 and Figure 10 for a juxtaposition of these values with those calculated in the present study). The similarity of maturity result from Ranasinghe & Crosdale (2022), Grosjean et al. (2022) and the present study provides convincing evidence that the Cambrian section of the Carrara 1 core is in the general maturity range to be generating liquid hydrocarbons.

5.1.2. Thermal maturity of Proterozoic stratigraphic sequence between 630 m and 1012 m

The thermal maturity of the Proterozoic sequence between 630-1012 m is characteristically more mature than the overlying Cambrian samples. All P and MP parameters report a similar maturity and R_c(MPDF) ranges from 0.69-1.09, R_c(MPI) ranges from 0.72-1.12 and R_c(MPR) ranges from 0.89-1.12 indicating that these samples are in the very late stages of oil generation and possibly producing wet gas (Table 7 and Figure 10). The break in the trend at 630m is also reported by Grosjean et al. (2022) and is the consequence of the loss of sediment at the unconformity that sits at this depth (Carson et al. 2022; Grosjean

et al. 2022). T_{max} data couldn't be used to determine thermal maturity in these samples due to poorly resolved S2 peaks which can often lead to inaccurate T_{max} values (Grosjean et al. 2022). Despite this, the VREq values calculated between 630 – 1012 m ranged from 1.30-1.69 (Table 7 and Figure 10) indicating that these samples are overmature in terms of oil generation and are likely producing wet gas (Ranasinghe and Crosdale 2022). However, there are two oil stains from this section which indicates that at least at some point, it has produced oil. Since the thermal maturity of the oils is consistent with surrounding sediments, it is likely they originated close to where they were found, providing further evidence that this section has been, and may still be generating liquid hydrocarbons.

5.1.3. Thermal maturity of Paleoproterozoic stratigraphic sequence between 1012 m and 1750.85 m

According to the thermal maturity parameters calculated using P and MP, R_c(MPI) ranges between 0.98-1.5%, R_c(MPDF) ranges form 1.10-1.46% and R_c(MPR) from 1.16-1.62% indicating that every sample in the Paleoproterozoic section of the core is overmature in terms of oil generation and is most likely producing wet or possible dry gas (Figure 10) (Tissot and Welte 1984). Compared to the VREq calculated by Ranasinghe and Crosdale (2022), which range between 1.69-2.96% (Table 7) R_c(MPI), R_c(MPDF) and R_c(MPR) in this study are much lower. As mentioned in chapter 4, P and MP can vary in unexpected ways in bitumens that have experienced extremely high thermal maturities, and in some cases, the trend in P/MP can reverse (Boreham et al. 1988; Brocks et al. 2003a). As the bitumen experiences increasing thermal maturity and pyrolytic degradation, several chemical processes will take place. These can include the demethylation of methyl, di-methyl, and tri-methyl phenanthrenes to P and to a lesser extent the re-alkylation of P to MP (Brocks et al. 2003a; Peters et al. 2005). It is generally considered that the demethylation mechanism reaches equilibrium at MPI ≈ 1.7% (Boreham et al. 1988) but if thermal degradation persists beyond this point, the re-alkylation of P into MP will continue and ultimately reverse the trend in P/MP (Boreham et al. 1988; Peters et al. 2005). Figure 6 illustrates an apparent reversal in P/MP values deeper than 1000 m, however, the MPI of these samples is < 1.7% which according to Boreham et al. (1988), is the point where demethylation of alkylated phenanthrenes should reach equilibrium. Boreham et al. (1988) mention that this estimate was made based on only four samples and is not well defined (Boreham et al. 1988, p. 291) and therefore, it is plausible that the Carrara samples > 1000 m have experienced a true reversal in P/MP. If this is the case, Boreham et al. (1988) define a separate equation to determine the MPI that considers the reversal trend (see equation 8 in chapter 4). Figure 10b illustrates the new R_c(MPI) for samples > 1000 m based on this alternative equation which range from 1.99-2.40%. These values are much more similar to the VREq values reported by Ranasinghe and Crosdale (2022), 1.69-2.96% and are possibly a better indication of the thermal maturity of the Carrara samples > 1000 m, although it has to be noted that it is unclear whether the reversal equation is applicable for the Carrara 1 samples given

the relative P and MP abundances are so different from those of Boreham (1988). If applicable however, both datasets now indicate that these deep samples are beyond the wet gas zone and are more likely producing dry gas or are completely overmature in terms of hydrocarbons generation (Tissot and Welte 1984; Ranasinghe and Crosdale 2022). The extreme maturity of the samples > 1000 m is further supported by the absence of saturated hydrocarbons (Figure 8) and the presence of PAHs such as benzo[a]pyrene and benzo[ghi]perylene (Figure 6), both of which are consistent with pyrolytically altered bitumen (Brocks et al. 2003a; George 1992).

5.2 Biomarker distribution in the Carrara 1 drill core

5.2.1. Biomarker distribution of Cambrian samples (top – 630 m)

Based on clean sand blanks and exterior/interior (E/I) experiments, the internal fractions of the Carrara 1 drill core have indigenous biomarkers in the Cambrian sediments as deep as 630 m (Table 4). These include steranes, hopanes, tricyclic terpanes and aryl isoprenoids. The most common eukaryote biomarkers are the trifecta steranes, C_{27} cholestane, C_{28} ergostane and C_{29} stigmastane (Brocks et al. 2017). The Cambrian samples of the Carrara 1 core have an abundance and distribution of these steranes that is expected and in keeping with the current biomarker record (Brocks et al. 2017; Brocks 2018). It is well established that by the Cambrian period, eukaryotes had diversified and surpassed bacteria as the dominant primary producers in the oceans, and this is reflected in the abundance of steranes in the Cambrian samples of the Carrara 1 core. Generally, C_{29} stigmastane and C_{28} ergostane are the predominant steranes in primary endosymbiotic algae and secondary endosymbiotic algae respectively (Brocks et al. 2017; Grice & Eisereck 2014). The C_{27} cholestane measured in the Cambrian samples is most likely derived from rhodophyte algae which were present in the Cambrian oceans and show a general sterol skeleton composed of 80:16:4% cholestane, ergostane and stigmastane respectively. Furthermore, the sterane/hopane (S/H) ratios calculated for the Cambrian samples are characteristically high compared to values during Precambrian (see Brocks et al. 2017), reflecting the ecological dominance of eukaryotes (Table 4 and Figure 4e). Hopanes are also detected in abundance in the Cambrian samples, especially in sample 7533159 (494.48 m) and 7533185 (610.47 m) illustrated by their relatively low S/H ratios of 0.35 and 0.29 compared to other samples, 0.68, 0.48 and 0.56 (Table 4 and Figure 4e). The abundance of hopanes and the corresponding S/H values is consistent with biomarker record reported by Brocks et al. (2017).

Trimethyl aryl isoprenoids (TMAI) are detected in Cambrian source rocks (but not the Cambrian oil stain) from C_{10} to C_{23}. TMAI can be produced by random isomerisation patterns at R_c(MPI) values > 0.8-1.0 (Vinnichenko et al. 2020). The Cambrian samples have an R_C(MPI) between, 0.68-0.83, indicating that it is unlikely that TMAI are isomerisation products and might be derived from a biogenic precursor. 2,3,6

TMAI and 2,3,4 TMAI are common break down products of C_{40} carotenoids which are produced by green and purple sulphur reducing bacteria respectively (Brocks et al. 2005; Palmisano et al. 1989; Vinnichenko et al. 2020). Green sulphur bacteria strictly inhabit anoxic waters within the photic zone down to depths of 100 m, while purple sulphur bacteria have a higher oxygen tolerance and light requirement (Brocks & Schaeffer 2008; Vinnichenko et al. 2020). Subsequently, purple sulphur bacteria often thrive just above the green sulphur bacteria at the anoxic-oxic boundary. Therefore, the presence of both TMAI isomers indicate that green and purple sulphur bacteria were part of the ocean ecosystem of the Carrara Sub-basin during the Cambrian, indicating that the depositional environment reflected a shallow, stratified environment with a strong chemocline (Vinnichenko 2020).

Acyclic saturated hydrocarbons are detected in all of the Cambrian samples and exhibit a typical Phanerozoic distribution characteristic of "facies 3" defined by Pawlowska et al. (2013) (Figure 8a-f). Facies 3 characteristics observed in these samples include a low unresolved complex mixture (UCM) and a high abundance of *n*-alkanes compared to mono-methyl alkanes (MMA) and dimethyl alkanes (DMA) both of which indicate low heterotrophic reworking characteristic of younger sediments (Alexander et al. 2011; Pawlowska et al. 2013) Based on all three CPI parameters, there is generally an odd/even predominance from C_{15}-C_{19} in the Cambrian samples, especially for the oil stain 6725604 (528.33 m) which is feature of many Palaeozoic bitumens (Jarrett et al. 2019b; Xianying et al. 2015). This is most likely as a result of the phototrophic organism *Gloeocapsomorpha prisca* of which the attribution as an algae or cyanobacterium is still debated (Evans 1994; Fowler 1992). Regularly branched isoprenoids, namely pristane and phytane are also identified in abundance in the Cambrian samples with pristane/phytane (Pr/Ph) ratios that range from 0.87 – 1.60 (Table 3). Generally, Pr/Ph < 1 or > 1 indicates anoxic or oxic source rock depositional environment respectively (Peters et al. 2005). Pr/Ph < 0.8 is often characteristic of anoxic, hypersaline or carbonate environments which is consistent with the depositional environment of the Carrara Sub-basin described by Crombez et al. (2022) between 630-800 and 965-1130 m.

5.2.2. Biomarker distribution of Proterozoic samples (630 – 1751.85 m)

Indigenous steranes, hopanes, tricyclic terpanes and TMAIs were all below detection limits in samples between the unconformity at 630 m and the total depth (TD) of 1750.85 m. However, acyclic saturated hydrocarbons were detected in the source rocks and oils between 689.85 – 925.50 m, and in sample 7533609 (1069.32 m). The lack of polycyclic biomarkers in all Proterozoic samples could be the consequence of several processes. First, the biological source of the biomarkers did not yet exist or played a very minor role in the ecosystem when the sediment was deposited. The earliest definitive evidence of eukaryotes, the most common source of the trifecta steranes, come from 1800-million-year-old sediments from the Changzougou formation in Northern China (Lamb et al. 2009). However, it is believed that they played a

very minor role in Earth's ecosystem until their diversification during the Neoproterozoic (Brocks et al. 2015; Brocks 2018; Erwin et al. 2011). According to Brocks et al. (2017) and Brocks (2018), cholestane is not detected until 820 Ma as a result of the rise in Rhodophyte algae, and stigmastane and ergostane don't appear until 635 Ma after the rise of green algae (Brocks et al. 2017; Brocks 2018; Grantham & Wakefield 1988; Porter 2020). SHRIMP zircon U-Pb geochronology illustrates that the sediment from 1200-1600m was deposited between 1600-1612 Ma (Carson et al. 2022) and thus it is in keeping with this evidence that steranes are below detection limits in the Proterozoic samples. In contrast, bacteria producing the parent molecules of hopanes and trimethyl aryl isoprenoids (TMAI), undoubtedly existed at the time when these samples were deposited (Brocks et al. 2017; Jarret et al. 2019a). Hopanes and TMAI have been previously reported in mid-late Paleoproterozoic sediments up to 1.64 Ga old (Brocks et al. 2005). Vinnichenko et al. (2020) analysed samples from the 1.73 Ga Wollogorang formation in the southern McArthur Basin and detected a continuous series of low molecular weight 2,3,6-trimethyl aryl isoprenoids which are interpreted as indigenous (Vinnichenko et al. 2020). As mentioned earlier, TMAIs are produced by cyanobacteria and or green and purple sulphur bacteria and are a relatively common element of the Proterozoic biomarker record since the Proterozoic oceans were anoxic, stratified and sulphidic creating the perfect habitat for these kinds of organisms (Brocks et al. 2005). The absence of TMAI in the Proterozoic section of the core is interesting because it would distinguish it from other nearby Proterozoic basins such as the Barney Creek formation (Brocks et al. 2005; Brocks and Lee 2011). The absence of TMAI was also observed by Jarret et al. (2019a) in the 1380 Ma Velkerri formation in the McArthur Basin. Based on the thermal maturity of the samples, they concluded that while thermal degradation affected the TMAI abundance of the sample, their absence is more likely the result of heterotrophic reworking and/or the fact that the basin was never inhabited by sulphur bacteria (Jarrett et al. 2019a). In the case of the Carrara 1 samples, the thermal maturity indicates that the absence of TMAI is the consequence of thermal degradation. It has been demonstrated that TMAI will be detectable to T_{max} values of 440-445°C before they are destroyed by thermal degradation (Brocks and Lee 2011). Based on Rock-Eval data for the Carrara 1 samples summarised from Grosjean et al. (2022) in Table 1, it would be unlikely to find indigenous TMAI in any of the Proterozoic samples. Furthermore, Jarrett et al. (2019b) demonstrate that hopanes drop below detection limits at MPDF > 0.39 and MPR > 1.03. The MPDF and MPR values for the Proterozoic samples range between 0.42-0.72 and 0.89-4.89 respectively indicating that hopanes once preserved in the Proterozoic sections of the Carrara 1 drill core have likely been destroyed by thermal degradation (See Figure 9).

5.3 Thermal maturity and biomarker evidence for a fault repeated system

Sample 7533204 (689.85 m) has a higher thermal maturity according to all P and MP parameters (Figure 9). For example, it has an MPI-1 value of 1.16 while in the overlying and underlying samples, MPI-1 =

0.42 and 0.89 respectively. (Figure 9c). This trend is also observed in the R_c values calculated based on these parameters (Table 7 and Figure 10). According to laboratory sand blanks and E/I experiments, the P and MP in the sample are indigenous and the unusually high thermal maturity is not caused by anthropogenic contamination. Crombez et al. (2022) analysed the sedimentology and sequence stratigraphy of the Carrara 1 core and found that between 630-800m, the sedimentology suddenly reverts to silt and shale intervals with detrital deposits that would indicate the detrital source was in close proximity to the well (Crombez et al. 2022). This is the same sedimentology that they report further downcore between 925-1130m. Based on this evidence, they cautiously conclude that there may be a fault-repeated section at 630-800 m from 925-1130 m (Crombez et al. 2022). Interestingly, the elevated thermal maturity of sample 7533204 (689.82 m, MPI-1 = 1.16) correlates well with the thermal maturity of the two samples between 925-1130m in this study (MPI-1 = 1.29 and 1.23). Furthermore, sample 7533204 (689.85 m) and 7533210 (719.21 m), are characteristically Proterozoic, reflecting a typical Proterozoic distribution defined as "facies 1" by Pawlowska et al. (2013). Facies 1 characteristics include, a high UCM, relatively abundant MMAs and DMAs compared to Phanerozoic counterparts and conspicuously depleted pristane and phytane (Pawlowska et al. 2013). However, the underlying sample 7533225 (794.80 m) has notably higher abundances of *n*-alkanes relative to MMA and UCM, characteristics that could somewhat resemble facies 3, possibly indicating less heterotrophic reworking of original biomass compared to typical facies 1 (Pawlowska et al. 2013). Interestingly, the underlying sample, 7533569 (925.50 m) reverts to a clear facies 1 distribution and resembles 7533204 (689.85 m) and 7533210 (719.21 m) (Figure 8). One explanation for this inconsistent trend is that sample 7533204 (689.85 m) and 7533210 (719.21 m) were originally deposited at a similar depth to 7533569 (925.50 m) which is in the range of the fault repeated system described by Crombez et al. (2022). As a consequence of this repetition, sample 7533204 (689.85 m) and 7533210 (719.21 m) now overlie 7533225 (794.80 m).

Polyaromatic hydrocarbons (PAHs) can provide a crude estimate of thermal degradation of a bitumen by comparing the more stable parent PAHs (pPAHs) to the less stable alkylated PAHs (aPAHs). Table 6, Figure 6 and inserts in Figure 8 illustrate pPAH/aPAH ratios for all samples as a function of depth. F/MF values for sample 7533204 (689.85 m) and 7533210 (719.21 m) are actually lower compared with the underlying sample 7533225 (794.80 m) while P/MP and Py/Mpy report similar values for all three samples (Table 6 and Figure 6). According to PAHs, it is inconclusive whether samples 7533204 (689.85 m) and 7533210 (719.21 m) were deposited earlier than sample 7533225 (794.80 m). Nevertheless, the thermal maturity estimated using P and MP data in addition to the distribution of acyclic saturated hydrocarbons are consistent with the interpretations that sample 7533204 (689.85 m) and 7533210 (719.21 m) are part of the repeated section from 925-1130 m. described by Crombez et al. 2022 and were originally deposited earlier than the now underlying sample 7533225 (794.80 m). However, additional data is required to validate the trend and draw more solid conclusions.

5.4 Unexpected distribution of saturated and aromatic biomarkers between 689m and 1069m as potential evidence of oil migration

One of the most notable characteristics of the Proterozoic samples of the Carrara 1 drill core is the trend in saturated hydrocarbons with depth. As previously discussed, the shallowest Proterozoic samples, 7533204, 7533210, 7533225 and 7533569 (689-925m) contain a typical biomarker distribution for the corresponding maturity (Pawlowska et al. 2013) (See Figure 8). Below this depth, saturated hydrocarbons are detected only in trace concentrations with the notable exception of sample 7533609 (1069.32 m). It exhibits a typical Proterozoic distribution of saturated hydrocarbons despite the fact that the overlying sample 7533584 (998 m) is devoid of these molecules (Figure 8m). The T_{max} of 494°C of sample 7533584 (998 m) indicates that the lack of hydrocarbons in sample 7533584 is likely a consequence of thermal degradation and since sample 7533609 (1069.32 m, T_{max} = 500°C) is underlying this sample, it should have a similar thermal maturity, which is confirmed by R_c (Figure 10) and thus, the bitumen should have experienced a similar level of thermal degradation. Figure 6 and Table 6 illustrates the pPAH/aPAH ratio which as previously discussed, can provide a crude estimate of thermal degradation of bitumens (Brocks et al. 2003b; Wang et al. 2022; Zylstra & Gibson 1991). Sample 7533584 (998 m) and 7533609 (1069.32 m) have very similar pPAH/aPAH ratios which, supports the hypothesis that they have experienced similar amounts of thermal degradation. This makes the presence of saturated hydrocarbons in sample 7533609 (1069.32 m) all the more intriguing. Below, two hypotheses are considered that could explain their presence.

5.4.1. Contamination

The first hypothesis for the presence of saturated and aromatic hydrocarbons in sample 7533609 (1069.32 m) is that they are anthropogenic contaminants derived from drilling fluids and diesel introduced when the sample was collected. It is well understood that these products can quickly contaminate and overprint indigenous signals, leading to misinterpretations (Brocks 2011; Brocks et al. 2008; Jarrett et al. 2013; Schinteie et al. 2019). As discussed in chapter 4, exterior/interior (E/I) analysis can be performed to determine the extent of exterior contamination and how much of this contamination has penetrated the interior portion of the sample (Brocks 2011). Figure 2b illustrates the E/I values for *n*-alkanes in sample 7533609 (1069.32 m) which are well in the range to confidently interpret them as indigenous (Brocks 2011). Furthermore, if anthropogenic contaminants were to blame, other biomarkers that are more characteristic of Phanerozoic bitumens, should be detected (Brocks 2011). These could include steranes, hopanes, tricyclic terpanes and trimethyl aryl isoprenoids, none of which are detected in this sample (see section 5.2.2). Furthermore, anthropogenic contaminants should also be detected in the aromatic fraction, however, the computed ratios of PAHs for this sample are consistent with the expected distribution for a Proterozoic

bitumen at the given depth (Brocks et al. 2003a; George 1992; Pawlowska et al. 2013;). It is therefore unlikely that the presence of saturated hydrocarbons in this sample are derived from anthropogenic contaminants.

5.4.2. Secondary migration of liquid hydrocarbons

An alternate hypothesis for the presence of saturated hydrocarbons in sample 7533609 (1069.32 m) is that is has been contaminated by secondary oil migration. Secondary oil migration is the process by which hydrocarbons are released via cracks and fissures in the rock and migrate to adjacent sequences and towards reservoirs and seeps (Larter et al. 1996; Selley & Richard 2014). In this case, the indigenous signal of the bitumen could have been overprinted by a locally migrated oil. In a similar way to anthropogenic contamination, migrating oil will also affect the aromatic fraction. The insert in Figure 8m illustrates chromatograms for the aromatic fraction between 34 and 76 minutes which contains important PAHs including the P and MP. The Figure illustrates that the peaks are less defined, and the chromatogram is noisier compared to other Proterozoic samples which could indicate that this sample has been partially overprinted. Since the thermal maturity based on P and MP values and other PAH ratios are consistent with overlying and underlying Proterozoic samples in the core, the migrated oil must have originated nearby. The two oil stains at 763.10 m illustrate that source rocks in this section have at least experienced primary migration of liquid hydrocarbons (the release of oil through cracks and fissured in the rock). As previously mentioned, the maturity of these oil stains indicates that they originate very close to where they were found providing further evidence that a nearby oil might have overprinted the indigenous signal of 7533609 (1069.32 m). The evidence is relatively crude and inconclusive and further investigation is required to determine if secondary oil migration is the source of saturated hydrocarbons in sample 7533609 (1069.32 m).

6: Conclusion

The Carrara 1 drill core intersects several interesting intervals in terms of geobiological research and resource exploration. The Georgina basin, which represents the top 630 m of the core is rich in prokaryote and eukaryote biomarkers identified using GC/MS analysis which are interpreted as indigenous biomarkers according to exterior/interior experiments and comparison of samples to laboratory sand blanks. This section of the core spans the early-middle Cambrian period providing valuable data to support and strengthen the current biomarker record. According phenanthrene (P) and methylphenanthrenes (MP) thermal maturity assessment, the samples above 630 m are in the peak oil window and are likely highly generative in terms of liquid hydrocarbons, which is further supported by the presence of an oil stain at 528.33 m. These findings compliment and support the previous findings reported by Ranasinghe & Crosdale (2022) and Grosjean et al. (2022) further cementing the importance of the Carrara sub-basin for future hydrocarbon exploration in line with the objectives of the Exploring for the Future initiative. Thermal maturity and biomarker data provide strong evidence for an unconformity at 630 m, initially postulated by Carr et al. (2019) separating the Cambrian samples from the much older Proterozoic samples. According to calculated vitrinite reflectance (R_c) using P and MPs, the thermal maturity increases steeply across this boundary and polycyclic biomarkers are below detection limits in the Proterozoic package. Acyclic saturated hydrocarbons, including pristane and phytane, are detected in the shallower Proterozoic samples.

In addition, the peculiar thermal maturity value, and the distribution of aromatic and acyclic saturated hydrocarbons in sample 7533204 (689.85) suggests that this sample may have originally been deposited between 998-1069m, which is consistent with a fault-repeating system between 630-800 m from 925-1130 m, hypothesised by Crombez et al. (2022). The absence of most biomarkers in the samples and distribution of acyclic saturated hydrocarbons in parallel with high R_c values strongly suggest that the Proterozoic interval is part of the Paleoproterozoic Lawn Hill Platform, and it is either in the late stages of wet gas generation or is producing dry gas.

Finally, the data presented here in addition to the oil stains discovered at 763.10 m indicates that secondary migration of liquid hydrocarbons may have overprinted at least one of the Paleoproterozoic samples of Carrara 1 affecting the distribution of saturated hydrocarbons. If secondary oil migration is responsible for the peculiar distributions of these hydrocarbons, the source of the migrating oil is not far from the sample. However, further work will be required to determine the extent of secondary oil migration in Carrara 1.

The data collected to compile this master's project is part of a much larger initiative to understand the geology, resource potential and paleobiology of Northern Australia. Though we still have much to learn about these basins, the data presented here is instrumental to our understanding of the Carrara Sub-

basin and will provide a strong foundation for further exploration as we continue to uncover the secrets of the early Earth that would otherwise remain locked away in deep time.

VI. References

Abdullah, E.S., Ebiad, M.A., Rashad, A.M., El Nady, M.M., El-Sabbagh, S.M., 2021. Thermal maturity assessment of some Egyptian crude oils as implication from naphthalene, phenanthrene and alkyl substituents. Egyptian Journal of Petroleum 30, 17–24. https://doi.org/10.1016/j.ejpe.2020.12.004

Alalade, B. and Tyson, R.V., 2013. Influence of igneous intrusions on thermal maturity of Late Cretaceous shales in the Tuma well, Chad Basin, NE Nigeria. *Journal of African Earth Sciences*, *77*, pp.59-66. https://doi.org/10.1016/j.jafrearsci.2012.09.006

Alexander, R., Berwick, L. and Pierce, K., 2011. Single carbon surface reactions of 1-octadecene and 2, 3, 6-trimethylphenol on activated carbon: implications for methane formation in sediments. *Organic Geochemistry*, *42*(5), pp.540-547.

Anbar, A., Knoll, A., 2002. Anbar, A. D. & Knoll, A. H. Proterozoic ocean chemistry and evolution: A bioinorganic bridge? Science 297, 1137-1142. Science (New York, N.Y.) 297, 1137–42. https://doi.org/10.1126/science.1069651

Anderson, J., Carson, C., Lewis, C., Cross, A., Carr, L., Henson, P., Kositcin, N., 2019b. Exploring for the future: new U-Pb geochronology for the South Nicholson region and implications for stratigraphic correlations. ASEG Extended Abstracts 2019, 1–5. https://doi.org/10.1080/22020586.2019.12073005

Andrews, S.J., 1998a. Stratigraphy and depositional setting of the upper McNamara Group, Lawn Hills region, Northwest Queensland. Economic Geology 93, 1132–1152. https://doi.org/10.2113/gsecongeo.93.8.1132

Assessing the syngeneity and indigeneity of hydrocarbons in the ∼1.4 Ga Velkerri Formation, McArthur Basin, using slice experiments - ScienceDirect n.d. https://doi.org/10.1016/j.orggeochem.2014.10.008

Basin and Petroleum System Modeling , n.d. . SpringerLink. URL https://link.springer.com/chapter/10.1007/978-3-319-49347-3_11 (accessed 4.23.22).

Becker, B., Marin, B., 2009. Streptophyte algae and the origin of embryophytes. Ann Bot 103, 999–1004. https://doi.org/10.1093/aob/mcp044

Bennett, W.W., Canfield, D.E., 2020. Redox-sensitive trace metals as paleoredox proxies: A review and analysis of data from modern sediments. Earth-Science Reviews 204, 103175. https://doi.org/10.1016/j.earscirev.2020.103175

Betts, H.C., Puttick, M.N., Clark, J.W., Williams, T.A., Donoghue, P.C.J., Pisani, D., 2018. Integrated genomic and fossil evidence illuminates life's early evolution and eukaryote origin. Nature Ecology & Evolution 2, 1556–1562. https://doi.org/10.1038/s41559-018-0644-x

Bloch, K., 1964. The biological synthesis of cholesterol 23.

Blumenberg, M., Thiel, V., Riegel, W., Kah, L.C., Reitner, J., 2012a. Biomarkers of black shales formed by microbial mats, Late Mesoproterozoic (1.1Ga) Taoudeni Basin, Mauritania. Precambrian Research 196–197, 113–127. https://doi.org/10.1016/j.precamres.2011.11.010

Blumenberg, M., Seifert, R., Buschmann, B., Kiel, S., Thiel, V., 2012b. Biomarkers Reveal Diverse Microbial Communities in Black Smoker Sulfides from Turtle Pits (Mid-Atlantic Ridge, Recent)

and Yaman Kasy (Russia, Silurian). Geomicrobiology Journal 29, 66–75. https://doi.org/10.1080/01490451.2010.523445

Bobrovskiy, I., Hope, J., Brocks, J., 2019. Reinterpretation of the Sterane/Hopane Ratio and Sterane Homolog Distributions. https://doi.org/10.3997/2214-4609.201903055

Bobrovskiy, I., Hope, J.M., Ivantsov, A., Nettersheim, B.J., Hallmann, C., Brocks, J.J., 2018. Ancient steroids establish the Ediacaran fossil Dickinsonia as one of the earliest animals. Science 361, 1246–1249. https://doi.org/10.1126/science.aat7228

Bobrovskiy, I., Hope, J.M., Nettersheim, B.J., Volkman, J.K., Hallmann, C., Brocks, J.J., 2021. Algal origin of sponge sterane biomarkers negates the oldest evidence for animals in the rock record. Nat Ecol Evol 5, 165–168. https://doi.org/10.1038/s41559-020-01334-7

Boreham, C.J., Crick, I.H., Powell, T.G., 1988. Alternative calibration of the Methylphenanthrene Index against vitrinite reflectance: Application to maturity measurements on oils and sediments. Organic Geochemistry 12, 289–294. https://doi.org/10.1016/0146-6380(88)90266-5

Brasier, M.D., Lindsay, J.F., 1998. A billion years of environmental stability and the emergence of eukaryotes: New data from northern Australia 4. https://doi-org.virtual.anu.edu.au/10.1130/0091-7613(1998)026<0555:ABYOES>2.3.CO;2

Briggs, D.E.G., 2015. The Cambrian explosion. Current Biology 25, R864–R868. https://doi.org/10.1016/j.cub.2015.04.047

Brocks, J.J., 2018. The transition from a cyanobacterial to algal world and the emergence of animals. Emerging Topics in Life Sciences 2, 181–190. https://doi.org/10.1042/ETLS20180039

Brocks, J.J., 2011. Millimeter-scale concentration gradients of hydrocarbons in Archean shales: Live-oil escape or fingerprint of contamination? Geochimica et Cosmochimica Acta 75, 3196–3213. https://doi.org/10.1016/j.gca.2011.03.014

Brocks, J.J., Buick, R., Summons, R.E., Logan, G.A., 2003a. A reconstruction of Archean biological diversity based on molecular fossils from the 2.78 to 2.45 billion-year-old Mount Bruce Supergroup, Hamersley Basin, Western Australia. Geochimica et Cosmochimica Acta 67, 4321–4335. https://doi.org/10.1016/S0016-7037(03)00209-6

Brocks, J.J., Grosjean, E., Logan, G.A., 2008. Assessing biomarker syngeneity using branched alkanes with quaternary carbon (BAQCs) and other plastic contaminants. Geochimica et Cosmochimica Acta 72, 871–888. https://doi.org/10.1016/j.gca.2007.11.028

Brocks, J.J., Jarrett, A.J.M., Sirantoine, E., Hallmann, C., Hoshino, Y., Liyanage, T., 2017. The rise of algae in Cryogenian oceans and the emergence of animals. Nature 548, 578–581. https://doi.org/10.1038/nature23457

Brocks, J.J., Jarrett, A.J.M., Sirantoine, E., Kenig, F., Moczydłowska, M., Porter, S., Hope, J., 2016. Early sponges and toxic protists: possible sources of cryostane, an age diagnostic biomarker antedating Sturtian Snowball Earth. Geobiology 14, 129–149. https://doi.org/10.1111/gbi.12165

Brocks, J.J., Logan, G.A., Buick, R., Summons, R.E., 1999. Archean Molecular Fossils and the Early Rise of Eukaryotes. Science 285, 1033–1036. https://doi.org/10.1126/science.285.5430.1033

Brocks, J.J., Love, G.D., Snape, C.E., Logan, G.A., Summons, R.E., Buick, R., 2003b. Release of bound aromatic hydrocarbons from late Archean and Mesoproterozoic kerogens via hydropyrolysis. Geochimica et Cosmochimica Acta 67, 1521–1530. https://doi.org/10.1016/S0016-7037(02)01302-9

Brocks, J.J., Love, G.D., Summons, R.E., Knoll, A.H., Logan, G.A., Bowden, S.A., 2005a. Biomarker evidence for green and purple sulphur bacteria in a stratified Palaeoproterozoic sea. Nature 437, 866–870. https://doi.org/10.1038/nature04068

Brocks, J.J., Love, G.D., Summons, R.E., Knoll, A.H., Logan, G.A., Bowden, S.A., 2005b. Biomarker evidence for green and purple sulphur bacteria in a stratified Palaeoproterozoic sea. Nature 437, 866–870. https://doi.org/10.1038/nature04068

Brocks, J.J., Schaeffer, P., 2008. Okenane, a biomarker for purple sulfur bacteria (Chromatiaceae), and other new carotenoid derivatives from the 1640Ma Barney Creek Formation. Geochimica et Cosmochimica Acta 72, 1396–1414. https://doi.org/10.1016/j.gca.2007.12.006

Brocks, J.J., Summons, R.E., 2014. 10.3 - Sedimentary Hydrocarbons, Biomarkers for Early Life, in: Holland, H.D., Turekian, K.K. (Eds.), Treatise on Geochemistry (Second Edition). Elsevier, Oxford, pp. 61–103. https://doi.org/10.1016/B978-0-08-095975-7.00803-2

Brocks, J.J., Summons, R.E., n.d. 8.03 Sedimentary Hydrocarbons, Biomarkers for Early Life 53. https://doi.org/10.1016/B978-0-08-095975-7.00803-2

Budd, G.E., Mann, R.P., 2018. History is written by the victors: The effect of the push of the past on the fossil record. Evolution 72, 2276–2291. https://doi.org/10.1111/evo.13593

Budzinski, H., Garrigues, Ph., Connan, J., Devillers, J., Domine, D., Radke, M., Oudins, J.L., 1995. Alkylated phenanthrene distributions as maturity and origin indicators in crude oils and rock extracts. Geochimica et Cosmochimica Acta 59, 2043–2056. https://doi.org/10.1016/0016-7037(95)00125-5

Burlage, R.S., Atlas, R., Stahl, D., Sayler, G., Geesey, G., 1998. Techniques in Microbial Ecology. Oxford University Press.

Butterfield, N.J., 2018. Oxygen, animals and aquatic bioturbation: An updated account. Geobiology 16, 3–16. https://doi.org/10.1111/gbi.12267

Butterfield, N.J., 2015. Early evolution of the Eukaryota. Palaeontology 58, 5–17. https://doi.org/10.1111/pala.12139

Butterfield, N.J., 2003. Exceptional Fossil Preservation and the Cambrian Explosion1. Integrative and Comparative Biology 43, 166–177. https://doi.org/10.1093/icb/43.1.166

Butterfield, N. J., Knoll, A.H., Swett, K., 1990. A bangiophyte red alga from the Proterozoic of arctic Canada. Science 250, 104–107. https://doi.org/10.1126/science.11538072

Canfield, D.E., Farquhar, J., 2009. Animal evolution, bioturbation, and the sulfate concentration of the oceans. Proc Natl Acad Sci U S A 106, 8123–8127. https://doi.org/10.1073/pnas.0902037106

Carr, L., Southby, C., Henson, P., Carson, C., Anderson, J., Macfarlane, S., Jarrett, A., Fomin, T., Costelloe, R., 2019a. Exploring for the Future: South Nicholson Basin region project outcomes and sequence stratigraphy.

Carr, L., Southby, C., Henson, P., Costelloe, R., Anderson, J., Jarrett, A., Carson, C., Macfarlane, S., Gorton, J., Hutton, L., Troup, A., Williams, B., Khider, K., Bailey, A., Fomin, T., 2019b. Exploring for the Future: South Nicholson Basin Geological summary and seismic data interpretation. https://doi.org/10.11636/Record.2019.021

Carson, C.J., Kositcin, N., Henson, P.A., Delle Piane, C., Crombez, V., Grosjean, E., Jarrett, A.J.M., Butcher, G., 2022. Exploring for the Future - SHRIMP U–Pb zircon geochronology from NDI Carrara 1 and implications for regional stratigraphic correlations, resource potential and geological evolution of the Carrara Sub-basin. AGES 2022 Proceedings, NT Geological Survey.

Chai, Z., Chen, Z., Liu, H., Cao, Z., Cheng, B., Wu, Z., Qu, J., 2020. Light hydrocarbons and diamondoids of light oils in deep reservoirs of Shuntuoguole Low Uplift, Tarim Basin: Implication for the evaluation on thermal maturity, secondary alteration and source characteristics. Marine and Petroleum Geology 117, 104388. https://doi.org/10.1016/j.marpetgeo.2020.104388

Chen, J., Fu, J., Sheng, G., Liu, D., Zhang, J., 1996. Diamondoid hydrocarbon ratios: novel maturity indices for highly mature crude oils. Organic Geochemistry 25, 179–190. https://doi.org/10.1016/S0146-6380(96)00125-8

Chernikova, D., Motamedi, S., Csürös, M., Koonin, E.V., Rogozin, I.B., 2011. A late origin of the extant eukaryotic diversity: divergence time estimates using rare genomic changes. Biology Direct 6, 26. https://doi.org/10.1186/1745-6150-6-26

Crombez, V., n.d. NDI Carrara 1 sedimentology and sequence stratigraphy 18. https://dx.doi.org/10.26186/146338

De Grande, S.M.B., Aquino Neto, F.R., Mello, M.R., 1993. Extended tricyclic terpanes in sediments and petroleums. Organic Geochemistry 20, 1039–1047. https://doi.org/10.1016/0146-6380(93)90112-O

Dembicki, H., Jr., 2009. Three common source rock evaluation errors made by geologists during prospect or play appraisals. AAPG Bulletin 93, 341–356. https://doi.org/10.1306/10230808076

Des Marais, D.J., 1995. The Biogeochemistry of Hypersaline Microbial Mats, in: Jones, J.G. (Ed.), Advances in Microbial Ecology, Advances in Microbial Ecology. Springer US, Boston, MA, pp. 251–274. https://doi.org/10.1007/978-1-4684-7724-5_6

Dow, W.G., 1977. Kerogen studies and geological interpretations. Journal of Geochemical Exploration 7, 79–99. https://doi.org/10.1016/0375-6742(77)90078-4

Dutkiewicz, A., Volk, H., Ridley, J. and George, S., 2003. Biomarkers, brines, and oil in the Mesoproterozoic, Roper Superbasin, Australia. *Geology*, *31*(11), pp.981-984. 10.1130/G19754.1

Eigenbrode, J., 2011. Molecular Fossils, in: Gargaud, M., Amils, R., Quintanilla, J.C., Cleaves, H.J. (Jim), Irvine, W.M., Pinti, D.L., Viso, M. (Eds.), Encyclopedia of Astrobiology. Springer, Berlin, Heidelberg, pp. 1070–1076. https://doi.org/10.1007/978-3-642-11274-4_1015

Erwin, D.H., Laflamme, M., Tweedt, S.M., Sperling, E.A., Pisani, D., Peterson, K.J., 2011. The Cambrian Conundrum: Early Divergence and Later Ecological Success in the Early History of Animals. Science 334, 1091–1097. https://doi.org/10.1126/science.1206375

Evans, W.G., 1994. Volatile organic chemicals of a shore-dwelling cyanobacterial mat community. *Journal of chemical ecology*, *20*(2), pp.219-230.

Farrimond, P., Bevan, J.C., Bishop, A.N., 1999. Tricyclic terpane maturity parameters: response to heating by an igneous intrusion. Organic Geochemistry 30, 1011–1019. https://doi.org/10.1016/S0146-6380(99)00091-1

Farrimond, P., Taylor, A., TelnÆs, N., 1998. Biomarker maturity parameters: the role of generation and thermal degradation. Organic Geochemistry 29, 1181–1197. https://doi.org/10.1016/S0146-6380(98)00079-5

Fournier, G.P., Moore, K.R., Rangel, L.T., Payette, J.G., Momper, L., Bosak, T., 2021. The Archean origin of oxygenic photosynthesis and extant cyanobacterial lineages. Proceedings of the Royal Society B: Biological Sciences 288, 20210675. https://doi.org/10.1098/rspb.2021.0675

Fowler, M.G., 1992. The influence of Gloeocapsomorpha prisca on the organic geochemistry of oils and organic-rich rocks of Late Ordovician age from Canada. In *Early organic evolution* (pp. 336-356). Springer, Berlin, Heidelberg.

French, K.L., Hallmann, C., Hope, J.M., Schoon, P.L., Zumberge, J.A., Hoshino, Y., Peters, C.A., George, S.C., Love, G.D., Brocks, J.J., Buick, R., Summons, R.E., 2015. Reappraisal of hydrocarbon biomarkers in Archean rocks. PNAS 112, 5915–5920. https://doi.org/10.1073/pnas.1419563112

George, S.C., 1992. Effect of igneous intrusion on the organic geochemistry of a siltstone and an oil shale horizon in the Midland Valley of Scotland. Organic Geochemistry 18, 705–723. https://doi.org/10.1016/0146-6380(92)90097-H

George, S.C., Ahmed, M., 2002. Use of Aromatic Compound Distributions to Evaluate Organic Maturity of the Proterozoic Middle Velkerri Formation, Mcarthur Basin, Australia 253.

Geoscience Australia, Carrara 1 portal , n.d. URL https://portal.ga.gov.au/bhcr/minerals/648482 (accessed 5.27.21).

Gibson, G.M., Meixner, A.J., Withnall, I.W., Korsch, R.J., Hutton, L.J., Jones, L.E.A., Holzschuh, J., Costelloe, R.D., Henson, P.A., Saygin, E., 2016. Basin architecture and evolution in the Mount Isa mineral province, northern Australia: Constraints from deep seismic reflection profiling and implications for ore genesis. Ore Geol. Rev. 76, 414–441. https://doi.org/10.1016/j.oregeorev.2015.07.013

Gibson, T.M., Shih, P.M., Cumming, V.M., Fischer, W.W., Crockford, P.W., Hodgskiss, M.S.W., Wörndle, S., Creaser, R.A., Rainbird, R.H., Skulski, T.M., Halverson, G.P., 2018. Precise age of Bangiomorpha pubescens dates the origin of eukaryotic photosynthesis. Geology 46, 135–138. https://doi.org/10.1130/G39829.1

Gold, D.A., Caron, A., Fournier, G.P., Summons, R.E., 2017. Paleoproterozoic sterol biosynthesis and the rise of oxygen. Nature 543, 420–423. https://doi.org/10.1038/nature21412

Grantham, P.J., Wakefield, L.L., 1988. Variations in the sterane carbon number distributions of marine source rock derived crude oils through geological time. Organic Geochemistry 12, 61–73. https://doi.org/10.1016/0146-6380(88)90115-5

Grice, K., Cao, C., Love, G.D., Böttcher, M.E., Twitchett, R.J., Grosjean, E., Summons, R.E., Turgeon, S.C., Dunning, W., Jin, Y., 2005. Photic Zone Euxinia During the Permian-Triassic Superanoxic Event. Science 307, 706–709. https://doi.org/10.1126/science.1104323

Grice, K. and Eiserbeck, C., 2013. The analysis and application of biomarkers. In *Treatise on geochemistry* (pp. 47-78). Elsevier Science.

Grosjean, E., Love, G.D., Stalvies, C., Fike, D.A., Summons, R.E., 2009. Origin of petroleum in the Neoproterozoic–Cambrian South Oman Salt Basin. Organic Geochemistry 40, 87–110. https://doi.org/10.1016/j.orggeochem.2008.09.011

Grosjean, E., Jarrett, A., Boreham, C., Butcher, G., CJ, C., L, W., Munson, T., Henson, P., 2022. Reassessing stromatolite biostratigraphy in the East Tennant region, northern Australia: Implications for regional mineral prospectivity.

Gueneli, N., McKenna, A.M., Ohkouchi, N., Boreham, C.J., Beghin, J., Javaux, E.J., Brocks, J.J., 2018. 1.1-billion-year-old porphyrins establish a marine ecosystem dominated by bacterial primary producers. Proc Natl Acad Sci USA 115, E6978–E6986. https://doi.org/10.1073/pnas.1803866115

Gürgey, K. and Zühtü, B.A.T.I., 2018. Palynological and petroleum geochemical assessment of the lower Oligocene Mezardere Formation, Thrace Basin, NW Turkey. *Turkish Journal of Earth Sciences*, *27*(5), pp.349-383.

Hackley, P.C., Ryder, R.T., Trippi, M.H., Alimi, H., 2013. Thermal maturity of northern Appalachian Basin Devonian shales: Insights from sterane and terpane biomarkers. Fuel 106, 455–462. https://doi.org/10.1016/j.fuel.2012.12.032

Menneken, M., Nemchin, A.A., Geisler, T., Pidgeon, R.T. and Wilde, S.A., 2007. Hadean diamonds in zircon from Jack Hills, Western Australia. *Nature*, *448*(7156), pp.917-920. https://doi:10.1038/nature06083

Hallmann, C., Kelly, A.E., Gupta, S.N., Summons, R.E., 2011. Reconstructing Deep-Time Biology with Molecular Fossils, in: Laflamme, M., Schiffbauer, J.D., Dornbos, S.Q. (Eds.), Quantifying the Evolution of Early Life: Numerical Approaches to the Evaluation of Fossils and Ancient Ecosystems, Topics in Geobiology. Springer Netherlands, Dordrecht, pp. 355–401. https://doi.org/10.1007/978-94-007-0680-4_14

Harvey, H.R., Mcmanus, G.B., 1991. Marine ciliates as a widespread source of tetrahymanol and hopan-3β-ol in sediments. Geochimica et Cosmochimica Acta, The Macalpine Hills Lunar Meteorite Consortium 55, 3387–3390. https://doi.org/10.1016/0016-7037(91)90496-R

He, C., Huang, H., Wang, Q., Li, Z., 2019. Correlation of Maturity Parameters Derived from Methylphenanthrenes and Methyldibenzothiophenes in the Carboniferous Source Rocks from Qaidam Basin, NW China. Geofluids 2019, 1–12. https://doi.org/10.1155/2019/5742902

He, J., Zhang, S., Zhang, X., Qian, Y., He, H., Wu, H., 2016. Composition and Distribution Characteristics and Geochemical Significance of n-Alkanes in Core Sediments in the Northern Part of the South Yellow Sea. Journal of Chemistry 2016, e4741939. https://doi.org/10.1155/2016/4741939

Henson, P., Carson, C., Doublier, M., Williams, B., Simmons, J., Hutton, L., Close, D., 2020. Structural evolution of the South Nicholson region: insight from the 2017 L210 reflection seismic survey. https://doi.org/10.11636/133051

Hoefs, M.J.L., Rijpstra, W.I.C., Sinninghe Damsté, J.S., 2002. The influence of oxic degradation on the sedimentary biomarker record I: evidence from Madeira Abyssal Plain turbidites. Geochimica et Cosmochimica Acta 66, 2719–2735. https://doi.org/10.1016/S0016-7037(02)00864-5

Holba, A.G., Dzou, L., Masterson, D., Hughes, W.B., Huizinga, B., Singletary, M.S., Moldowan, J.M., Mello, M.R., Tegelaar, E., 1998. Application of 24-norcholestanes for constraining source age of petroleum. Organic Geochemistry 29, 1269–1283. https://doi.org/10.1016/S0146-6380(98)00184-3

Jahnke, L.L., Embaye, T., Hope, J., Turk, K.A., Van Zuilen, M., Des Marais, D.J., Farmer, J.D., Summons, R.E., 2004. Lipid biomarker and carbon isotopic signatures for stromatolite-forming, microbial mat communities and Phormidium cultures from Yellowstone National Park. Geobiology 2, 31–47. https://doi.org/10.1111/j.1472-4677.2004.00021.x

Jarrett, A., Cox, G., Southby, C., Hong, Z., Palatty, dr. P., Carr, L., Henson, P., 2018. Source rock geochemistry of the McArthur Basin, northern Australia. https://doi.org/10.11636/Record.2018.024

Jarrett, A., Hall, L., Carr, L., Anderson, J., orr, meredith, bradshaw, barry, Henson, P., Gorton, J., 2019a. Source rock geochemistry of the Isa Superbasin and South Nicholson Basin, Northern Australia: Baseline regional hydrocarbon prospectivity. https://doi.org/10.11636/Record.2018.038

Jarrett, A., Bailey, A.E.H., Boreham, C.J., Palu, T., Hall, L., Shannon, A., Collins, A.S., Vinnichenko, G., Brocks, J., Li, Z., Munson, T.J., Edwards, S., Carr, L., Henson, P., 2020. A geochemical investigation into the resource potential of the Lawn Hill Platform, northern Australia. The APPEA Journal 60, 722. https://doi.org/10.1071/AJ19118

Jarrett, A., Cox, G.M., Brocks, J.J., Grosjean, E., Boreham, C.J., Edwards, D.S., 2019b. Microbial assemblage and palaeoenvironmental reconstruction of the 1.38 Ga Velkerri Formation, McArthur Basin, northern Australia. Geobiology 17, 360–380. https://doi.org/10.1111/gbi.12331

Jarrett, A.J.M., Schinteie, R., Hope, J.M., Brocks, J.J., 2013. Micro-ablation, a new technique to remove drilling fluids and other contaminants from fragmented and fissile rock material. Organic Geochemistry 61, 57–65. https://doi.org/10.1016/j.orggeochem.2013.06.005

Jarvie, D.M., Morelos, A. and Han, Z., 2001. Detection of pay zones and pay quality, Gulf of Mexico: Application of geochemical techniques.

Javaux, E.J., Knoll, A.H., 2017. Micropaleontology of the lower Mesoproterozoic Roper Group, Australia, and implications for early eukaryotic evolution. J. Paleontol. 91, 199–229. https://doi.org/10.1017/jpa.2016.124

Javaux, E.J., Knoll, A.H., Walter, M., 2003. Recognizing and Interpreting the Fossils of Early Eukaryotes. Orig Life Evol Biosph 33, 75–94. https://doi.org/10.1023/A:1023992712071

Jiang, C., Chen, Z., Lavoie, D., Percival, J.B., Kabanov, P., 2017. Mineral carbon MinC(%) from Rock-Eval analysis as a reliable and cost-effective measurement of carbonate contents in shale source and reservoir rocks. Marine and Petroleum Geology 83, 184–194. https://doi.org/10.1016/j.marpetgeo.2017.03.017

Katz, B.J., Lin, F., 2021. Consideration of the limitations of thermal maturity with respect to vitrinite reflectance, Tmax, and other proxies. AAPG Bulletin 105, 695–720. https://doi.org/10.1306/09242019261

Knoll, A. h, Javaux, E. j, Hewitt, D., Cohen, P., 2006. Eukaryotic organisms in Proterozoic oceans. Philosophical Transactions of the Royal Society B: Biological Sciences 361, 1023–1038. https://doi.org/10.1098/rstb.2006.1843

Kodner, R.B., Summons, R.E., Knoll, A.H., 2004. A Molecular Approach to the Study of Green Algal Evolution and Early Terrestrial Ecosystems 2004, B33B-0254.

Kunzmann, M., Blaikie, T.N., 2019. The ca 1640 Ma Barney Creek Formation in the McArthur Basin: Targeting diagenetic mineralisation and depocentre shift 5.

Kvalheim, O.M., Christy, A.A., Telnæs, N., Bjørseth, A., 1987. Maturity determination of organic matter in coals using the methylphenanthrene distribution. Geochimica et Cosmochimica Acta 51, 1883–1888. https://doi.org/10.1016/0016-7037(87)90179-7

Lamb, D. M., Awramik, S.M., Chapman, D.J., Zhu, S., 2009. Evidence for eukaryotic diversification in the ~1800 million-year-old Changzhougou Formation, North China. Precambrian Research, World Summit on Ancient Microscopic Fossils 173, 93–104. https://doi.org/10.1016/j.precamres.2009.05.005

Larter, S.R., Bowler, B.F.J., Li, M., Chen, M., Brincat, D., Bennett, B., Noke, K., Donohoe, P., Simmons, D., Kohnen, M., Allan, J., Telnaes, N., Horstad, I., 1996. Molecular indicators of secondary oil migration distances. Nature 383, 593–597. https://doi.org/10.1038/383593a0

Laurie, J.R., 2022. Biostratigraphy of the Georgina Basin succession in NDI Carrara 1.

Lee, C., Brocks, J.J., 2011. Identification of carotane breakdown products in the 1.64billion year old Barney Creek Formation, McArthur Basin, northern Australia. Organic Geochemistry 42, 425–430. https://doi.org/10.1016/j.orggeochem.2011.02.006

Leider, A., Schumacher, T.C., Hallmann, C., 2016. Enhanced procedural blank control for organic geochemical studies of critical sample material. Geobiology 14, 469–482. https://doi.org/10.1111/gbi.12183

Liyanage, T., n.d. Comprehensive Identification Guide Cheilanthanes C_{19}-C_{46}. Unpublished

Love, G.D., Grosjean, E., Stalvies, C., Fike, D.A., Grotzinger, J.P., Bradley, A.S., Kelly, A.E., Bhatia, M., Meredith, W., Snape, C.E., Bowring, S.A., Condon, D.J., Summons, R.E., 2009. Fossil steroids record the appearance of Demospongiae during the Cryogenian period. Nature 457, 718–721. https://doi.org/10.1038/nature07673

Lu, H., Shen, C., Zhang, Z., Liu, M., Sheng, G., Peng, P., Hsu, C.S., 2015. 2,3,6-/2,3,4-Aryl Isoprenoids in Paleocene Crude Oils from Chinese Jianghan Basin: Constrained by Water Column Stratification. Energy Fuels 29, 4690–4700. https://doi.org/10.1021/acs.energyfuels.5b00110

Luo, G., Hallmann, C., Xie, S., Ruan, X., Summons, R.E., 2015. Comparative microbial diversity and redox environments of black shale and stromatolite facies in the Mesoproterozoic Xiamaling Formation. Geochimica et Cosmochimica Acta 151, 150–167. https://doi.org/10.1016/j.gca.2014.12.022

Luo, Q., Zhang, L., Zhong, N., Wu, Jin, Goodarzi, F., Sanei, H., Skovsted, C.B., Suchý, V., Li, M., Ye, X., Cao, W., Liu, A., Min, X., Pan, Y., Yao, L., Wu, Jia, 2021. Thermal evolution behavior of the organic matter and a ray of light on the origin of vitrinite-like maceral in the Mesoproterozoic and Lower Cambrian black shales: Insights from artificial maturation. International Journal of Coal Geology 244, 103813. https://doi.org/10.1016/j.coal.2021.103813

Lyons, T.W., Reinhard, C.T., Planavsky, N.J., 2014. The rise of oxygen in Earth's early ocean and atmosphere. Nature 506, 307–315. https://doi.org/10.1038/nature13068

Ma, A., Jin, Z., Zhu, C., Bai, Z., 2017. Cracking and thermal maturity of Ordovician oils from Tahe Oilfield, Tarim Basin, NW China. Journal of Natural Gas Geoscience 2, 239–252. https://doi.org/10.1016/j.jnggs.2017.12.001

Mackenzie, A.S., 1984. Applications of Biological Markers in Petroleum Geochemistry, in: Brooks, J., Welte, D. (Eds.), Advances in Petroleum Geochemistry, Advances in Petroleum Geochemistry. Academic Press, London, pp. 115–214. https://doi.org/10.1016/B978-0-12-032001-1.50008-0

Marek, S., Rospondek, M., 2014. Controls on distributions of methylphenanthrenes in sedimentary rock extracts: Critical evaluation of existing geochemical data from molecular modelling. Organic Geochemistry 41, 1297–1311. https://doi.org/10.1016/j.orggeochem.2010.09.009

Marshall, C.R., 2006. Explaining the Cambrian "Explosion" of Animals. Annual Review of Earth and Planetary Sciences 34, 355–384. https://doi.org/10.1146/annurev.Earth.33.031504.103001

Miao, L., Moczydłowska, M., Zhu, S., Zhu, M., 2019. New record of organic-walled, morphologically distinct microfossils from the late Paleoproterozoic Changcheng Group in the Yanshan Range, North China. Precambrian Research 321, 172–198. https://doi.org/10.1016/j.precamres.2018.11.019

Moczydłowska, M., Liu, P., 2021. Ediacaran algal cysts from the Doushantuo Formation, South China. Geological Magazine 1–21. https://doi.org/10.1017/S0016756820001405

Moldowan, J.M., Seifert, W.K., Gallegos, E.J., 1983. Identification of an extended series of tricyclic terpanes in petroleum. Geochimica et Cosmochimica Acta 47, 1531–1534. https://doi.org/10.1016/0016-7037(83)90313-7

Mukhopadhyay, P.K., 1994. Vitrinite Reflectance as Maturity Parameter, in: Vitrinite Reflectance as a Maturity Parameter, ACS Symposium Series. American Chemical Society, pp. 1–24. https://doi.org/10.1021/bk-1994-0570.ch001

Nazir, A., Fazeelat, T., 2017. Geochemistry of cretaceous rocks, Pakistan: I. Biomarker approach to assess thermal maturity of OM. Petroleum Science and Technology 35, 875–882. https://doi.org/10.1080/10916466.2017.1283523

Neto, F.R.A., Restle, A., Connan, J., Albrecht, P., Ourisson, G., 1982. Novel tricyclic terpanes (C19, C20) in sediments and petroleums. Tetrahedron Letters 23, 2027–2030. https://doi.org/10.1016/S0040-4039(00)87251-2

Nguyen, K., Love, G.D., Zumberge, J.A., Kelly, A.E., Owens, J.D., Rohrssen, M.K., Bates, S.M., Cai, C., Lyons, T.W., 2019. Absence of biomarker evidence for early eukaryotic life from the Mesoproterozoic Roper Group: Searching across a marine redox gradient in mid-Proterozoic habitability. Geobiology 17, 247–260. https://doi.org/10.1111/gbi.12329

Niu, C., Hou, D., Cheng, X., Han, X., Li, Yan, Li, Yaxi, 2021. Origin and Geochemical Implications of Hopanoids in Saline Lacustrine Crude Oils from Huanghekou East Sag and Laizhouwan Northeastern Sag, Bohai Bay Basin. ACS Omega 6, 30298–30314. https://doi.org/10.1021/acsomega.1c02762

Ourisson, G., Albrecht, P., Rohmer, M., 1979. The Hopanoids: palaeochemistry and biochemistry of a group of natural products. Pure and Applied Chemistry 51, 709–729. https://doi.org/10.1351/pac197951040709

Pagès, A., Schmid, S., Edwards, D., Barnes, S., He, N., Grice, K., 2016. A molecular and isotopic study of palaeoenvironmental conditions through the middle Cambrian in the Georgina Basin, central Australia. Earth and Planetary Science Letters 447, 21–32. https://doi.org/10.1016/j.epsl.2016.04.032

Palmisano, A.C., Summons, R.E., Cronin, S.E. and Des Marais, D.J., 1989. Lipophilic pigments from cyanobacterial (blue-green algal) and diatom mats in Hamelin pool, shark bay, western Australia 1. *Journal of phycology*, *25*(4), pp.655-661.

Pawlowska, M.M., Butterfield, N.J., Brocks, J.J., 2013. Lipid taphonomy in the Proterozoic and the effect of microbial mats on biomarker preservation. Geology 41, 103–106. https://doi.org/10.1130/G33525.1

Peters, C.A., George, S.C., 2018. Hydrocarbon biomarkers preserved in carbonate veins of potentially Paleoproterozoic age, and implications for the early biosphere. Geobiology 16, 577–596. https://doi.org/10.1111/gbi.12305

Peters, K.E., 2000. Petroleum tricyclic terpanes: predicted physicochemical behavior from molecular mechanics calculations. Organic Geochemistry 31, 497–507. https://doi.org/10.1016/S0146-6380(00)00029-2

Peters, K.E., 1998. Biomarker: Assessment of thermal maturity, in: Geochemistry. Springer Netherlands, Dordrecht, pp. 36–39. https://doi.org/10.1007/1-4020-4496-8_28

Peters, K.E., 1986. Guidelines for Evaluating Petroleum Source Rock Using Programmed Pyrolysis1. AAPG Bulletin 70, 318–329. https://doi.org/10.1306/94885688-1704-11D7-8645000102C1865D

Peters, K.E., Curry, D.J., Kacewicz, M., 2012. An Overview of Basin and Petroleum System Modeling: Definitions and Concepts 1–16. https://doi.org/10.1306/13311426H4139

Peters, K. E., Walters, C.C., Moldowan, J.M., 2005. The Biomarker Guide. Cambridge University Press.

Planavsky, N.J., Reinhard, C.T., Wang, X., Thomson, D., McGoldrick, P., Rainbird, R.H., Johnson, T., Fischer, W.W., Lyons, T.W., 2014. Low Mid-Proterozoic atmospheric oxygen levels and the delayed rise of animals. Science 346, 635–638. https://doi.org/10.1126/science.1258410

Porter, S.M., 2020. Insights into eukaryogenesis from the fossil record. Interface Focus. https://doi.org/10.1098/rsfs.2019.0105

Radke, M., Horsfield, B., Littke, R., Rullkötter, J., 1997. Maturation and Petroleum Generation, in: Welte, D.H., Horsfield, Brian, Baker, D.R. (Eds.), Petroleum and Basin Evolution: Insights from

Petroleum Geochemistry, Geology and Basin Modeling. Springer, Berlin, Heidelberg, pp. 169–229. https://doi.org/10.1007/978-3-642-60423-2_4

Radke, M., Leythaeuser, D., Teichmüller, M., 1984. Relationship between rank and composition of aromatic hydrocarbons for coals of different origins. Organic Geochemistry 6, 423–430. https://doi.org/10.1016/0146-6380(84)90065-2

Radke, M., Welte, D.H., Willsch, H., 1982. Geochemical study on a well in the Western Canada Basin: relation of the aromatic distribution pattern to maturity of organic matter. Geochimica et Cosmochimica Acta 46, 1–10. https://doi.org/10.1016/0016-7037(82)90285-X

Ranasinghe, S.P., Crosdale, P.J., 2022. Source rock type, maturation levels and hydrocarbon potential of a suite of samples from NDI Carrara 1 well, Northern Territory. https://doi.org/10.26186/146260

Rashid, H., Grosjean, E., 2006. Detecting the source of Heinrich layers: An organic geochemical study. Paleoceanography 21. https://doi.org/10.1029/2005PA001240

Reddy, C.M., Eglinton, T.I., Palić, R., Benitez-Nelson, B.C., Stojanović, G., Palić, I., Djordjević, S., Eglinton, G., 2000. Even carbon number predominance of plant wax n-alkanes: a correction. Organic Geochemistry 31, 331–336. https://doi.org/10.1016/S0146-6380(00)00025-5

Reinhard, C.T., Planavsky, N.J., Robbins, L.J., Partin, C.A., Gill, B.C., Lalonde, S.V., Bekker, A., Konhauser, K.O., Lyons, T.W., 2013. Proterozoic ocean redox and biogeochemical stasis. Proceedings of the National Academy of Sciences 110, 5357–5362. https://doi.org/10.1073/pnas.1208622110

Reinhard, C.T., Planavsky, N.J., Ward, B.A., Love, G.D., Le Hir, G., Ridgwell, A., 2020. The impact of marine nutrient abundance on early eukaryotic ecosystems. Geobiology 18, 139–151. https://doi.org/10.1111/gbi.12384

Roger, Andrew J, Hug, L.A., 2006. The origin and diversification of eukaryotes: problems with molecular phylogenetics and molecular clock estimation. Philosophical Transactions of the Royal Society B: Biological Sciences 361, 1039–1054. https://doi.org/10.1098/rstb.2006.1845

Safarik, I. and Strausz, O.P., 1996. The thermal decomposition of hydro-carbons. Part 1. n-alkanes (C≥ 5). *Research on chemical intermediates*, *22*(3), pp.275-314.

Sassen, R., Chinn, E.W., 1989. Effects of elemental sulfur during programmed pyrolysis of kerogen. Organic Geochemistry 14, 475–477. https://doi.org/10.1016/0146-6380(89)90012-0

Scheeder, G., Weniger, P. and Blumenberg, M., 2020. Geochemical implications from direct Rock-Eval pyrolysis of petroleum. *Organic Geochemistry*, *146*, p.104051.

Schinteie, R., Colangelo-Lillis, J.R., Hope, J.M., Chen, J., Nelson, D.B., Jarrett, A.J.M., Brocks, J.J., 2019. Impact of drill core contamination on compound-specific carbon and hydrogen isotopic signatures. Organic Geochemistry 128, 161–171. https://doi.org/10.1016/j.orggeochem.2019.01.003

Selley, C., Sonnenber, S.A., 2014 Elements of Petroleum Geology - 3rd Edition , ISBN: 9780123860316

Senftle, J.T., Landis, C.R., 1991. Vitrinite Reflectance as a Tool To Assess Thermal Maturity. https://doi.org/10.1306/TrHbk543C12

Shang, X., Liu, P., 2022. Diverse multicellular algae from the early Ediacaran Doushantuo chert nodules and their palaeoecological implications. Precambrian Research 368, 106508. https://doi.org/10.1016/j.precamres.2021.106508

Stewart, A.K., Massey, M., Padgett, P.L., Rimmer, S.M., Hower, J.C., 2005. Influence of a basic intrusion on the vitrinite reflectance and chemistry of the Springfield (No. 5) coal, Harrisburg, Illinois. International Journal of Coal Geology, TSOP 2003 63, 58–67. https://doi.org/10.1016/j.coal.2005.02.005

Summons, R.E., Powell, T.G., 1986. Chlorobiaceae in Palaeozoic seas revealed by biological markers, isotopes and geology. Nature 319, 763–765. https://doi.org/10.1038/319763a0

Summons, R.E., Powell, T.G., Boreham, C.J., 1988. Petroleum geology and geochemistry of the Middle Proterozoic McArthur Basin, Northern Australia: III. Composition of extractable hydrocarbons. Geochimica et Cosmochimica Acta 52, 1747–1763. https://doi.org/10.1016/0016-7037(88)90001-4

Summons, R.E., Welander, P.V., Gold, D.A., 2022. Lipid biomarkers: molecular tools for illuminating the history of microbial life. Nat Rev Microbiol 20, 174–185. https://doi.org/10.1038/s41579-021-00636-2

Tang, Q., Pang, K., Yuan, X., Xiao, S., 2020. A one-billion-year-old multicellular chlorophyte. Nat Ecol Evol 4, 543–549. https://doi.org/10.1038/s41559-020-1122-9

Tissot, B.P., Welte, D.H., 1984. Petroleum formation and occurrence, 2nd, rev.enl. ed ed. Springer-Verlag, Berlin ; New York.

Tomazic, M.L., Poklepovich, T.J., Nudel, C.B. and Nusblat, A.D., 2014. Incomplete sterols and hopanoids pathways in ciliates: gene loss and acquisition during evolution as a source of biosynthetic genes. Molecular phylogenetics and evolution, 74, pp.122-134. https://doi.org/10.1016/j.ympev.2014.01.026

van Maldegem, L.M., Kipp, M., Hope, J.M., Brocks, J.J., 2019. Lipid Biomarkers Reveal a Bacterial Dominated Ecosystem after the Sturtian Glaciation, in: 29th International Meeting on Organic Geochemistry. Presented at the 29th International Meeting on Organic Geochemistry, European Association of Geoscientists & Engineers, Gothenburg, Sweden, pp. 1–1. https://doi.org/10.3997/2214-4609.201902748

van Maldegem, L.M., Nettersheim, B.J., Leider, A., Brocks, J.J., Adam, P., Schaeffer, P., Hallmann, C., 2021. Geological alteration of Precambrian steroids mimics early animal signatures. Nat Ecol Evol 5, 169–173. https://doi.org/10.1038/s41559-020-01336-5

Vinnichenko, G., Hope, J.M., Jarrett, A.J.M., Williams, N., Brocks, J.J., 2021. Reassessment of thermal preservation of organic matter in the Paleoproterozoic McArthur River (HYC) Zn-Pb ore deposit, Australia. Ore Geology Reviews 133, 104129. https://doi.org/10.1016/j.oregeorev.2021.104129

Vinnichenko, G., Jarrett, A.J.M., Hope, J.M., Brocks, J.J., 2020. Discovery of the oldest known biomarkers provides evidence for phototrophic bacteria in the 1.73 Ga Wollogorang Formation, Australia. Geobiology 18, 544–559. https://doi.org/10.1111/gbi.12390

Wang, Q., Huang, H., He, C., Li, Z. and Zheng, L., 2022. Methylation and demethylation of naphthalene homologs in highly thermal mature sediments. *Organic Geochemistry*, *163*, p.104343.

Wang, Y.-P., Zhan, X., Gao, Y., Xia, J., Wang, S., Zou, Y.-R., 2020. Geochemical Signatures and Controlling Factors of Rearranged Hopanes in Source Rocks and Oils from Representative Basins of China. ACS Omega 5, 30160–30167. https://doi.org/10.1021/acsomega.0c04615

Welander, P.V., 2019. Deciphering the evolutionary history of microbial cyclic triterpenoids. Free Radical Biology and Medicine, Early Life on Earth and Oxidative Stress 140, 270–278. https://doi.org/10.1016/j.freeradbiomed.2019.05.002

Wilde, S.A., Valley, J.W., Peck, W.H., Graham, C.M., 2001. Evidence from detrital zircons for the existence of continental crust and oceans on the Earth 4.4 Gyr ago. Nature 409, 175–178. https://doi.org/10.1038/35051550

Willman, S., Moczydłowska, M., 2007. Wall ultrastructure of an Ediacaran acritarch from the Officer Basin, Australia. Lethaia 40, 111–123. https://doi.org/10.1111/j.1502-3931.2007.00023.x

Woltz, C.R., Porter, S.M., Agić, H., Dehler, C.M., Junium, C.K., Riedman, L.A., Hodgskiss, M.S.W., Wörndle, S., Halverson, G.P., 2020. Total organic carbon and the preservation of organic-walled microfossils in Precambrian shale. Geology 49, 556–560. https://doi.org/10.1130/G48116.1

Wood, D.A., Hazra, B., 2017. Characterization of organic-rich shales for petroleum exploration & exploitation: A review-Part 2: Geochemistry, thermal maturity, isotopes and biomarkers. Journal of Earth Science 28, 758–778. http://dx.doi.org.virtual.anu.edu.au/10.1007/s12583-017-0733-9

Xianying, L., Zongju, Z. and Yuanlin, M., 2015. Application of an odd/even predominance of n-alkanes in oil–source rock correlation: taking the lower Paleozoic strata of the Tarim Basin as an example. *Toxicological & Environmental Chemistry*, *97*(3-4), pp.409-416.

Yang, E.C., Boo, S.M., Bhattacharya, D., Saunders, G.W., Knoll, A.H., Fredericq, S., Graf, L., Yoon, H.S., 2016. Divergence time estimates and the evolution of major lineages in the florideophyte red algae. Scientific Reports 6, 21361. https://doi.org/10.1038/srep21361

Yang, S., Horsfield, B., 2020. Critical review of the uncertainty of Tmax in revealing the thermal maturity of organic matter in sedimentary rocks. International Journal of Coal Geology 225, 103500. https://doi.org/10.1016/j.coal.2020.103500

Zhang, S., Huang, H., Xiao, Z., Liang, D., 2005. Geochemistry of Palaeozoic marine petroleum from the Tarim Basin, NW China. Part 2: Maturity assessment. Organic Geochemistry 36, 1215–1225. https://doi.org/10.1016/j.orggeochem.2005.01.014

Zhang, X., Shen, B., Yang, J., Sun, W., Hou, D., 2021. Evolution characteristics of maturity-related sterane and terpane biomarker parameters during hydrothermal experiments in a semi-open system under geological constraint. Journal of Petroleum Science and Engineering 201, 108412. https://doi.org/10.1016/j.petrol.2021.108412

Zumberge, J.A., Love, G.D., Cárdenas, P., Sperling, E.A., Gunasekera, S., Rohrssen, M., Grosjean, E., Grotzinger, J.P., Summons, R.E., 2018. Demosponge steroid biomarker 26-methylstigmastane provides evidence for Neoproterozoic animals. Nat Ecol Evol 2, 1709–1714. https://doi.org/10.1038/s41559-018-0676-2

Zylstra, G.J., Gibson, D.T., 1991. Aromatic Hydrocarbon Degradation: A Molecular Approach, in: Setlow, J.K. (Ed.), Genetic Engineering: Principles and Methods, Genetic Engineering. Springer US, Boston, MA, pp. 183–203. https://doi.org/10.1007/978-1-4615-3760-1_8

VII. Appendix

Appendix A – Table of samples

Sample ID	Depth top (m)	Depth bottom (m)	Age	Lithology
7533132	361.71	361.79	Drumian	Micritic limestone with wavy irregular muddy laminae and small concentrations of calcite (Geoscience Australia 2020).
7533139	394.97	395.12	Drumian	Micritic limestone with wavy irregular muddy laminae and small concentrations of calcite (Geoscience Australia 2020).
7533159	494.48	494.60	Wuliuan	Micritic limestone with low concentrations of calcite (Geoscience Australian 2020).
6725604	528.33	n.d	Wuliuan	Oil Stain
7533185	610.47	610.62	Wuliuan	Mostly micritic limestone, but it also has sections of dolostone (Geoscience Australia 2020) which might be an indication of sulphur reducing bacteria (Vasconcelos et al. 1995).
7533204	689.82	689.95	Proterozoic	Carbonaceous shale (Geoscience Australia 2020).
7533210	719.31	719.38	Proterozoic	Calcareous mudstone and micritic limestone (Geoscience Australia 2020).
7373044	763.10	n.d	Proterozoic	Oil stain
7373046	763.10	n.d	Proterozoic	Oil stain
7533225	794.71	794.86	Proterozoic	Calcareous mudstone and micritic limestone (Geoscience Australia 2020).
7533569	925.37	925.53	Proterozoic	Mudstone (Geoscience Australia 2020).
7533584	998.66	998.76	Proterozoic	Mudstone (Geoscience Australia 2020).
7533609	1069.16	1069.32	Proterozoic	Micritic limestone with calcite minerals (Geoscience Australia 2020).
7533625	1150.08	1150.21	Proterozoic	Micritic limestone with calcite minerals (Geoscience Australia 2020).
7533635	1199.60	1199.72	≈1600Ma (Carson et al. 2022)	Mudstone with some limestone (Geoscience Australia 2020).
7533644	1244.79	1244.95	≈1600Ma (Carson et al. 2022)	Mudstone with some limestone (Geoscience Australia 2020).

7533668	1345.03	1345.17	≈1600Ma (Carson et al. 2022)	Turbidite (Geoscience Australia 2020).
7533682	1405.10	1405.26	≈1600Ma (Carson et al. 2022)	Turbidite (Geoscience Australia 2020).
7533705	1461.32	1461.45	≈1612Ma (Carson et al. 2022)	Turbidite (Geoscience Australia 2020).
7533872	1593.64	1593.78	≈1612Ma (Carson et al. 2022)	Sandstone (Geoscience Australia 2020).

Appendix B – Photos of samples

2021330020
7533132 (361.71-361.19 m)

CARRARA 1_SLICE_7533132_361.71-361.79

20213300207
7533139 (394.97-395.12 m)

CARRARA 1_SLICE_7533139_394.97-395.12

2021330047
7533159 (494.48-494.6 m)

CARRARA 1_SLICE_7533159_494.48-494.6

20200005
6725604 (528.33 m)
Intact core (a) and split core (b) (Grosjean et al. 2022).

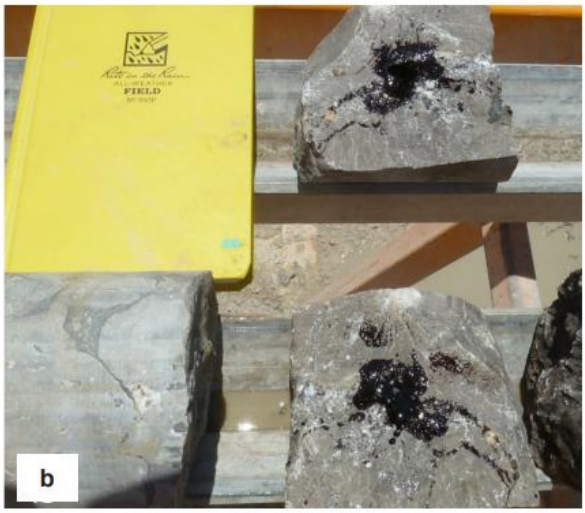

2021330073
7533185 (610.47-610.62 m)

2021330092
7533204 (689.82-689.95 m)

2021330098
7533210 (719.21-719.38 m)

20210010 and 20210012
7373044 and 7373046 (763.10 m)
Grosjean et al. 2022)

2021330113
7533225 (794.71-719.38 m)

2021330139
7533569 (925.37-925.53 m)

CARRARA 1 QUARTER 7533569 925.37-925.53

2021330154
7533584 (998.66-998.76 m)

2021330179
7533609 (1069.16-1069.32 m)

2021330195

7533625 (1150.08-1150.21 m)

CARRARA 1_QUARTER_7533625_1150.08-1150.21

2021330205
7533635 (1199.60-1199.72 m)

CARRARA 1_QUARTER_7533635_1199.6-1199.72

2021330214
7533644 (1244.79-1244.95 m)

CARRARA 1_QUARTER_7533644_1244.79-1244.95

2021330238
7533668 (1345.03-1345.17 m)

CARRARA 1_QUARTER_7533668_1345.03-1345.17

2021330252
7533682 (1405.10-1405.26 m)

CARRARA 1_QUARTER_7533682_1405.1-1405.26

2021330275
7533705 (1461.32-1461.45 m)

CARRARA 1_QUARTER_7533705_1461.32-1461.45

2021330397
7533872 (1593.64-1593.78 m)

CARRARA 1_QUARTER_7534872_1593.64-1593.78